PB81-156481

The Behavior of Bonded Doubler Splices for Composite Sandwich Panels

Virginia Polytechnic Inst. and State Univ.
Blacksburg

Prepared for

National Aeronautics and Space Administration
Hampton, VA

Jul 80

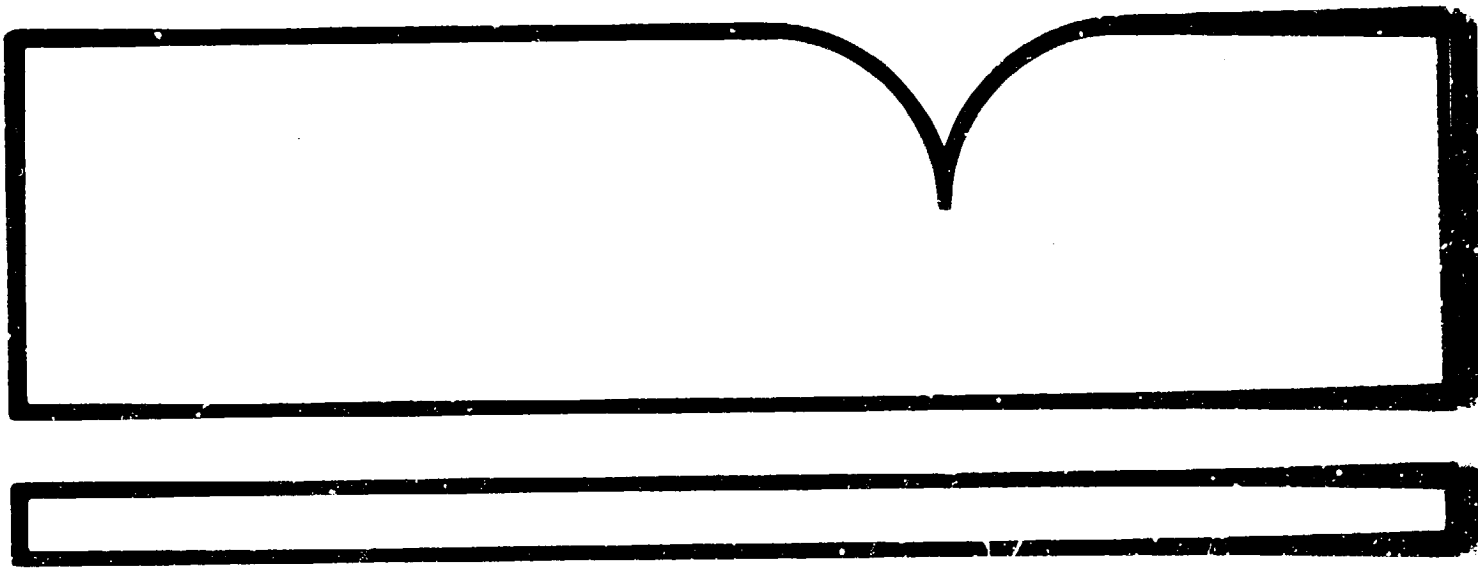

College of Engineering
Virginia Polytechnic Institute and State University
Blacksburg, Virginia 24061

VPI-E-80-20 July, 1980

THE BEHAVIOR OF BONDED DOUBLER SPLICES FOR COMPOSITE SANDWICH PANELS

Thomas A. Zeiler[1]

Terry A. Weisshaar[2]

Department of Engineering Science and Mechanics

Interim Report 19
The NASA-Virginia Tech Composites Program

NASA Grant NGR 47-004-129 and NASA Cooperative Agreement NCCI-15

Prepared for: Structural Mechanics Branch
National Aeronautics & Space Administration
Langley Research Center
Hampton, Virginia 23665

[1]Research Assistant - Virginia Tech

[2]Associate Professor of Aerospace and Ocean Engineering - Virginia Tech

SECURITY CLASSIFICATION OF THIS PAGE *(When Data Entered)*

REPORT DOCUMENTATION PAGE

READ INSTRUCTIONS BEFORE COMPLETING FORM

1. REPORT NUMBER: VPI-E-80-20	2. GOVT ACCESSION NO.
3. RECIPIENT'S CATALOG NUMBER	
4. TITLE *(and Subtitle)*: THE BEHAVIOR OF BONDED DOUBLER SPLICES FOR DOUBLER SPLICES FOR COMPOSITE SANDWICH PANELS	5. TYPE OF REPORT & PERIOD COVERED
	6. PERFORMING ORG. REPORT NUMBER: VIP-E-80-20
7. AUTHOR(s): Thomas A. Zeiler and Terry A. Weisshaar	8. CONTRACT OR GRANT NUMBER(s): NASA Grant NCCI-15 and NGR 47-004-129
9. PERFORMING ORGANIZATION NAME AND ADDRESS: Virginia Polytechnic Institute & State University Engineering Science and Mechanics Blacksburg, Virginia 24061	10. PROGRAM ELEMENT, PROJECT, TASK AREA & WORK UNIT NUMBERS
11. CONTROLLING OFFICE NAME AND ADDRESS: National Aeronautics & Space Administration Langley Research Center Hampton, Virginia 23665	12. REPORT DATE: July, 1980
	13. NUMBER OF PAGES
14. MONITORING AGENCY NAME & ADDRESS *(if different from Controlling Office)*: Virginia Polytechnic Institute & State University Engineering Science & Mechanics Blacksburg, Virginia 24061	15. SECURITY CLASS. *(of this report)*: unclassified
	15a. DECLASSIFICATION/DOWNGRADING SCHEDULE

16. DISTRIBUTION STATEMENT *(of this Report)*

Approved for public release, distribution unlimited

17. DISTRIBUTION STATEMENT *(of the abstract entered in Block 20, if different from Report)*

Approved for public release, distribution unlimited

18. SUPPLEMENTARY NOTES

19. KEY WORDS *(Continue on reverse side if necessary and identify by block number)*

graphite-polyimide, sandwich panels, bonded doublers, lap joints

20. ABSTRACT *(Continue on reverse side if necessary and identify by block number)*

See page iv

DD FORM 1 JAN 73 1473 EDITION OF 1 NOV 65 IS OBSOLETE

SECURITY CLASSIFICATION OF THIS PAGE *(When Data Entered)*

ACKNOWLEDGEMENTS

This investigation was supported by the NASA-Virginia Tech Composites Program (NASA Cooperative Agreement #NCCI-15 and NASA Grant NGR 47-004-129). The authors gratefully acknowledge the assistance of Dr. J. W. Sawyer of NASA-Langley Research Center, whose support and advice during all stages of this project was invaluable. In addition, the assistance of Dr. Paul Cooper of NASA-Langley was particularly helpful during the initial phase of the investigation. Typing and reproduction of this report was skillfully and patiently handled by Mrs. Frances Hale.

THE BEHAVIOR OF BONDED DOUBLER SPLICES FOR COMPOSITE SANDWICH PANELS

(ABSTRACT)

The results of an investigation into the behavior of adhesively bonded doubler splices of two composite material sandwich panels is presented. The splices are studied from three approaches: analytical; numerical (finite elements); and experimental.

Several parameters that characterize the splice are developed to determine their influence upon joint strength. These parameters are: doubler overlap length; core stiffness; laminate bending stiffness; the size of the gap between the spliced sandwich panels; and room and elevated temperatures. Similarities and contrasts between these splice and the physically similar single and double lap joints are discussed. The results of this investigation suggest several possible approaches to improving the strength of the sandwich splices.

TABLE OF CONTENTS

Table of Contents - continued

LIST OF FIGURES

List of Figures - continued

List of Figures - continued

LIST OF TABLES

Chapter 1

INTRODUCTION

Core-stiffened sandwich panels are intrinsically stiff, lightweight structural elements. As such, they have many applications in the weight and stiffness-critical structures of aerospace vehicles. However, any extensive use of sandwich panels in a major structure may require the joining of two or more panels. Also, if an area of a large sandwich panel on an in-service structure becomes damaged, repair might involve splicing a piece of sandwich panel tc replace the damaged area. The method by which the panels are joined depends largely upon the conditions in the region of the structure in which the splice occurs. This is because of the numerous possible loading conditions present throughout the structure, as well as the requirements of local and overall structural geometry. Indeed, sandwich panels are typically spliced together to another structural member, such as a frame, which becomes a part of the splice itself.

There are very few published discussions of sandwich panel splices available; these studies are, for the most part, experimental. This is because many of the splices considered worth testing were geometrically complex and not easily analyzed. Analytical complexity is exacerbated when the panel materials involved are laminated, orthotropic materials.

The sandwich splice to be considered is an adhesively bonded, doubler splice of two sandwich panels (Figure 1). The sandwich face sheets and the doublers are constructed of laminated Graphite/Polyimide

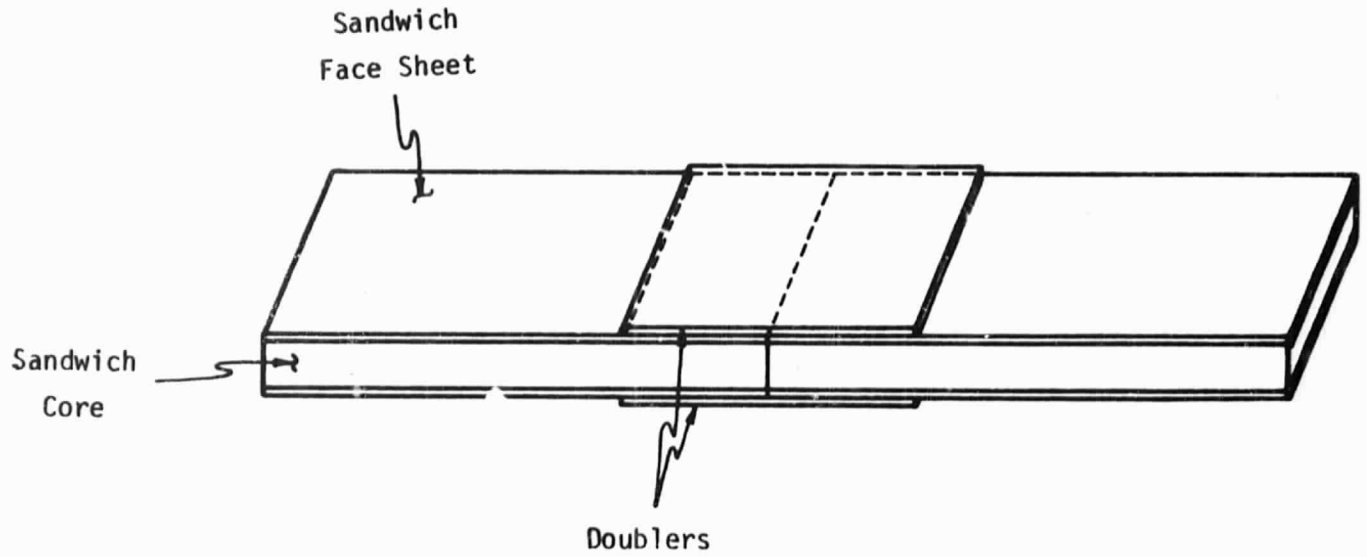

Figure 1: Sandwich Panel Splice

plies, and the sandwich core is Glass/Polyimide honeycomb. This splice does not involve an additional structural member.

This relatively simple splice is geometrically similar to both single and double lap joints. The sandwich splice model of Mallon and Beck [1], which is based fundamentally on the single lap joint model of Goland and Reissner [2], was adopted and improved to form the analytical model presented here. The results of this analysis will show the general influence of several parameters upon internal loads of the face-sheet and doubler. The parameters that characterize the splice include: applied load level; doubler overlap length; doubler and face-sheet bending stiffnesses; sandwich core stiffness; and the length of the gap between the spliced panels. Also studied with this analytical formulation are the critical buckling loads for the face sheets.

Curing and mechanical stress distributions within the splice are analyzed with the SPAR finite element program. Geometric nonlinearity under load is accounted for through the use of a one-step geometric stiffness matrix iteration. Additionally, face-sheet and doubler internal loads predicted by the finite element analysis are compared to the results of the analytical model. In the finite element model of the splice, each layer of the laminated face sheet and doubler is assigned its particular lamina properties.

Experimental results are also presented. The variables in the testing program are: doubler overlap length; face sheet and doubler stiffnesses; and temperature. The panels are tested in both tension and compression for failure loads and modes.

Chapter 2

LITERATURE SURVEY

Most of the analytical studies of structural sandwich panels done in the past have concentrated on the overall behavior of a single flat or curved sandwich panel under load. However, there seems to be very little published literature available that treats the problem of splicing together two or more separate sandwich panels.

Mallon and Beck [1] analysed the compressive behavior of a sandwich panel splice similar to that being considered here. Their report includes results of an optimization study, as well as some experimental results. However, the validity of their boundary conditions is questionable.

Some experimental work on sandwich panel splices has also been done. Lutter and Bonassar [3] present several types of laminated composite sandwich panel splices, each designed for efficiency in a particular type of loading condition. They report failure loads and theoretical efficiencies. Conclusions are drawn as to which splices show the most promise; in addition, some suggestions are made for improvement in strength and weight characteristics.

The sandwich splice being considered in the present study is geometrically similar to adhesive bonded lap joints. Goland and Reissner [2] were the first to establish analytically the load relief effect afforded by both the characteristic deformation of a lap joint under load, and an increase in overlap length. Hart-Smith [4]

later improved upon the Goland-Reissner analysis by approximating the nature of the load transfer through the adhesive layer, and including its effect upon the internal loads of the adherends. Hart-Smith also considers temperature effects and the occurrence of plasticity in both the adhesive and metal adherends. He accounts for laminated composite adherends by including a bending-extension coupling factor in the expression for adherend bending stiffness. Hart-Smith [5] also studied the double lap joint with attention to temperature, adhesive plasticity, and laminated composite adherends.

Early finite element analyses of adhesive bonded lap joints were characterized by mesh sizes that were too coarse to adequately handle the large shear stress gradients near the free edges of the overlap. A typical example is the investigation by Amijima, et al [6]. Humphreys and Herakovich [7] account for temperature and nonlinear material behavior in finite element analyses of composite adherend lap joints. Up to this point, however, no finite element analyses have accounted for the geometric nonlinearity which is characteristic of the lap joint problem. This nonlinearity is caused by the interdependence of the bending moment and deflection due to inplane loads.

Cooper and Sawyer [8] have examined the effects of geometric nonlinearity in both finite element and finite difference analyses of single lap joints. They investigate the stress distributions through the adhesive and adherend thicknesses. Previous studies are typified by the analysis of stress distributions along the adhesive centerline only.

Chapter 3

ELASTIC AXIS BEAM MODEL

3.1 General Description

A two-dimensional plate bending model was developed to study the effects of various parameters such as overlap length, gap width, load level, and core and plate stiffnesses upon the behavior of sandwich plate joints subjected to in-plane loads. The model assumes unidirectional beam bending of the face-sheets with an axial end load, and a distributed transverse load provided by an elastic core. The result is a fourth-order differential equation of equilibrium that describes the face-sheet deflection. Solutions from this model provide the transverse face-sheet deflections, and values of internal moments and shears at either end of the overlap.

The sandwich panel splice, simplified through symmetry conditions (Fig. 2) is divided into three separate regions (I, II, and III). The elastic axes of the three regions are discontinuous at the two junctions between the regions. Regions I and II are both modeled as a plate on an elastic foundation, while region III has no elastic foundation, since it represents half of the gap between the two spliced sandwich panels. The elastic axis model is shown in Figure 3, complete with characteristic lengths.

The three elastic axis regions can be replaced by a single continuous axis with applied moments occurring at the locations of the axis offsets at the region junctions. This representation is shown in

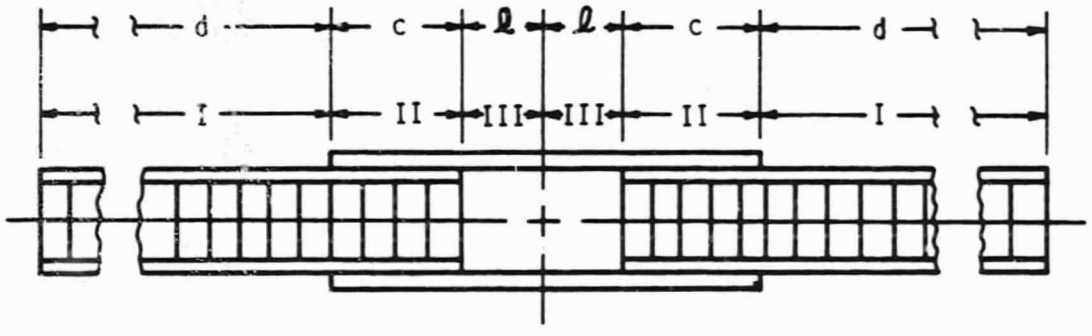

Figure 2: Sandwich Panel Splice (Side View)

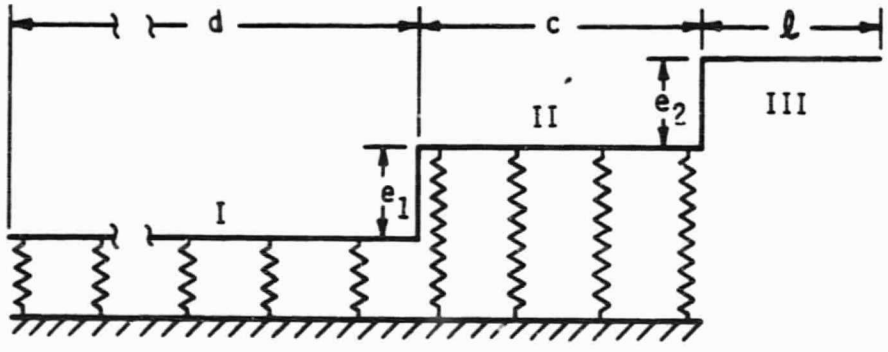

Figure 3: Discontinuous Elastic Axis Representation

Figure 4, with regional coordinate systems and support conditions at each end of the model structure.

The symbols x_i and z_i represent the longitudinal and transverse coordinates for region i, while w_i is the transverse deflection of the elastic axis in region i.

The plate bending equation is written in each of the three regions. In each region, there is a plate bending stiffness and four boundary conditions. Three of the boundary conditions at each junction represent continuity of deflection, slope, and shear. The fourth boundary condition required at each junction accounts for the prescribed elastic axis offsets. These offsets, and the fact that axial loading is present, cause discontinuities or jumps in the internal bending moments of the plates. To solve for the deflection in each region, it is necessary to join together the three separate solutions to the bending equation. The method of analyzing the three solution regions and of defining the elastic axis offsets as jumps in the plates' internal moments is adapted from that used by Mallon and Beck (Ref. 1).

The boundary conditions form a system of simultaneous linear algebraic equations. The unknowns are the undetermined constant coefficients in the deflection solutions to the three separate fourth-order differential equations of bending. Because of the size of the system of boundary condition equations, a closed-form solution for the equation coefficients is not practical. Therefore, a digital computer program was developed to obtain numerical solutions for the coefficients for a range of axial loads. A detailed development of the system

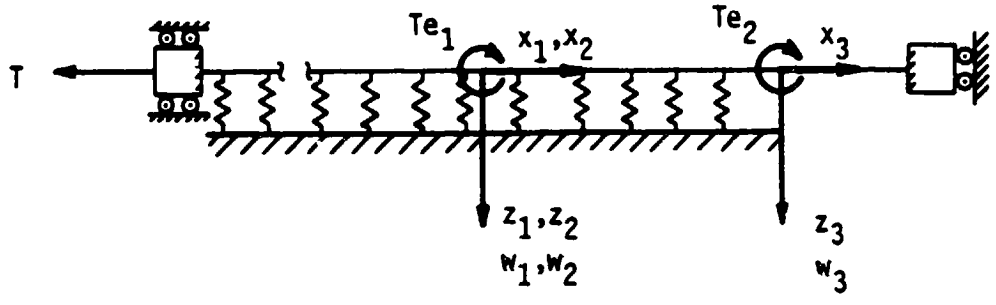

Figure 4: Continuous Elastic Axis Representation

of boundary condition equations follows in the next section.

3.2 Development of Analytical Model

The governing equations for the analytical model consist of a set of fourth-order differential equations for plates under unidirectional bending and axial edge-loads, with a distributed transverse load due to the elastic foundation. The basic equation is:

$$D \frac{d^4w}{dx^4} - T \frac{d^2w}{dx^2} + kw = 0, \tag{1}$$

where D is the plate bending stiffness, T is the applied edge-load (tension positive), and k is the elastic foundation stiffness of the sandwich core. Dividing equation (1) by the plate bending stiffness yields,

$$\frac{d^4w}{dx^4} - \alpha \frac{d^2w}{dx^2} + \beta w = 0, \tag{2}$$

where

$$\alpha = \frac{T}{D},$$

and

$$\beta = \frac{k}{D}. \tag{3}$$

Considering the characteristic equation of equation (2)

$$m^4 - \alpha m^2 + \beta = 0 \tag{4}$$

it is found that

$$m^2 = \frac{\alpha}{2} \pm \sqrt{\left(\frac{\alpha}{2}\right)^2 - \beta} \tag{5}$$

Since β is always greater than or equal to zero, three solution types are possible depending upon the sign of the term under the radical in Eqn. (5). These are:

(1) $(\frac{\alpha}{2})^2 < \beta$, complex m^2 (low in-plane load level)

(2) $(\frac{\alpha}{2})^2 = \beta$, repeated m^2 (transition between low load level and high load level)

(3) $(\frac{\alpha}{2})^2 > \beta$, real m^2 (high in-plane load level).

The above references to "low" and "high" load level are used to distinguish between the solution cases that occur depending upon the magnitude of α in comparison to β.

The low load level solution is as follows:

$$w(x) = C_1 e^{Rx}\cos(Ix) + C_2 e^{-Rx}\cos(Ix) + C_3 e^{Rx}\sin(Ix) + C_4 e^{-Rx}\sin(Ix) \tag{6}$$

where

$$R = \sqrt{\frac{\alpha}{4} + \sqrt{\frac{\beta}{4}}}$$

and (7)

$$I = \sqrt{\sqrt{\frac{\beta}{4}} - \frac{\alpha}{4}}\,.$$

R and I are, respectively, the real and imaginary parts of the roots,

$$m = \pm (R \pm Ii).$$

For low load level, there is no distinction between the solution forms for tension and compression.

The high load level case has two special subcases - one for a nonzero β and one for a zero β. The non-zero β case has two separate

forms for tension and for compression. These are:

TENSION ($\alpha > 0$)

$$w(x) = C_1 e^{m_1 x} + C_2 e^{-m_1 x} + C_3 e^{m_2 x} + C_4 e^{-m_2 x} \tag{8}$$

$$m_1 = \sqrt{\frac{\alpha}{2} + \sqrt{\left(\frac{\alpha}{2}\right)^2 - \beta}}$$

$$m_2 = \sqrt{\frac{\alpha}{2} - \sqrt{\left(\frac{\alpha}{2}\right)^2 - \beta}}$$

COMPRESSION ($\alpha < 0$)

$$w(x) = C_1 \cos(m_1 x) + C_2 \sin(m_1 x) + C_3 \cos(m_2 x) + C_4 \sin(m_2 x) \tag{9}$$

$$m_1 = \sqrt{-\frac{\alpha}{2} - \sqrt{\left(\frac{\alpha}{2}\right)^2 - \beta}}$$

$$m_2 = \sqrt{-\frac{\alpha}{2} + \sqrt{\left(\frac{\alpha}{2}\right)^2 - \beta}}$$

The special case of a zero β applies to region III of the elastic axis model and corresponds to a plate without an elastic foundation. The governing equation becomes

$$\frac{d^4 w}{dx^4} - \alpha \frac{d^2 w}{dx^2} = 0 \tag{10}$$

The solution forms for this case are:

TENSION ($\alpha > 0$)

$$w(x) = C_1 + C_2 x + C_3 e^{\sqrt{\alpha}\, x} + C_4 e^{-\sqrt{\alpha}\, x} \tag{11}$$

COMPRESSION ($\alpha < 0$)

$$w(x) = C_1 + C_2 x + C_3 \cos(\sqrt{-\alpha}\, x) + C_4 \sin(\sqrt{-\alpha}\, x) \qquad (12)$$

The other solution case, the case where $(\frac{\alpha}{2})^2$ is equal to β, is the transition point between the low and high load level solution cases. This case is not considered in detail since it appears to be of little significance. This point becomes somewhat important for the compressive stability of a pinned-pinned plate/column on an elastic foundation. The edge-load at the transition point is close to, though still below, the critical buckling load in certain ranges of elastic foundation stiffness. As the stiffness of the elastic foundation is increased, the compressive edge-load at this point assymptotically approaches, from below, the critical buckling load. However, for clamped-clamped boundary conditions, which are the conditions for face sheets of the sandwich panel splice, bifurcation points exist well within the high load level regime only.

There are twelve boundary conditions necessary to define the model as depicted in Figure 4. Certain of these boundary conditions are dependent upon the assumption that the slopes of the elastic axes at their two junctions are small. These particular boundary conditions are the ones of equal deflections at the junctions of the elastic axes.

Considering the first junction between regions I and II (Figure 5), it is seen that the rigid junction must rotate to insure equal, non-zero slopes at the junction.

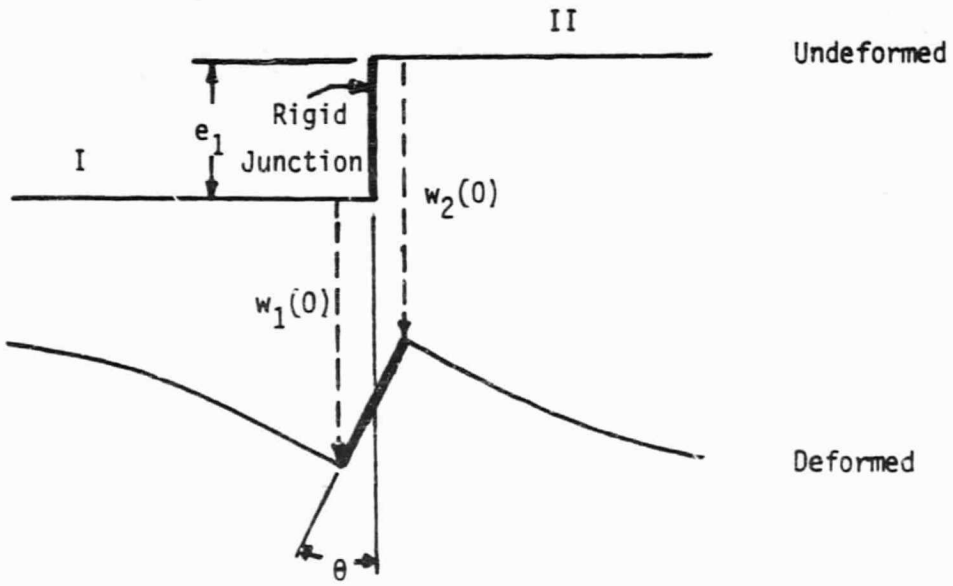

Figure 5: Deformation at the First Regional Junction

It is evident that

$$w_1(0) = w_2(0) - e_1(1 - \cos\theta)$$

For small slopes, θ is small, and $\cos\theta \simeq 1$.

Thus,

$$w_1(0) \simeq w_2(0).$$

By a similar argument, it can be shown that (refer to figure 4 for coordinate system definitions)

$$w_2(c) \simeq w_3(0).$$

If the same junction is considered in closer detail (Figure 6), it is seen that moment equilibrium requires that

$$M_1(0) = M_2(0) - Te_1$$

Similarly, for the second junction,

$$M_2(c) = M_3(0) - Te_2.$$

The boundary conditions are summarized below (refer to Figure 4 for support conditions and coordinate system definitions).

Left Hand Edge ($x_1 = -d$)

$$w_1 = 0 \qquad (13.a)$$

$$\frac{dw_1}{dx_1} = 0 \qquad (13.b)$$

First Junction ($x_1 = x_2 = 0$)

$$w_1 = w_2 \qquad (13.c)$$

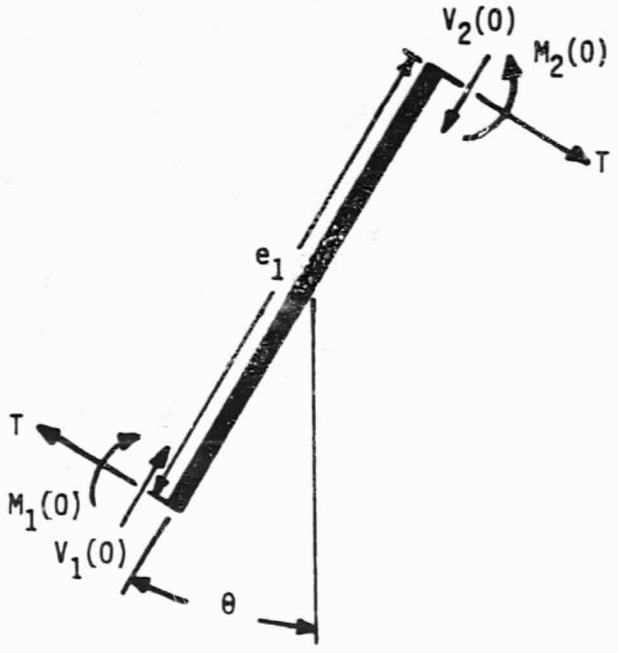

Figure 6: Loads and Rotation at the First Regional Junction

$$\frac{dw_1}{dx_1} = \frac{dw_2}{dx_2} \tag{13.d}$$

$$M_1 = M_2 - Te_1$$

or

$$D_1 \frac{d^2w_1}{dx_1^2} = D_2 \frac{d^2w_2}{dx_2^3} + Te_1 \tag{13.e}$$

$$V_1 = V_2$$

or

$$D_1 \frac{d^2w_1}{dx_1^3} = D_2 \frac{d^3w_2}{dx_2^3} \tag{13.f}$$

Second Junction ($x_2 = c$, $x_3 = 0$)

$$w_2 = w_3 \tag{13.g}$$

$$\frac{dw_2}{dx_2} = \frac{dw_3}{dx_3} \tag{13.h}$$

$$M_2 = M_3 - Te_2$$

or

$$D_2 \frac{d^2w_2}{dx_2^2} = D_3 \frac{d^2w_3}{dx_3^2} + Te_2 \tag{13.i}$$

$$V_2 = V_3$$

or

$$D_2 \frac{D^3w_2}{dx_2^3} = D_3 \frac{d^3w_3}{dx_3^3} \tag{13.j}$$

At $x_3 = \ell$,

$$\frac{dw_3}{dx_3} = 0 \tag{13.k}$$

$$V_3 = 0$$

or

$$\frac{d^3w_3}{dx_3^3} = 0 \tag{13.l}$$

3.3 Discussion of Analytical Model

This analytical model has several features in common with the Goland-Reissner, single lap-joint analysis of Reference 4. Like part I of the Goland-Reissner analysis, this analysis provides solutions for transverse deflections, and values of internal moment and shear at either end of the overlap. And like the initial Goland-Reissner solution, the present solution cannot account for axial deformation, shear flexibility or plasticity in the adhesive layer between the face sheet and doubler. As a result, the present model is somewhat stiffer than a more detailed analytical model. This fact has been demonstrated by Hart-Smith (Refs. 4,5) in his lap joint analyses.

Despite some deficiencies of the present model, it accounts for the presence of a continuous elastic support, and has relative analytical and computational simplicity. The advantages of simplicity are a necessity, because of the complications caused by the elastic foundation and by the boundary conditions of this problem. Both

features necessitate the use of the full fourth-order form of the bending equation. In the lap joint analyses, the simpler structure permits the use of a second order form of the bending equation.

Goland and Reissner, and Hart-Smith, do not explicitly define how their lap joint models are restrained. However, Figure 7a illustrates the physical supports that are compatible with their analyses.

The simply supported lap joint can be considered as a two-force member, thus allowing the convenience of an incline line of action, as shown in Figure 7b. In the case of the present analysis, these conditions are inappropriate. As is evident from Figure 4, the right hand end of the sandwich panel splice (the center of the doubler) is free to move vertically with a non-zero moment, while the shear and slope at this point are necessarily zero. These conditions require the direction of the load at the right-hand end to be horizontal, prohibiting the definition of a line of action.

a: Simply Supported Single Lap Joint

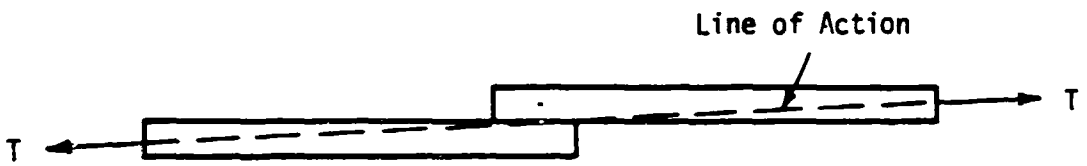

b: Single Lap Joint as a Two-Force Member

Figure 7: Single Lap Joint

Chapter 4

FINITE ELEMENT MODEL

The SPAR finite element program, described in reference 9, was also used to analyze the present sandwich splice problem. The two-dimensional finite element mesh used, shown in Figure 8, includes both triangular and quadrilateral membrane elements. A very fine mesh was used at the ends of the overlap region where lap joint analyses have shown the existence of large stress gradients. Each ply of the laminated face-sheet and doubler is modeled individually. Because of the difficulties involved in altering the mesh geometry, only the 8-ply laminate and two overlap lengths were studied. The constraints and applied loads on the model structure are illustrated in Figure 9.

As in the case of a lap joint, the internal loads and the deformation of the splice are interdependent, thus making the problem geometrically nonlinear. The nonlinear behavior is approximated in the SPAR analysis through a geometric (or initial stress) stiffness matrix iteration. This is accomplished by first obtaining a linear solution and then computing the associated geometric stiffness matrix; this matrix is then added to the initial stiffness matrix. The analysis is repeated with the modified stiffness matrix. Previous experience with this method of approximating geometrically nonlinear behavior in single lap joints has shown that convergence is rapid (Reference 8).

SPAR output includes stresses at the element centroids. The

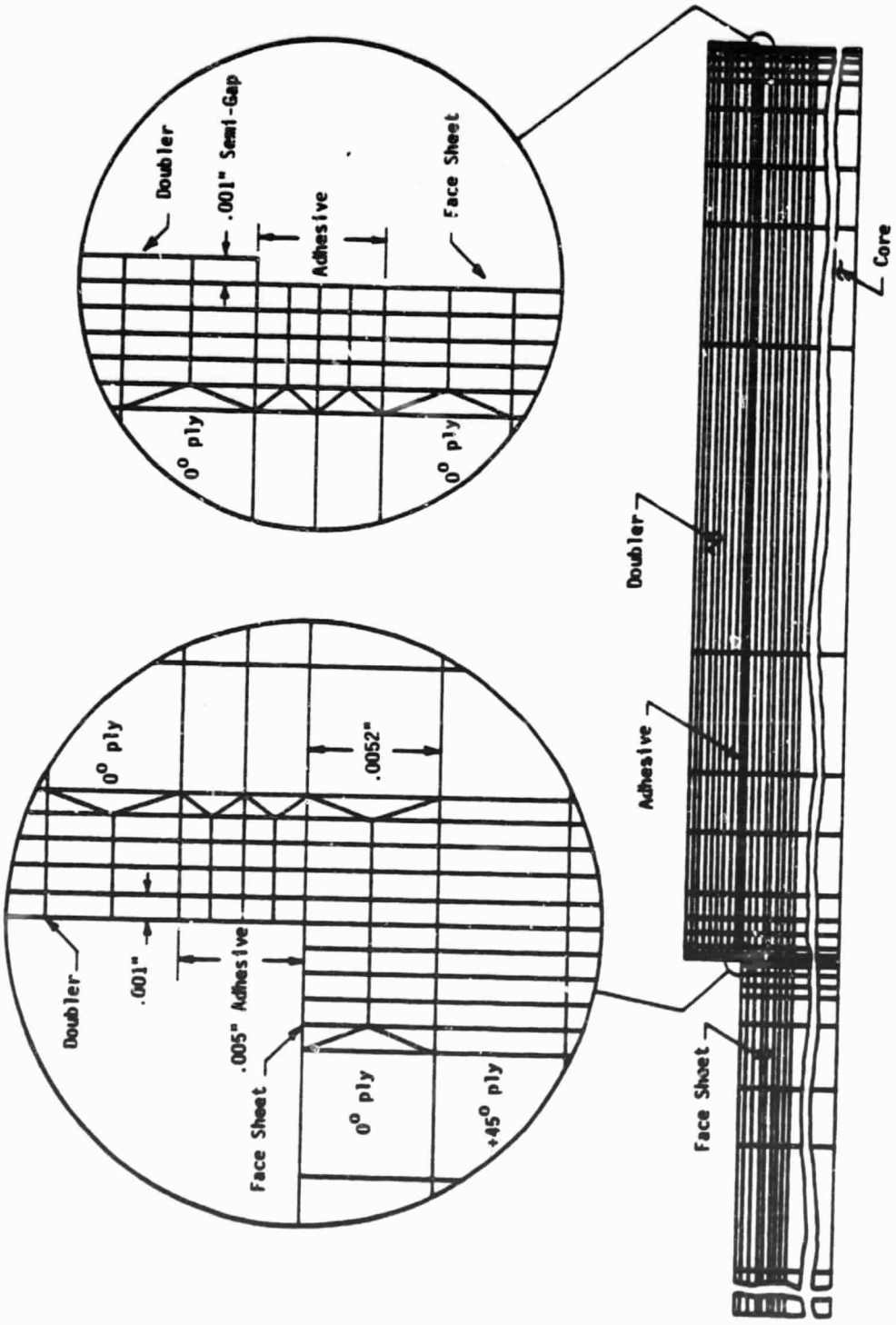

Figure 8: SPAR Finite Element Mesh of the Overlap Region of a Sandwich Panel Splice

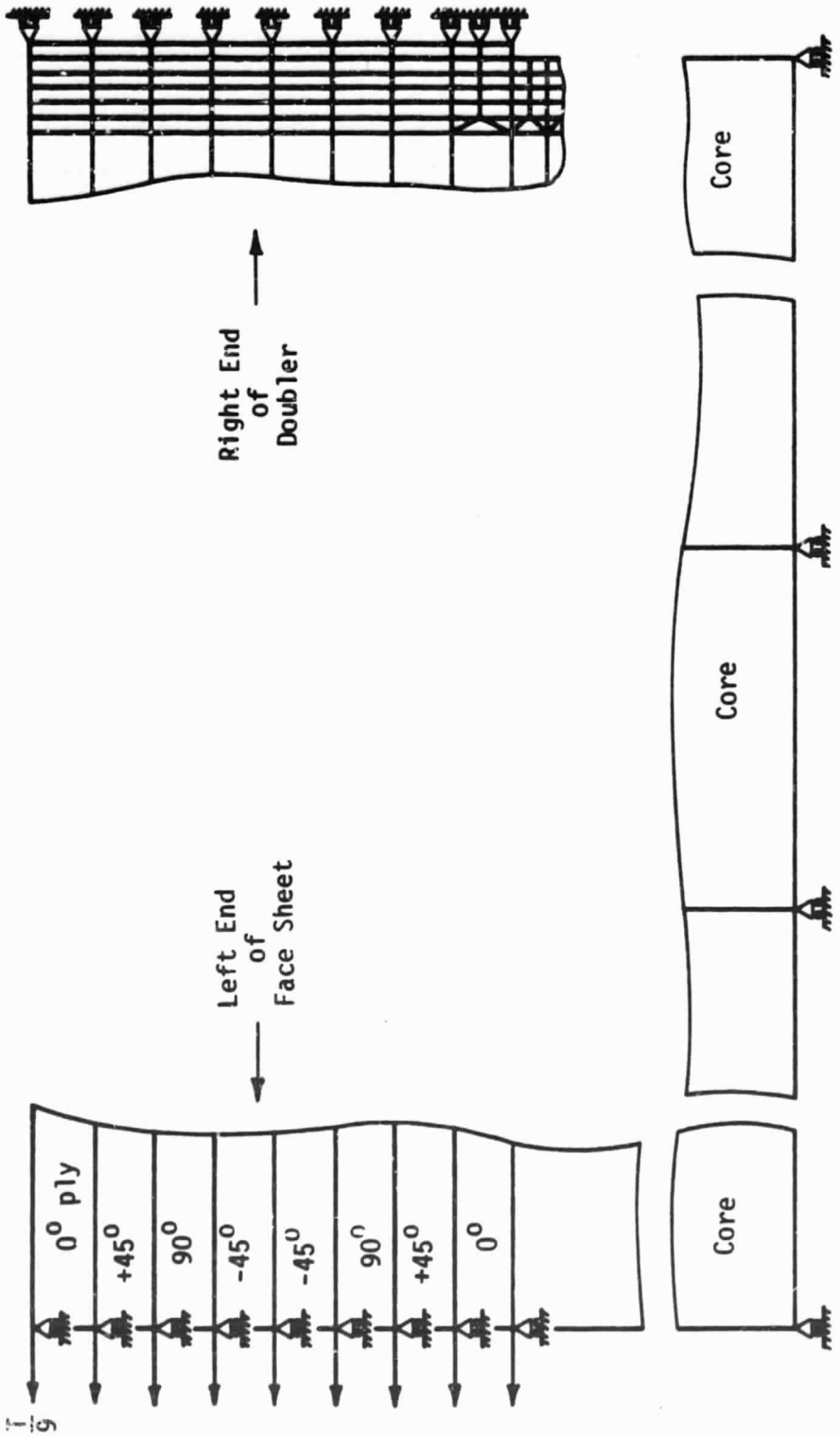

Figure 9: Finite Element Model Constraints and Applied Loads

distribution of these stresses in the overlap region was studied, as well as the face sheet and doubler internal loads at the overlap ends. The internal loads (moment and shear) were calculated from the stresses in elements just outside of the overlap with the following equations:

$$\text{Moment,} \quad M = \sum_{i=1}^{9} \bar{z}_i \sigma_{xi} t_i \tag{14}$$

$$\text{Shear,} \quad V = \sum_{i=1}^{9} \tau_{xzi} t_i \tag{15}$$

The quantities in the above equations are defined for the face sheet in Figure 10.

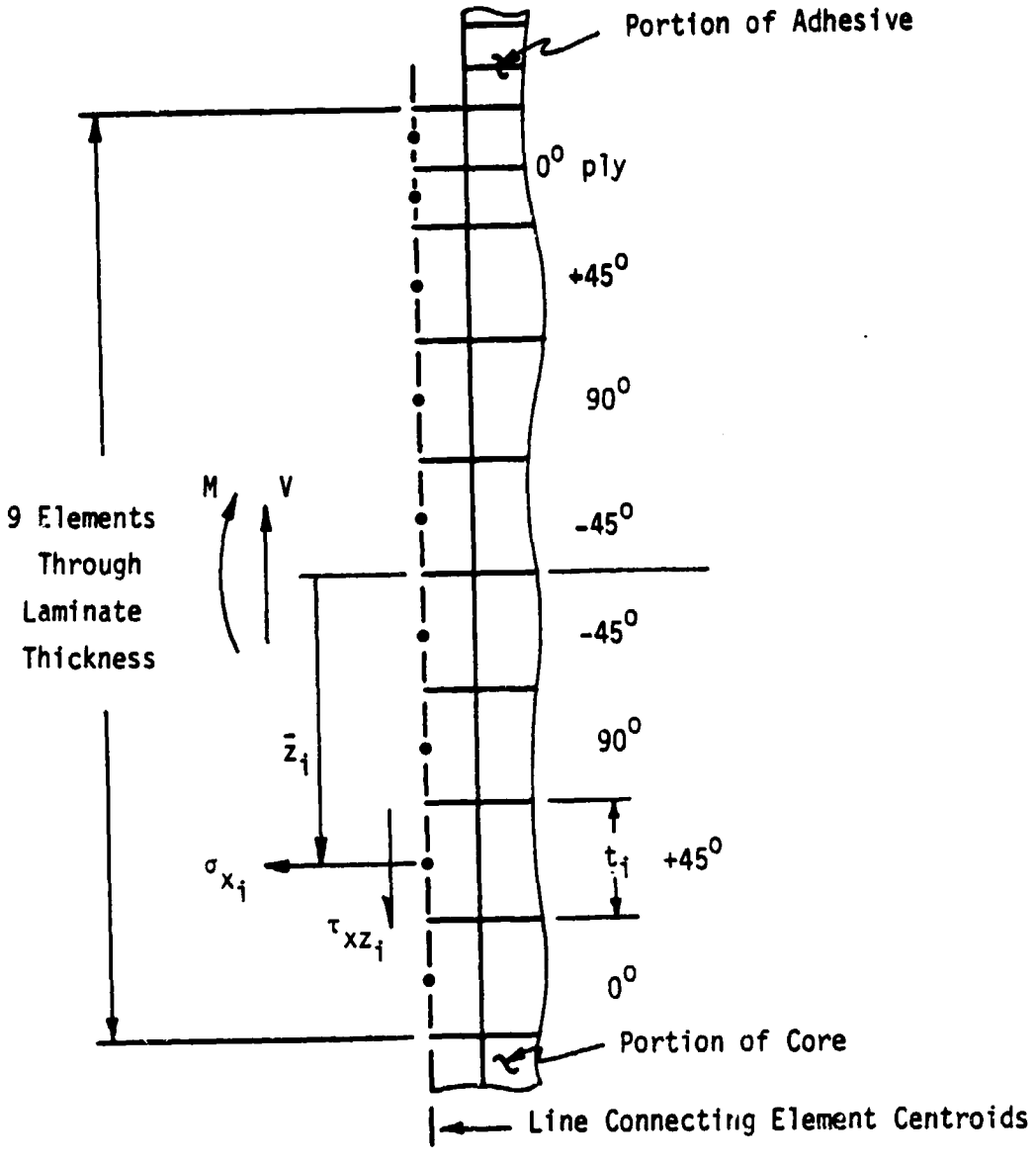

Figure 10: Definition of Quantities in Equations 13 and 14 for the Face Sheet

Chapter 5

EXPERIMENTAL PROGRAM

5.1 Test Specimens and Special Equipment

Drawings of typical test specimens are shown in Figures 11.a and 11.b. The doublers, face sheets, and load tab padups are made from Celion 6000/PMR-15 (Graphite/Polyimide) laminates. The core is HEXEL HRH-327-316-4.0, Glass/Polyimide honeycomb with a density of 4.0 lbs/ft^3. The core filler, or "potting" material, is BR34B. The face sheets and core are bonded together with FM-34 adhesive and the doublers and padups are bonded together with LARC-13 adhesive.

The general procedure used by Rockwell International to fabricate the test specimens is diagrammed in Figure 12. The laminate material provides the face sheets, doublers, and load tab padups for five specimens. When the individual specimens were cut from the larger fabricated sandwich panel, the best three specimens, as evaluated through an ultrasonic inspection technique (C-scan), were retained for testing. The excess trim material from the laminates was used by the manufacturer to measure such laminate characteristics as their volume fraction and void content.

Figure 13 depicts one of the two specimen grips designed for testing the specimens. To reduce the likelihood of a specimen failure occurring in the load tabs, the pressure plates are squeezed against the load tab padups using the pressure plate screws.

In Figure 14 is shown the general test setup. The specimens were

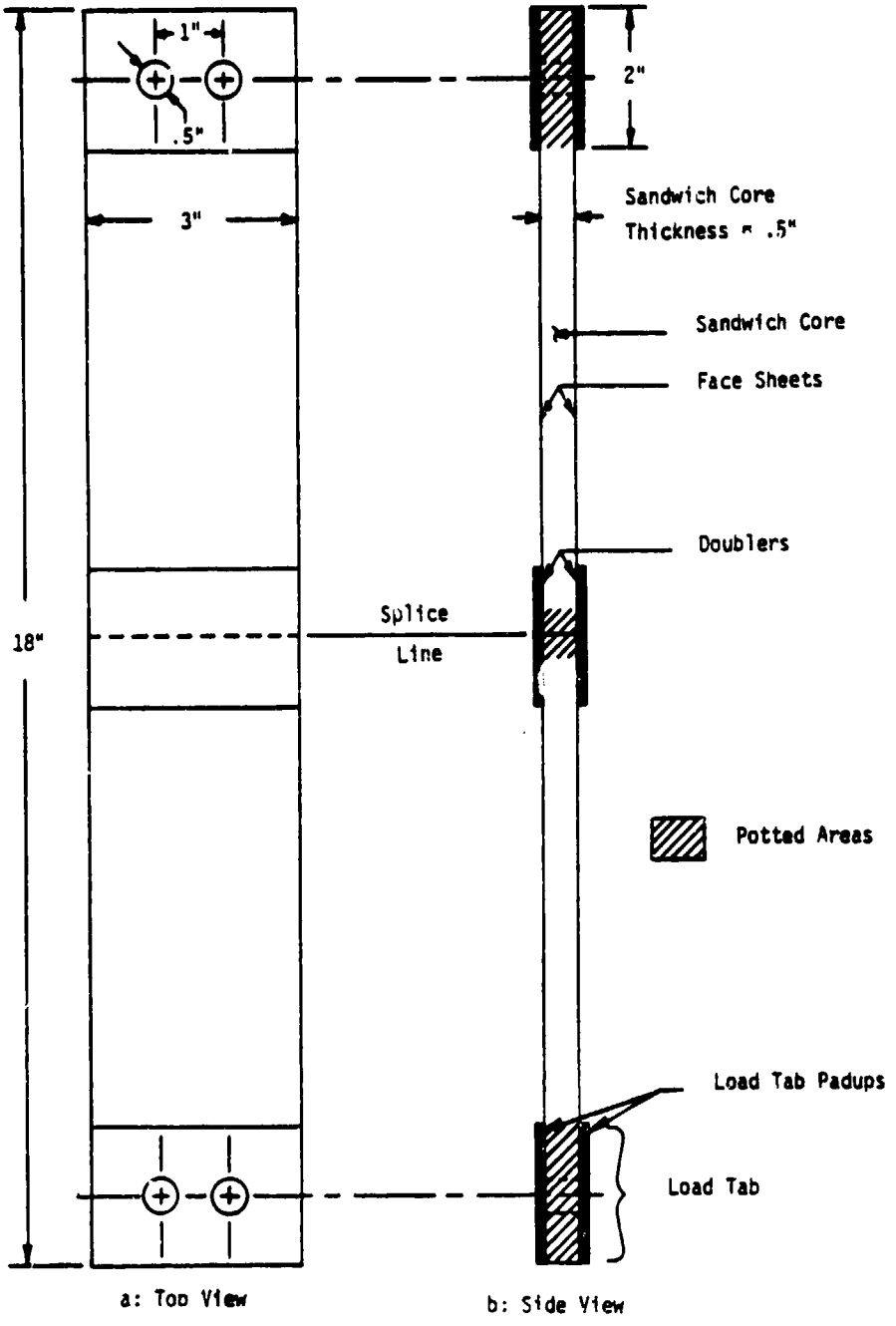

Figure 11: General Test Specimen

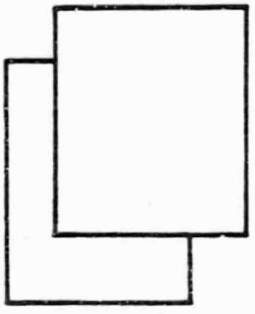

a: Fabricate Laminates A & B

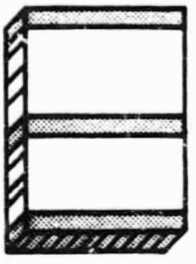

b: Pot Core

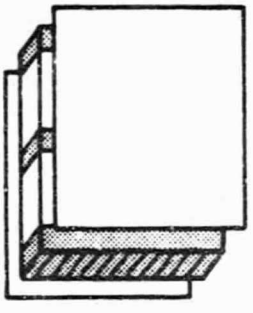

c: Bond Face Sheets, Trimmed From A & B, to Core

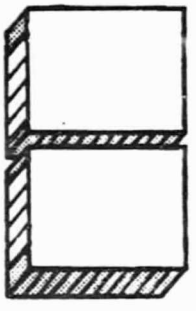

d: Cut Panel

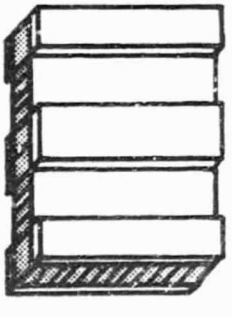

e: Bond Doublers and Load Tab Padups, Trimmed From A & B

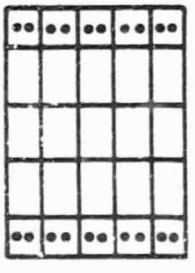

f: Cut Panel into Test Specimens and Drill Holes

Figures 12: General Specimen Fabrication Procedure

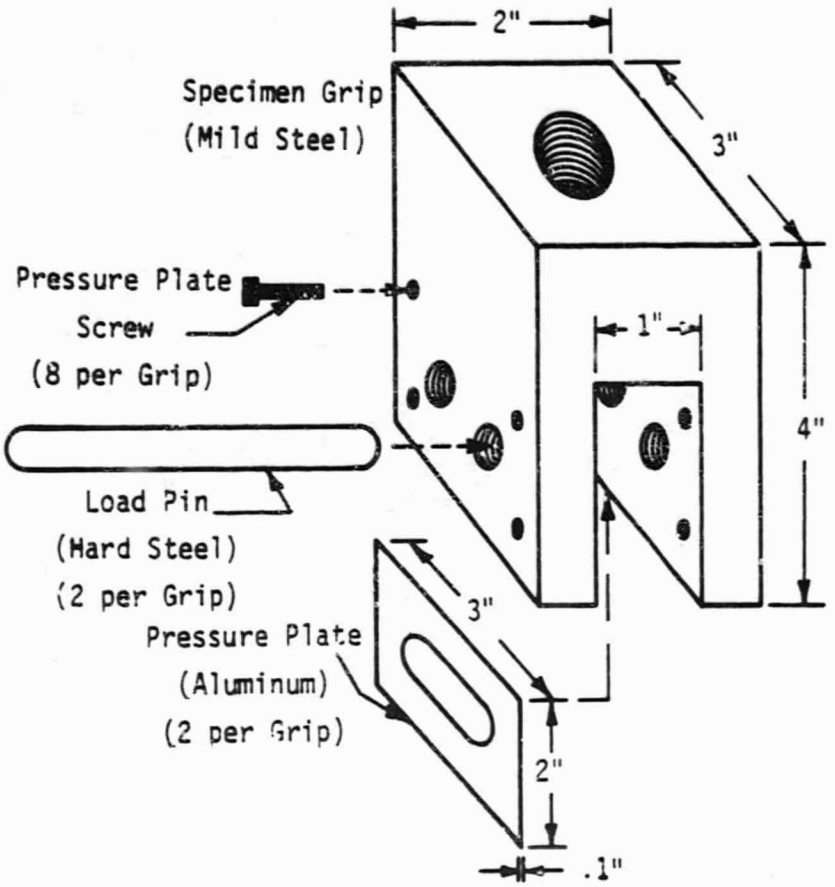

a: Specimen Grip Assembly

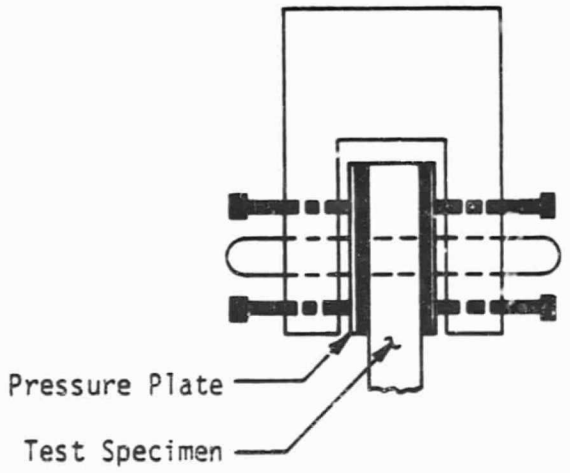

b: Specimen Mounted in Grip

Figure 13: Specimen Grip

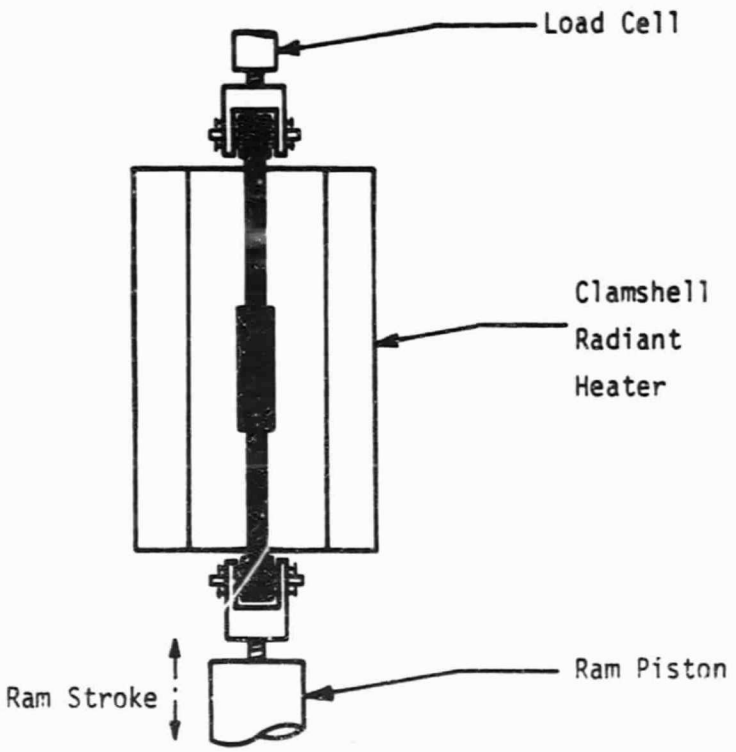

Figure 14: General Test Setup

mounted with the grips attached to the testing machine's ram piston at the bottom and to the load cell at the top. For the elevated temperature tests, a clamshell radiant heater heated the specimens to the 550°F to 600°F range. The clamshell produces heat with electrical resistance-type wire filaments.

5.2 Experimental Program

The objective of the experimental program was to test to failure several types of specimens under tension and compression loads both at room and elevated temperature. Each test provides both the failure load and mode. The specimens were made from three types of laminate and with three different doubler lengths. The laminate configurations were:

$$[0/+45/90/-45]_s,$$

$$[0_3/+45/90/-45]_s,$$

and

$$[0_5/+45/90/-45]_s.$$

The three doubler lengths are:

1.50 in.,

2.50 in.,

and

3.50 in.

The specimens fabricated for testing are tabulated in Figure 15. All three doubler lengths were used on the specimens with the 8-ply

Doubler Overlap	Laminate Type I	Laminate Type II	Laminate Type III
.75 in.	12 Specimens Fabricated	0	0
1.25 in.	12	12	12
1.75 in.	12	0	0

I - $[0/+45/90/-45]_s$

II - $[0_3/+45/90/-45]_s$

III - $[0_5/+45/90/-45]_s$

Figure 15: Test Specimen Description Matrix

laminates. The 12 and 16-ply laminate specimens were fabricated with 2.50 in. doublers only. For each particular set of test variables (loading, temperature, laminate type, and doubler length), three specimens were planned for testing. In all, a total of 60 tests were planned. However, not all the tests could be completed. This is discussed in Chapters 8 and 9.

Chapter 6

ELASTIC AXIS BEAM MODEL TENSION RESULTS

It is useful to compare the results of the elastic axis analysis of the doubler-spliced sandwich panel joint to results of single and double lap joint analyses. The splice bears a physical resemblance to both the single and double lap joints. If the elastic foundation in the elastic axis beam analysis of the sandwich splice has zero stiffness, then one might expect behavior similar to that of the single lap joint. If the foundation were rigid, then one might expect behavior similar to that of the double lap joint.

In addition to the elastic foundation, there are two other physical characteristics of this sandwich panel splice that are not included in any existing lap joint analyses. These are: the small size of the gap between the sandwich panels being spliced and the types of restraint applied to the ends of the symmetry-simplified splice. In lap joint analyses, the adherends (doublers and face-sheets) are treated as being both long and simply supported. In the case of the sandwich splice, the ends are treated as restrained against rotation.

A meaningful measure of comparison between the sandwich splice and the lap joint is the moment factor, k_{mi}, defined as (see Figure 16):

$$k_{mi} = \frac{M_i}{\overline{Te}_i} .$$

The moment factor has an intuitive appeal which makes it a good quantity for study. It is directly related to the internal moment and the load

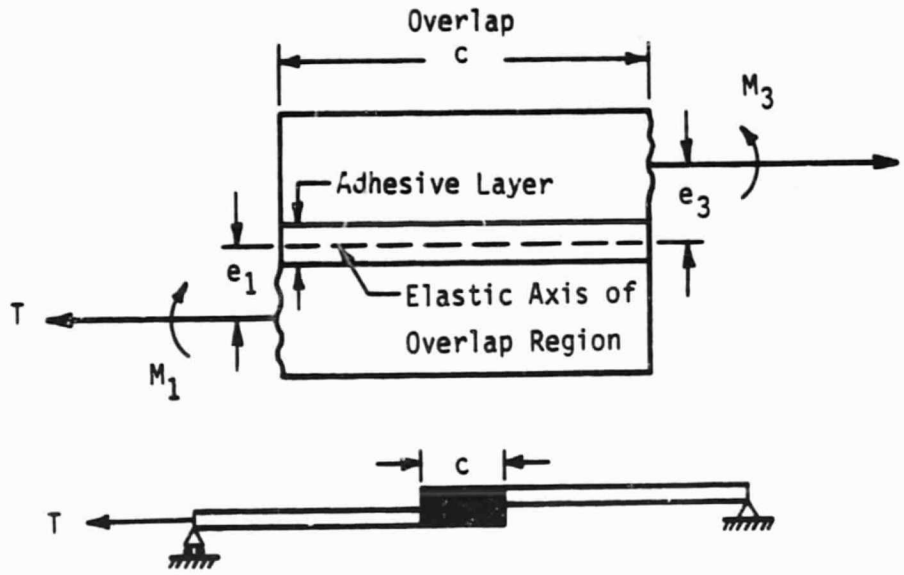

Figure 16 : Overlap Region of a
Single Lap Joint

path eccentricity characteristic of the splice. In addition, since the moment factor is related directly to the internal moment in the plates, it can be related directly to the plate curvatures.

In reference 3, the moment factor for a single lap joint is given as

$$k_m = \frac{1}{1 + \frac{D_2}{D_1} \frac{\tanh\left(\frac{c}{2}\sqrt{\frac{T}{D_2}}\right)}{\tanh\left(d\sqrt{\frac{T}{D_1}}\right)}}, \tag{16}$$

where

c is the overlap length

d is the adherend length less the overlap length

D_2 is the bending stiffness of the overlap region

and

D_1 is the bending stiffness of the adherends.

Eqn. 16 illustrates how the bending stiffnesses, overlap length, adherend length, and applied load affect the moment factor in a balanced single lap joint. Typically, the adherend length, applied load, and bending stiffnesses are such that eqn. 16 can be simplified to

$$k_m = \frac{1}{1 + \frac{D_2}{D_1} \tanh\left(\frac{c}{2}\sqrt{\frac{T}{D_2}}\right)}. \tag{17}$$

That is, d and T are large enough to make the term $\tanh\left(d\sqrt{\frac{T}{D_1}}\right)$ nearly equal to unity. This leaves k_m to be primarily a function of the parameter $\frac{c}{2}\sqrt{\frac{T}{D_2}}$. However, if d and T are not sufficiently large,

the moment factor becomes a much more complicated function of the quantities defining a single lap joint subjected to load. In this latter case, it would be necessary to evaluate eqn. 16 to find the moment factor.

It is important to note two aspects of eqn. 16. One is the fact that the moment factor approaches zero as adherend length, d, approaches zero. This limit occurs because the adherend ends are simply supported. When d is zero, the pin supports are at the overlap edges requiring zero moments there. But, this effect of shortening the adherends illustrates that the adherend boundary conditions can strongly affect the adherend moment factor at the overlap edges when the boundaries are in the near vicinity of the overlap.

The other aspect of eqn. 16 is the fact that it was derived for a lap joint model whose two adherends were identical in length and stiffness. This restriction permits considerable analytical simplification. In general, the moment factor would be a function of <u>two</u> adherend lengths as well as overlap length, two bending stiffnesses, and load level. The moment factor will also be different for the two overlap edges.

Similarly, the sandwich splice model has two adherend dimensions. These are the length of the sandwich panel face sheet and half of the gap between the sandwich panels. But, in contrast, the sandwich panel splice has zero rotation boundary conditions discussed previously. Also, the sandwich splice model has an elastic foundation. Thus, the moment factors at the overlap edges are a complicated function of

face sheet, gap, and overlap lengths, laminate bending stiffnesses, elastic foundation stiffness, and load level. This, in turn, makes any attempt at a comprehensive parametric study impractical. However, the face sheet length in a typical sandwich splice would likely be larger than either the overlap length or the gap length. So, in view of the small influence of long adherends on the moment factors in a lap joint, the assumption that a large face sheet length has little influence on the sandwich splice moment factors is reasonable. This leaves overlap and gap lengths, laminate bending stiffnesses, elastic foundation stiffness, and load level as parameters.

To further isolate parameters in some sort of natural grouping, one can consider the differential equation of plate bending for the overlap region. The characteristic values of this equation are given in general form by eqn. 5 as

$$m_2^2 = \frac{\alpha 2}{2} \pm \sqrt{(\frac{\alpha_2}{2})^2 - \beta_2} \ .$$

But this can be rewritten as

$$m_2^2 = \frac{\alpha_2}{2} \left(1 \pm \sqrt{1 - \frac{4\beta_2}{\alpha_2^2}}\right) \ . \qquad (18)$$

Substituting for α_2 and β_2,

$$m_2 = \pm \left[\frac{T}{2D_2} \left(1 \pm \sqrt{1 - \frac{4kD_2}{T^2}}\right)\right]^{\frac{1}{2}} \qquad (19)$$

In the boundary condition equations there are terms involving $m_2 c$. This provides two parameter groupings, $c\sqrt{\frac{T}{D_2}}$ and $\frac{kD_2}{T^2}$. For the sake of

comparison with the lap joint solution, $\frac{c}{2}\sqrt{\frac{T}{D_2}}$ can be used instead of $c\sqrt{\frac{T}{D_2}}$. Also, since the second parameter, $\frac{kD_2}{T^2}$, can become large for typical values of the quantities involved, $\sqrt[4]{\frac{kD_2}{T^2}}$ becomes a convenient form for plotting purposes.

If the moment factors were solely a function of the characteristic parameters derived above, then any two dissimilar splices would have the same moment factors, provided that the characteristic parameters were also the same. This situation would mean that, for two splices, 1 and 2,

$$c_1\sqrt{\frac{T_1}{D_{2_1}}} = c_2\sqrt{\frac{T_2}{D_{2_2}}} \tag{20.a}$$

and

$$\frac{k_1 D_{2_1}}{T_1^2} = \frac{k_2 D_{2_2}}{T_2^2} . \tag{20.b}$$

Rearranging equations 20.a and 20.b in various ways yields,

$$\frac{k_1}{k_2} = (\frac{c_2}{c_1})^2(\frac{T_1}{T_2}) = (\frac{D_{2_1}}{D_{2_2}})(\frac{c_2}{c_1})^4 = (\frac{D_{2_2}}{D_{2_1}})(\frac{T_1}{T_2})^2. \tag{21}$$

If splice #1 is considered to be completely defined (that is, D_{2_1}, c_1, T_1, and k_1 are specified), then there are four unknowns and two equations involving them. The unknowns are D_{2_2} through k_2 and the equations are 20.a and 20.b. If two of the unknowns are then specified, the remaining two quantities can be obtained from convenient forms of eqn. 21.

Of course, the moment factors will not strictly be functions of the characteristic parameters associated with the overlap region alone. So, it might be useful to know if and what conditions permit the moment factors to be matched when the characteristic parameters are matched. This study was done with the computer program, VTSP, developed to solve the system of boundary condition equations (eqns. 13) for the elastic axis beam model of the splice.

To start characteristic parameter matching, it is necessary to specify two of the characteristic quantities (D_2, c, T, or k). One obvious choice is to fix one of the four quantities for both splices. Inspection of eqns. 20.a and 20.b shows that equating two quantities will force all of the quantities to be identical. While this would produce matched moment factors, it is a trivial case. Continuing with this approach, there are four fundamental cases that can be considered. Each case involves holding one of the four characteristic quantities constant and identical between splices. For each fundamental case there are three subcases which involve specifying one of the three remaining quantities as constant, but distinct between splices. The remaining two quantities are varied over a range of values while the characteristic parameters are matched between splices. In the present study, only one subcase out of each of the four fundamental cases is considered.

The values of the four characteristic quantities used in the four case studies are summarized in Table I. Bending stiffnesses were computed from lamination theory with the quantities listed in Table II.

TABLE I: DATA FOR VTSP STUDY CASES

CASE	QUANTITY	SPLICE #1	SPLICE #2
I	D_2(lb-in)	540.4	540.4
		$[0/45/90/-45]_s$ laminates	
	c(in)	0.75	1.25
	T & k	variable	variable
II	D_2	540.4 $[0/45/90/-45]_s$	2466.8 $[0_3/45/90/-45]_s$
	c	0.75	0.75
	T & k	variable	variable
III	D_2	540.4	2466.8
	c & k	variable	variable
	T(lb/in)	1000	1000
IV	D_2	540.4	2466.8
	c & T	variable	variable
	k(lb/in^3)	4000	4000

Table II

MATERIAL AND GEOMETRIC CONSTANTS

Graphite/Polyimide*

E_{11} = 19.9 Msi

$E_{22} = E_{33}$ = 1.2 Msi

$G_{12} = G_{31}$ = .604 Msi

ν_{12} = .3

ν_{23} = .5

$\alpha_1 = 2.5 \times 10^{-6}$ in/in/°F

$\alpha_2 = 14.5 \times 10^{-6}$ in/in/°F

t = .0052 in/ply

FM-34 Adhesive (assumed for LARC 13 Adhesive)**

E = 2.6 Msi

G = .46 Msi

ν = .17

$\alpha = 14.5 \times 10^{-6}$ in/in/°F

t = .005 in

Glass/Polyimide Honeycomb (4 lbs/cu. ft.)***

E_T = .001 Msi

G_{LT} = .001 Msi

$\frac{1}{2}T$ = .25 in.

* Properties obtained from several sources and averaged
** Properties obtained from Reference 14
*** Properties obtained from Reference 10

The results of the case studies will also demonstrate the nature of the dependence of the moment factors upon the four characteristic quantities.

Since there are other quantities which characterize the splice and have an influence on the results, they can be kept constant and identical between splices to avoid confusion. These quantities are: the gap lengths, the adhesive thickness, and the face sheet length. For the cases presented here, the fixed quantities used are listed below:

semi-gap length = .001 in.

adhesive thickness = .005 in. (used in determining D_2)

face sheet length = 6.75 in.

Figure 17 summarizes the results for case I. The solid lines are for splice #1 with the core stiffnesses indicated. The symbols correspond to splice #2 points with the characteristic parameters matched with those of splice #1. Matching was done only for k_1 values of 1,000, 4,000, and 50,000 lb/in^3. It can be seen that matching characteristic parameters for case I matches the moment factors very closely. The figure also shows the general influence of the core stiffness and load level upon the moment factors. That is, the face sheet moment factor varies directly with both quantities, whereas the doubler moment factor varies inversely. These results suggest that

$$k_{m_i} = k_m \left(\frac{kD_2}{T^2},\ c\sqrt{\frac{T}{D_2}},\ i\right)_{D_2 = \text{const}} \qquad (22)$$

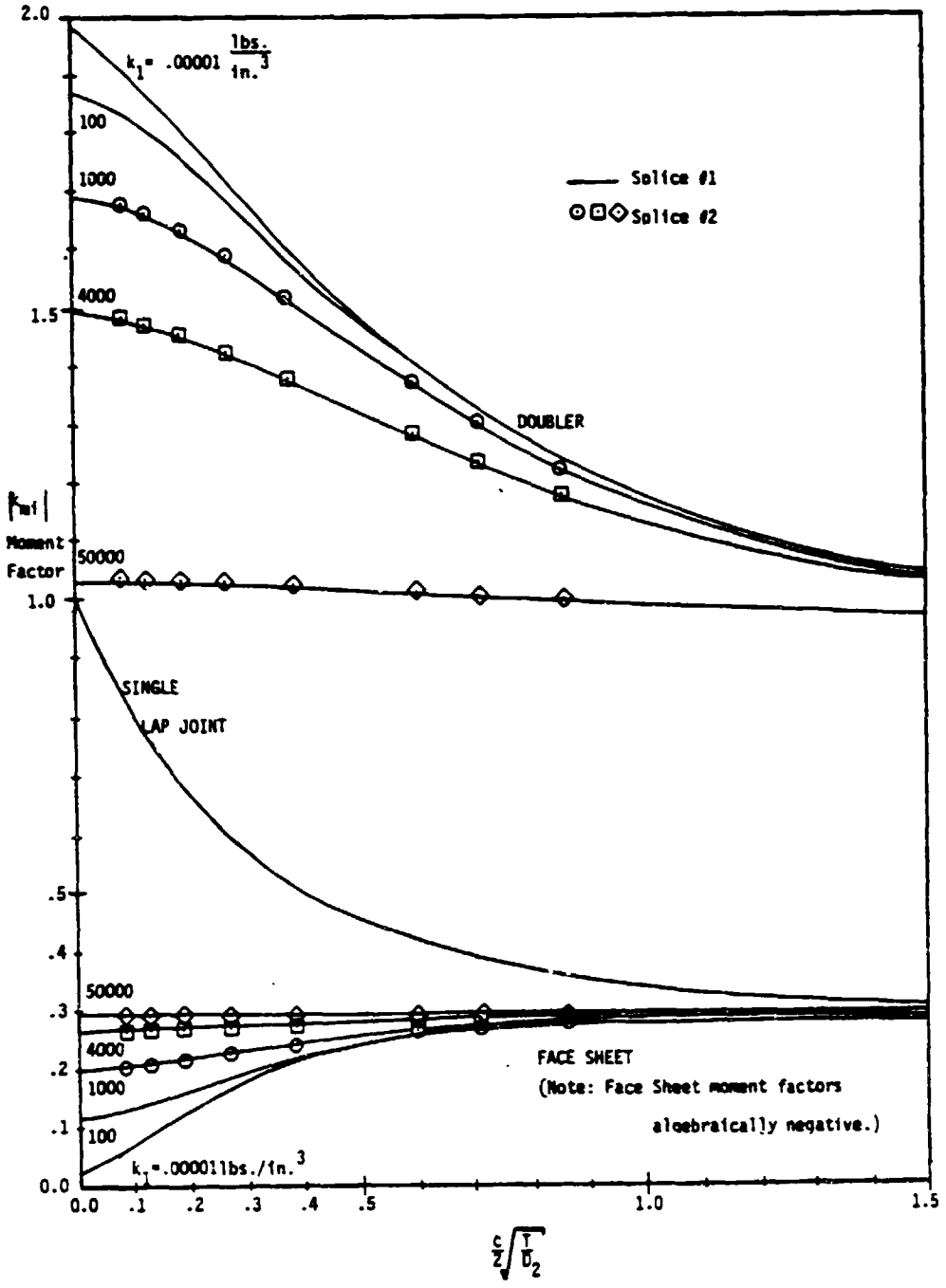

Figure 17: Moment Factor vs. $\frac{c}{2}\sqrt{\frac{T}{D_2}}$ - Case I

Figure 18 shows the results for case II. These curves were developed in the same fashion as those in case I (in fact, the splice #1 curves are identical), so the same general influences of core stiffness and load level are preserved. However, it is quite evident that case II does not permit matching moment factors by way of matching the overlap region's characteristic parameters. The figure shows that the matching deficiency is worsened by increasing core stiffness and slightly lessened by increasing load level.

The results for case III are shown in Figure 19. Case III also appears to permit moment factor matching to some degree. The curves, however, have a distinctly different shape than the curves in cases I and II. This is because the case I and II curves were developed by increasing load while the case III and IV (following) curves were developed by increasing overlap. This difference will be discussed later.

It can be seen that the general influence of the core stiffness demonstrated by cases I and II is preserved in case III. The figure also shows that the influence upon the moment factors of overlap is, for the most part, similar to that of core stiffness and load level. Case III suggests, then, that

$$k_{m_i} \simeq k_m \left(\frac{kD_2}{T^2},\ c\sqrt{\frac{T}{D_2}},\ i\right)\Big|_{T = \text{const.}} \qquad (23)$$

The case IV results are shown in Figure 20. It is evident that case IV permits moment factor matching to a certain degree with the

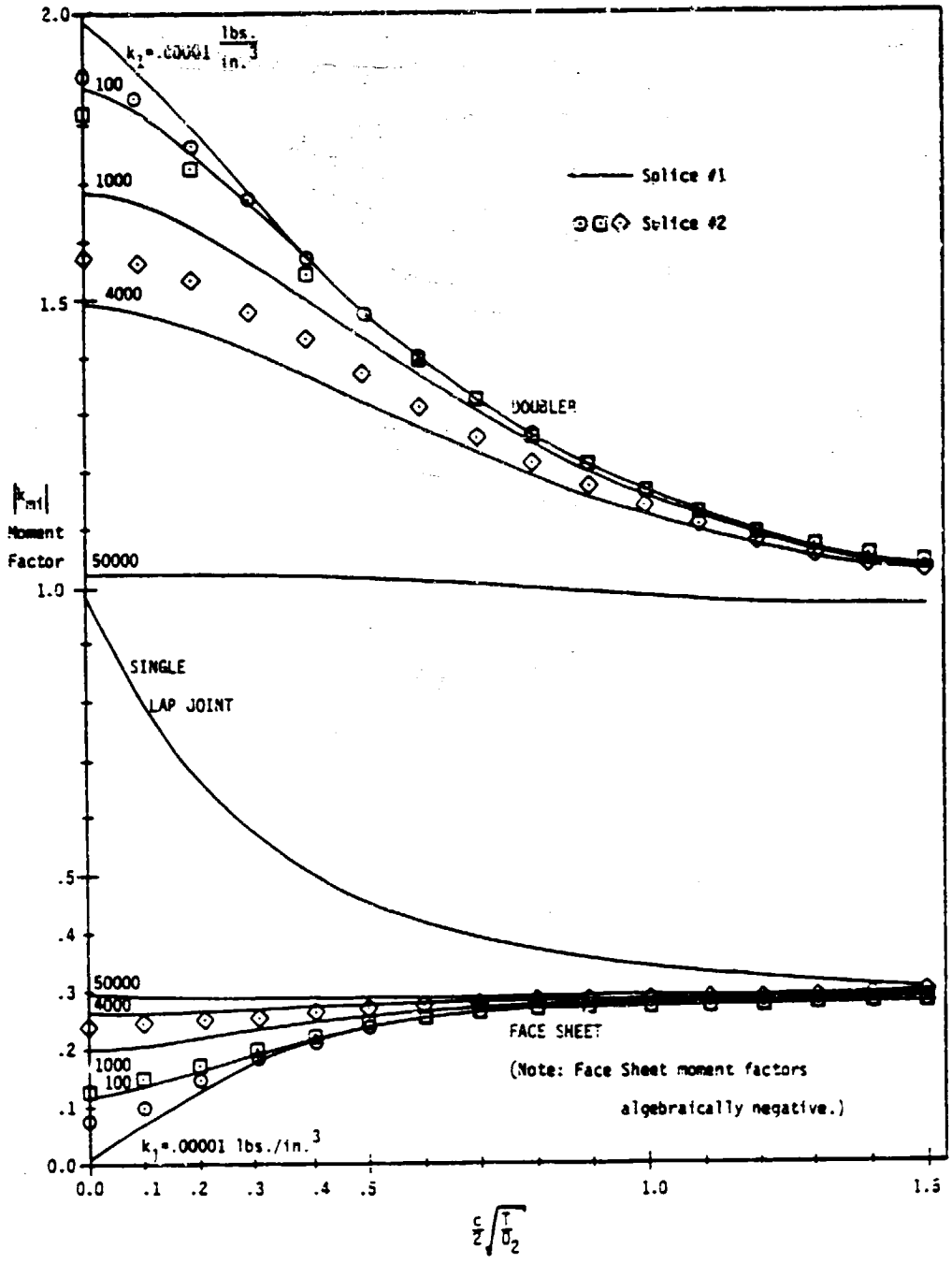

Figure 18: Moment Factor vs. $\frac{c}{2}\sqrt{\frac{T}{D_2}}$ - Case II

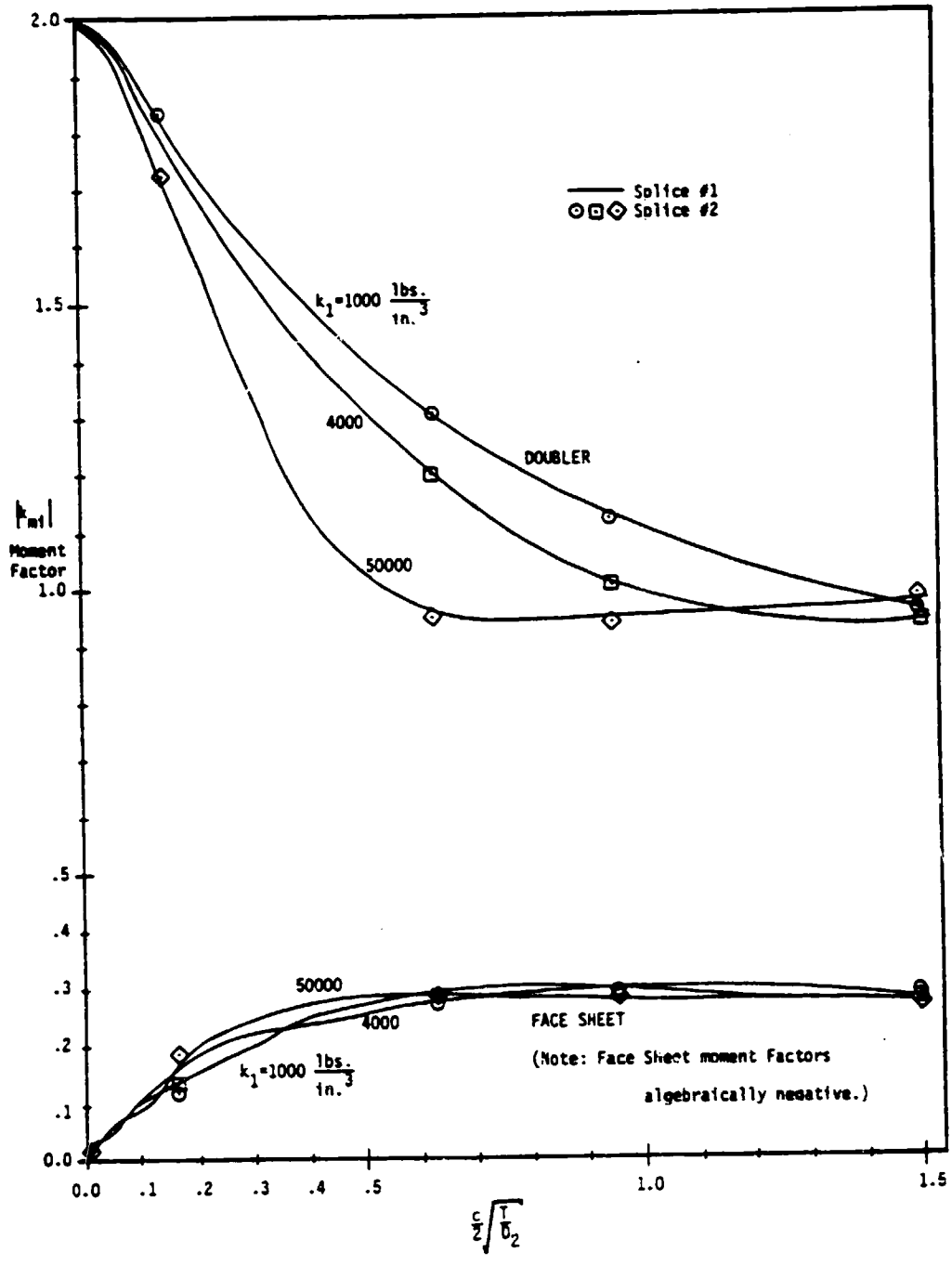

Figure 19: Moment Factor vs. $\frac{c}{2}\sqrt{\frac{T}{D_2}}$ - Case III

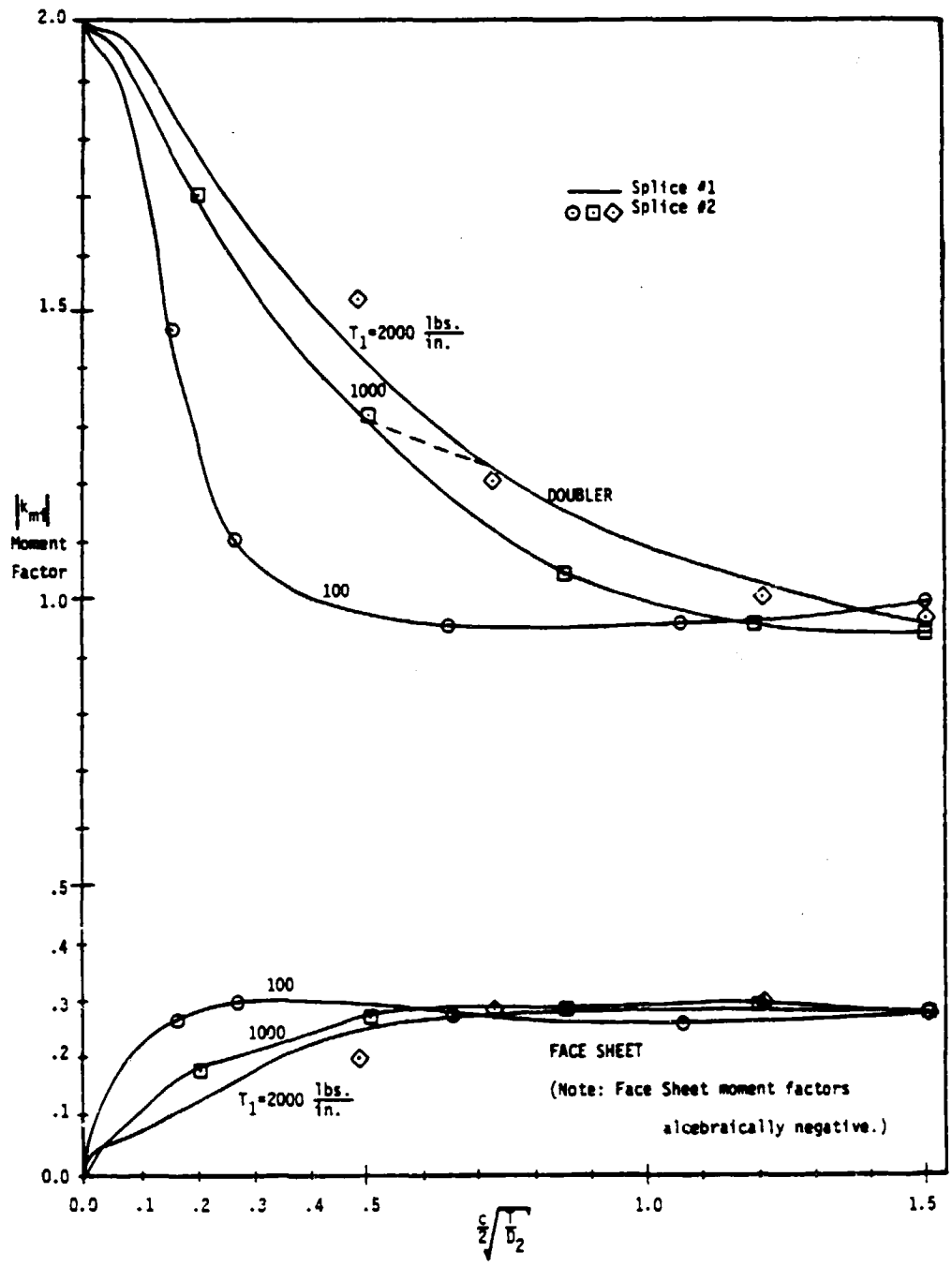

Figure 20: Moment Factor vs. $\frac{c}{2}\sqrt{\frac{T}{D_2}}$ - Case IV

matching showing deterioration for T_1 = 2000 lbs/in. The curves show the same influence of overlap previously noted. At first, it appears that the effect of load level in case IV is reversed from the effect demonstrated in cases I and II. This is a deceiving result because each curve in this set of curves can demonstrate only the effect of overlap. The dashed line is for a splice with overlap = 0.75 in., overlap bending stiffness = 540.4 lb/in., core stiffness = 4000 lb/in^3, and load level increased from 1000 to 2000 lb/in^3. The dashed line shows that the doubler moment factor is decreased by increasing load level for a given splice, which conforms to previous results. So, case IV suggests that

$$k_{m_i} \simeq k_m \left(\frac{kD_2}{T^2}, c\sqrt{\frac{T}{D_2}}, i\right|_{k = \text{const.}} \qquad (24)$$

A clearer understanding of the drastic difference between the results in cases I and II, and the results in cases III and IV can be realized by plotting the moment factors in three dimensions as a function of the characteristic parameters. Figures 21 and 22 show general "carpet" plots of the moment factors. These two figures were developed from the splice #1 curves for cases I through IV. While they may not match exactly at all points, they are quite close. Examples of this slight mismatch are shown in Figure 23. These curves were taken from cases III and IV for the indicated values of the parameter, $\sqrt[4]{\frac{kD_2}{T^2}}$. If the characteristic parameter matching were exact, the dashed lines would fall directly on the solid lines. However, the degree of mismatch is small enough to be practically insignificant.

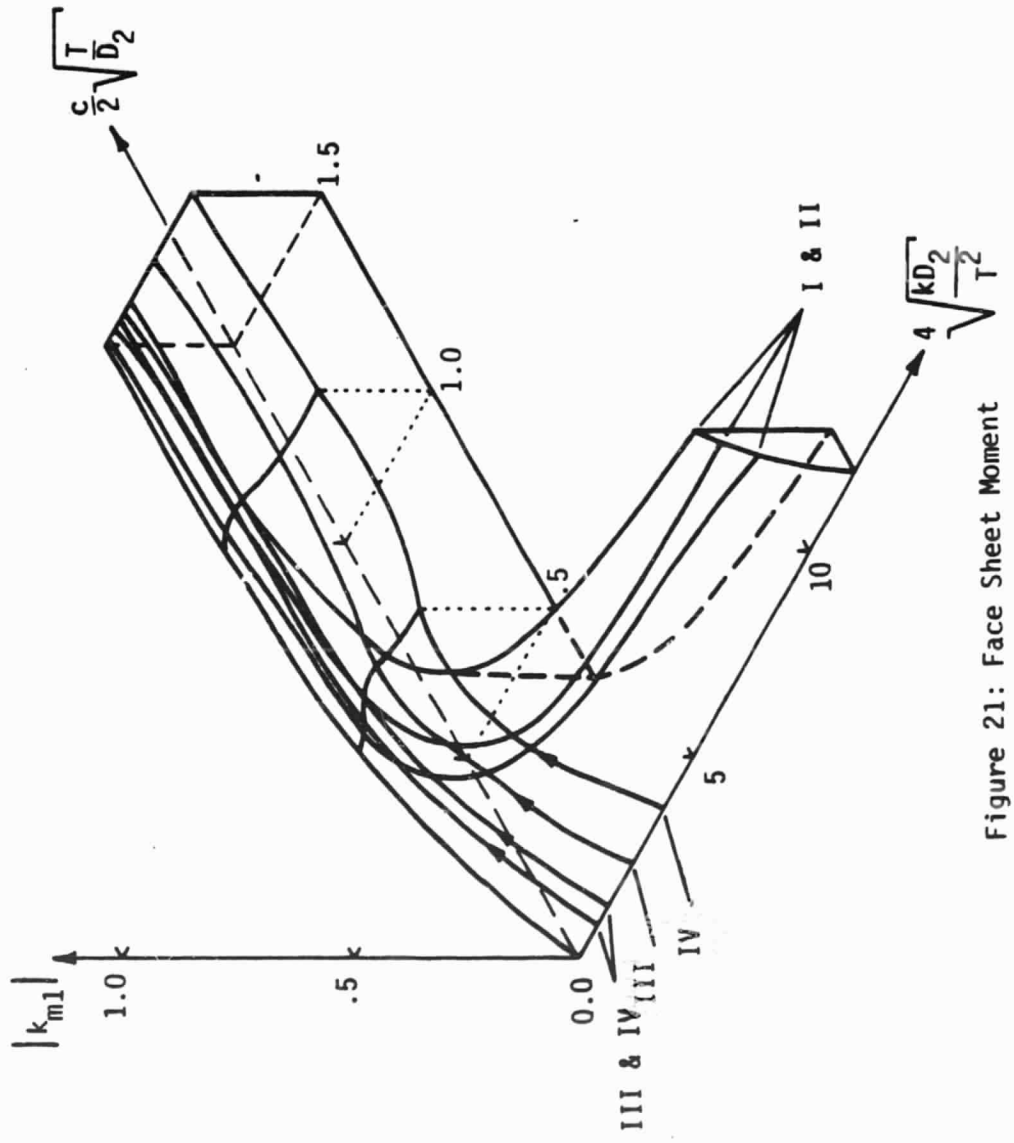

Figure 21: Face Sheet Moment Factor

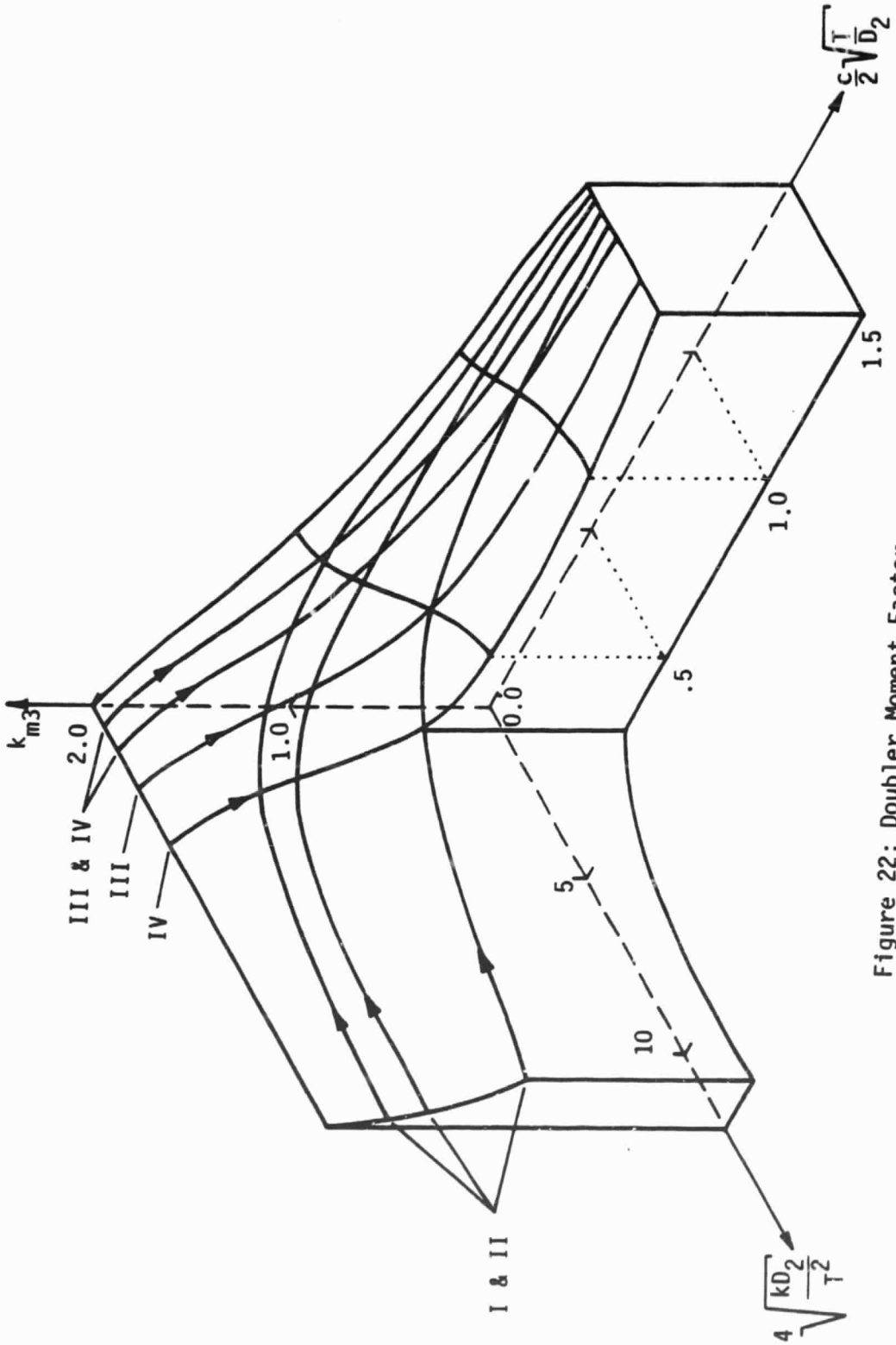

Figure 22: Doubler Moment Factor

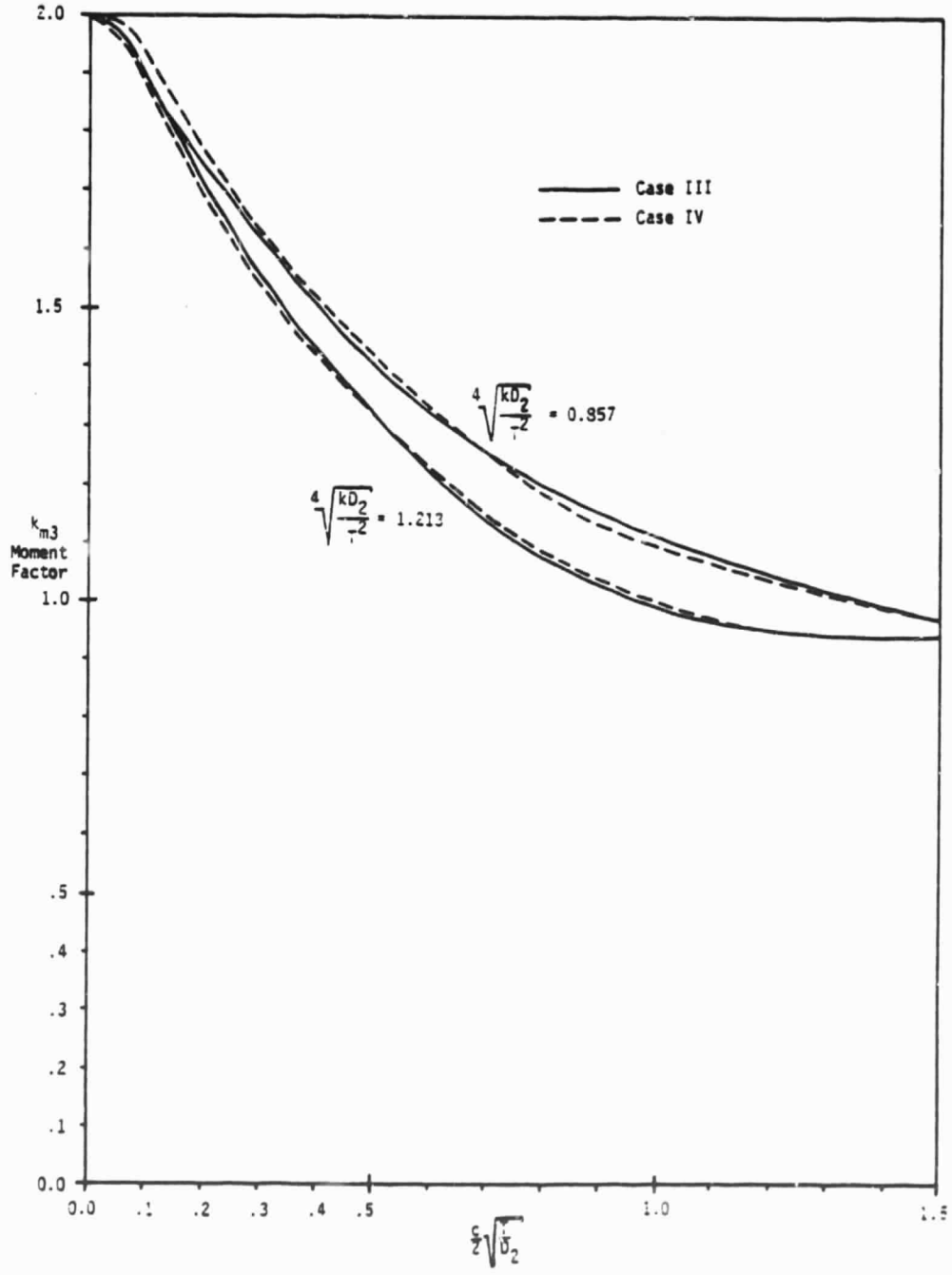

Figure 23: Typical Mismatch Between Splice #1 Curves

Figures 21 and 22 also show the paths taken by the curves in cases I through IV. These paths demonstrate why the curves in cases I and II differ in character from those of cases III and IV. In cases I and II the curves were developed by increasing load level (in the direction indicated by the arrows). Since load appears in both characteristic parameters, they are both changing as the loading path is traversed. However, the curves for cases III and IV were developed by increasing overlap (in the direction indicated by the arrows). Since overlap appears in only one characteristic parameter, the other parameter remains constant as the overlap path is traversed.

Thus far, the nature of the moment factor functions for the face sheet and doubler of an elastic-axis beam model of a sandwich panel splice have been studied. Some conditions have been found under which the moment factors are, very strongly, a function of two parameters only. These parameters were derived from the characteristic values of the differential equation governing the bending of the overlap region. They involve four quantities which characterize the splice to a large extent. These quantities are the overlap region's bending stiffness, overlap length, load level, and sandwich core stiffness. Also shown was the general influence of load level, overlap length, and core stiffness on the moment factors in the face sheet and doubler.

While the internal moments at the overlap region have been studied, nothing has been said of the internal shears. A supplementary analysis in Appendix A suggests that not only do the shears have little influence on the adhesive peel stresses, but that the gap side

of the overlap is much more critical than is the face sheet side in regard to these peel stresses. The second possible effect, suggested above, is supported by finite element and experimental results to be presented later.

A noticeable aspect of the moment factor carpet plots is the drastic difference in contour between the doubler and face sheet plots. The doubler in this sandwich splice is definitely being subjected to much more bending moment than the face sheet. As a result, the adhesive layer is subjected to a higher peel stress at the gap side of the overlap, as suggested by the analysis in Appendix A. It has been shown that the single lap joint's moment factor can be reduced toward zero by moving the simple-support boundary conditions toward the overlap edges. This suggests that, because the zero rotation boundary condition on the doubler at the gap center is so close to the gap side of the overlap, the doubler will always be subjected to a greater internal moment than the face sheet.

The effect of gap length was studied with the VTSP program. The basic splice used to study the gap length had the following characteristics:

overlap, c = .75 in.

face sheet length, d = 6.25 in.

adhesive thickness = .005 in.

laminates: $[0/45/90/-45]_s$

core stiffness and load level are variable over a range.

Figure 24 shows moment factor curves for semi-gap lengths of .001 and 6.25 inches, representing two extremes. The .001 inch semi-gap length curves include some of those in cases I and II presented previously. The curves show that a drastic reduction in the doubler moment factor is caused by increasing the semi-gap length from .001 inches to a length equal to the face sheet length. As would be expected, moment factor is reduced by increasing core stiffness.

In Figure 25 are shown curves of the doubler moment factor for a variety of semi-gap lengths, and a core stiffness of .00001 lb/in^3 (approximate single lap joints). It can be seen that increasing the semi-gap length will more rapidly reduce the moment factors at higher load levels.

The effect of laminate bending stiffness, as yet, has not been discussed. Figure 26 shows doubler moment factor curves for a splice with the following characteristics:

overlap, c = .75 in.

adhesive thickness = .005 in

T and k are variable over a range.

The effect of bending stiffness was studied by considering two types of graphite/polyimide laminates:

$$[0/45/90/-45]_s$$

and

$$[0_3/45/90/-45]_s.$$

It is evident that increasing the bending stiffness increases the doubler moment factor.

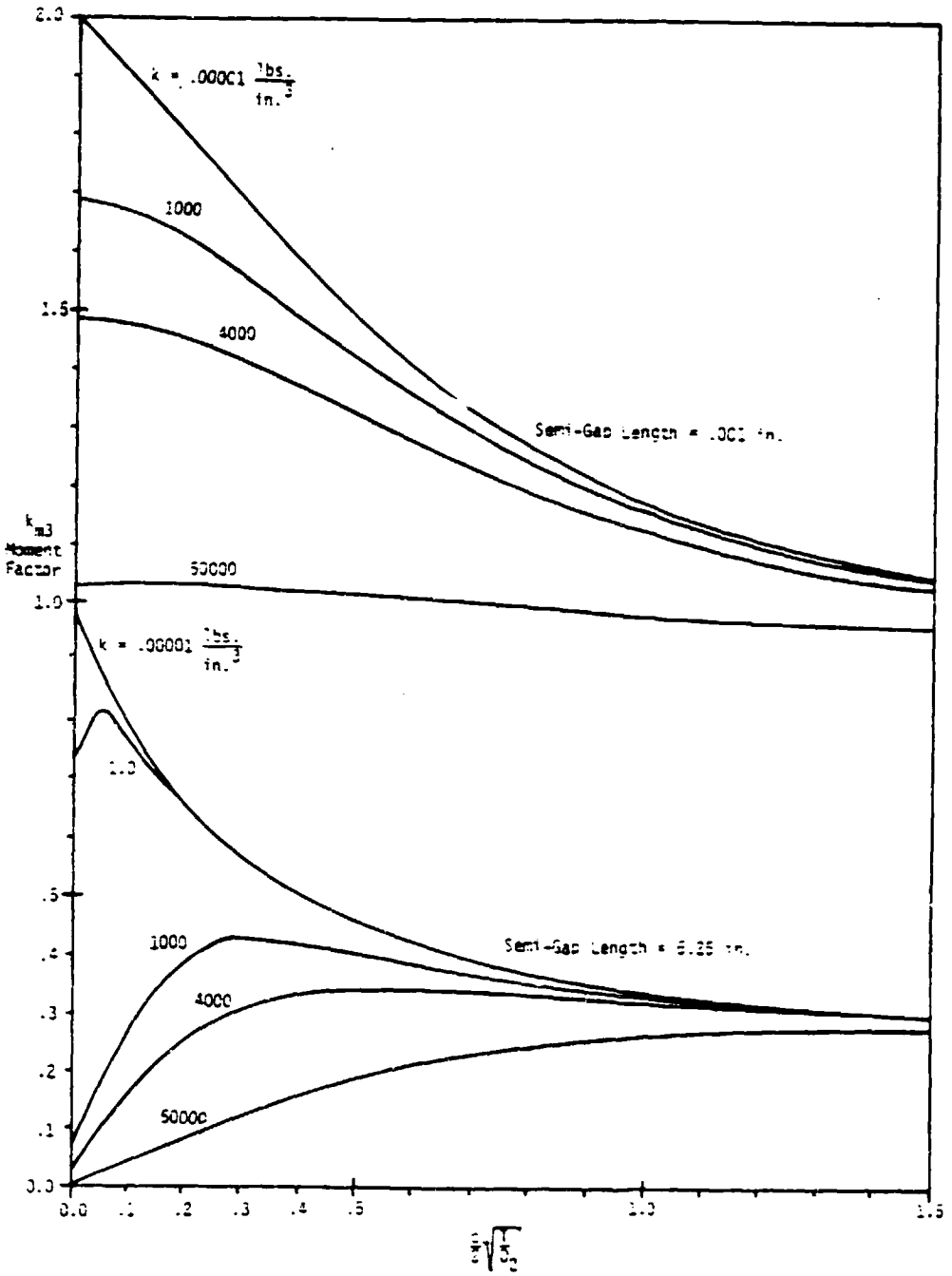

Figure 24: Effect of Gap Length on Doubler Moment Factor

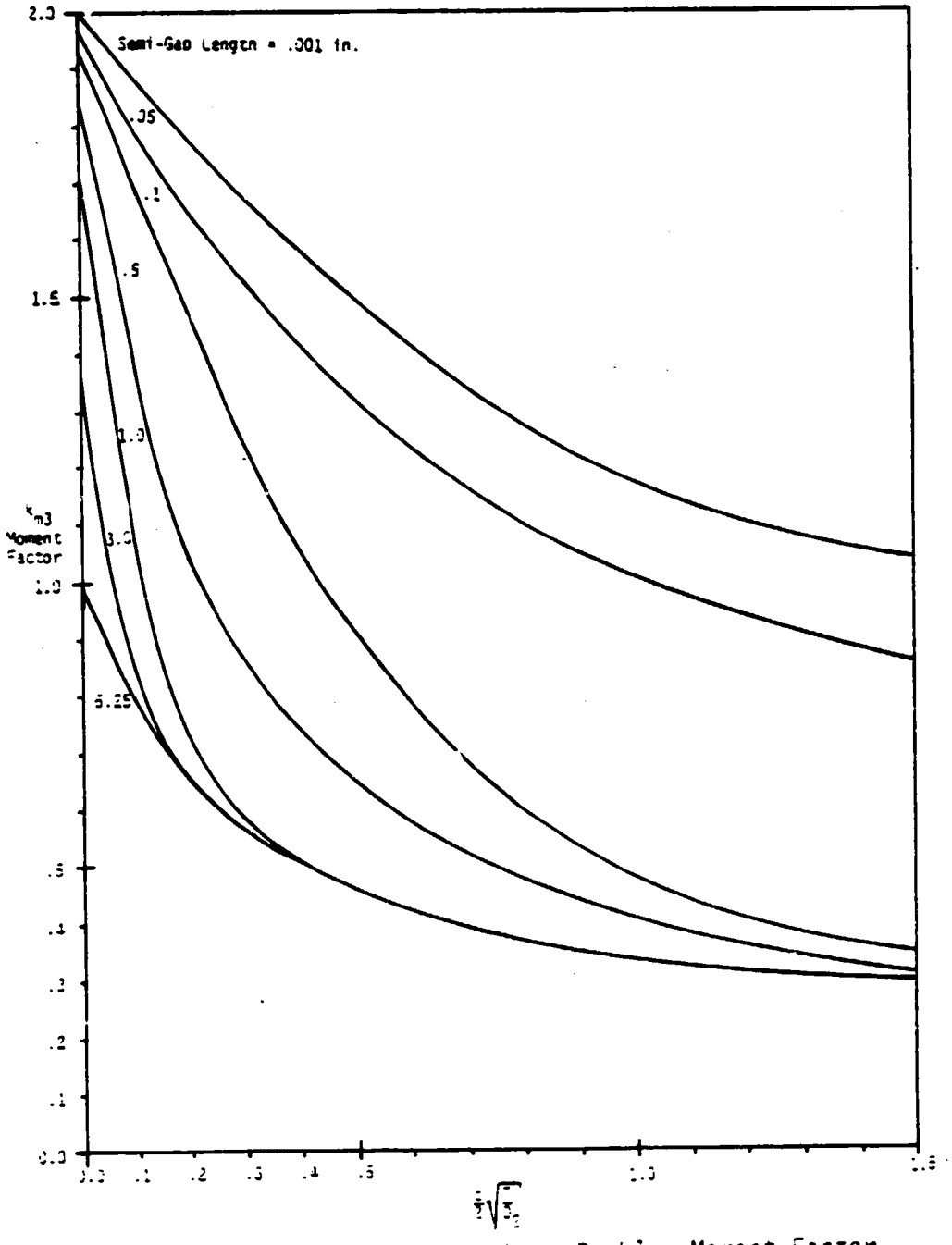

Figure 25: Effect of Gap Length on Doubler Moment Factor

- Low Core Stiffness

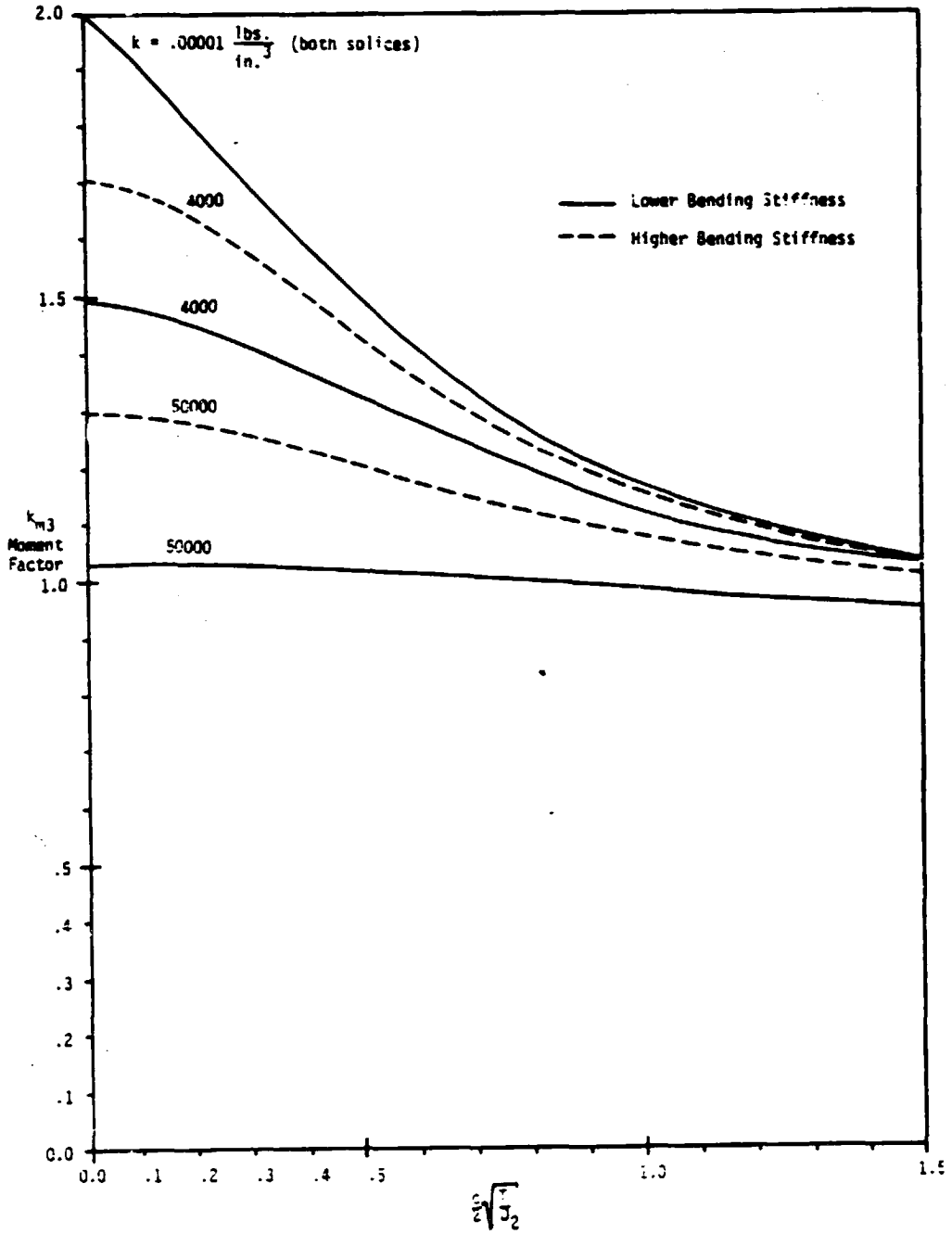

Figure 26: Effect of Bending Stiffness on Doubler Moment Factor

With the method of the analysis in Appendix A, the effects of the four quantities (D_2, C, T, and k) upon the adhesive peel stress at the gap side of the overlap was studied. It was found that anything that increases the doubler moment will increase the adhesive peel stress. This, in turn, would cause a degradation in the strength of the sandwich panel splice. The effects upon splice strength of variations in the quantities that characterize the splice (from the standpoint of the adhesive peel stresses) are summarized in Table III. In References 4 and 5, Hart-Smith reports that the critical failure mode for single and double lap joints made of composite laminates is peel failure in the adherends at the overlap edge. Thus, one can conclude that peel failure should also be the critical failure mode for the sandwich splice (the single and double lap joints being the two extreme cases of the sandwich splice).

It is interesting, in view of the physical similarity between the sandwich splice and the double lap joint, to note that the locations for critical peel stress in the adhesive differ between the two joints. In a double lap joint, the critical peel stress location is at the outer edge of the overlap (corresponding to the face sheet side of the overlap of the sandwich panel splice).

Table III

EFFECTS OF PHYSICAL VARIABLES ON JOINT STRENGTH

Increasing this Variable*	Has this effect on Splice Strength
Laminate Bending Stiffness	Degrades
Overlap Length	Improves
Core Stiffness	Improves
Gap Size	Improves

* Load level is not included in this table because the reduction in the doubler moment factor afforded by increasing load level is more of a demonstration of the geometric nonlinearity of the splice than it is a demonstration of strength improvement.

Chapter 7

FINITE ELEMENT MODEL TENSION RESULTS AND CURING STRESSES

7.1 Tension Results

Material properties and geometric constants used in the SPAR finite element analysis of the sandwich splice are to be found in Table II. Since properties for the LARC-13 adhesive were not available, they were assumed equal to those for the FM-34 adhesive. The LARC 13 adhesive's coefficient of thermal expansion was also unavailable, so it was assumed equal to α_2 for the Gr/Pi since the adhesive is a polyimide resin.

It was discussed in Chapter 4 how the geometric stiffness matrix (or initial stress matrix) associated with a given loading condition can be used to approximate the geometrically nonlinear behavior characteristic of lap joint-like structures (including the sandwich panel doubler splice). Figure 27 shows elastic axis deflections obtained from the following: VTSP; SPAR without the non-linear correction; and SPAR with the non-linear correction. It can be seen that the non-linear correction in the finite element solution effects a noticeable reduction in the elastic axis deflections predicted by the linear finite element solution. The gross effect of the non-linear correction, then, is the apparent stiffening of the structure that would be expected for tensile loading. However, one should not expect deflections from the finite element solution to be equal to or significantly close to the deflections from the elastic axis beam model results. This is because the finite element model is a more flexible structural model than is

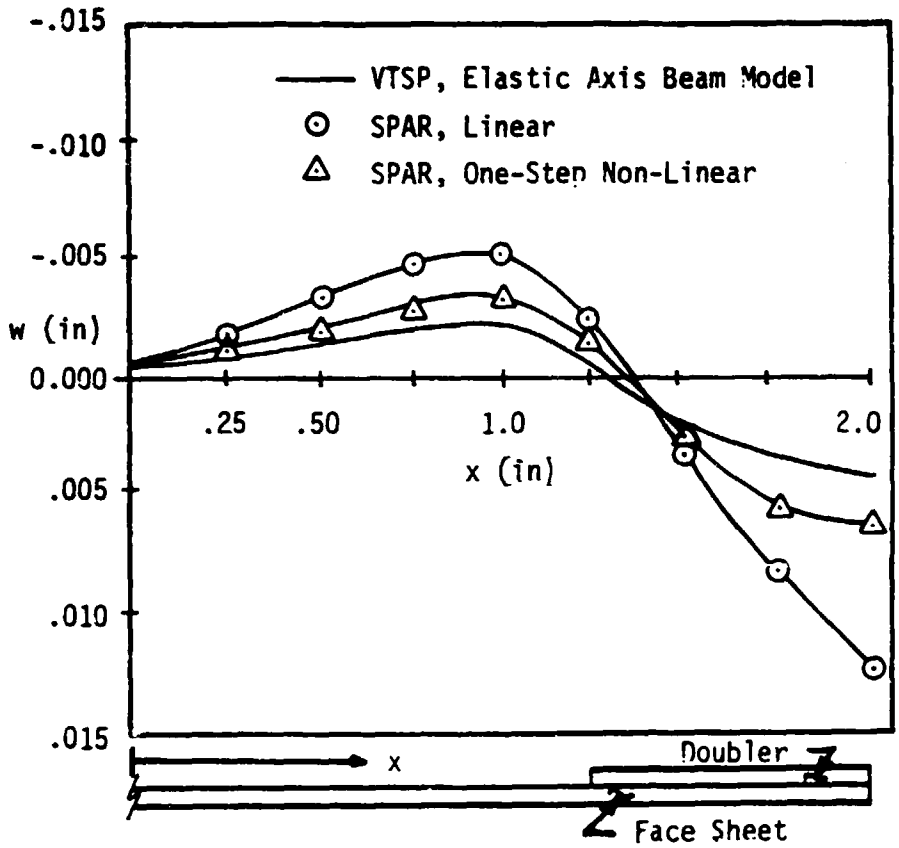

Figure 27: Elastic Axis Deflections

the elastic axis beam model. The finite element model places no restrictions on the flexibility of the plates or the adhesive, outside of assumed elemental displacement fields. The elastic axis beam model, however, does not include the effects of the extensional flexibility of the plates and of the load transfer through a flexible adhesive.

For a single lap joint, Hart-Smith has shown that accounting for the load transfer through the adhesive results in a lessening of the predicted internal loads of the adherends. This effect is also true of the sandwich splice, as evidenced by Figure 28. This figure shows doubler and face sheet moment factor curves for a particular splice configuration, developed by varying the applied load level (as was done for cases I and II in Chapter 6). One curve is from VTSP results while the other is from SPAR. Also shown in Figure 28 are several points calculated from SPAR results for which the characteristic parameters, derived in Chapter 6, were matched with those of the first splice. It is evident that matching the overlap region's characteristic parameters is not nearly sufficient for matching moment factors when a more realistic model of the sandwich splice is considered. It is likely, then, that any further attempts at such analytical unification are not feasible. However, as finite element results are composed principally of elemental stresses, some useful observations can be made regarding the critical regions for peak stresses and the effects of core stiffness and overlap length upon these stresses.

Figures 29 and 30 are contour plots of transverse normal stress, σ_z (the so-called peel stress), and shear stress, τ_{xz}, respectively.

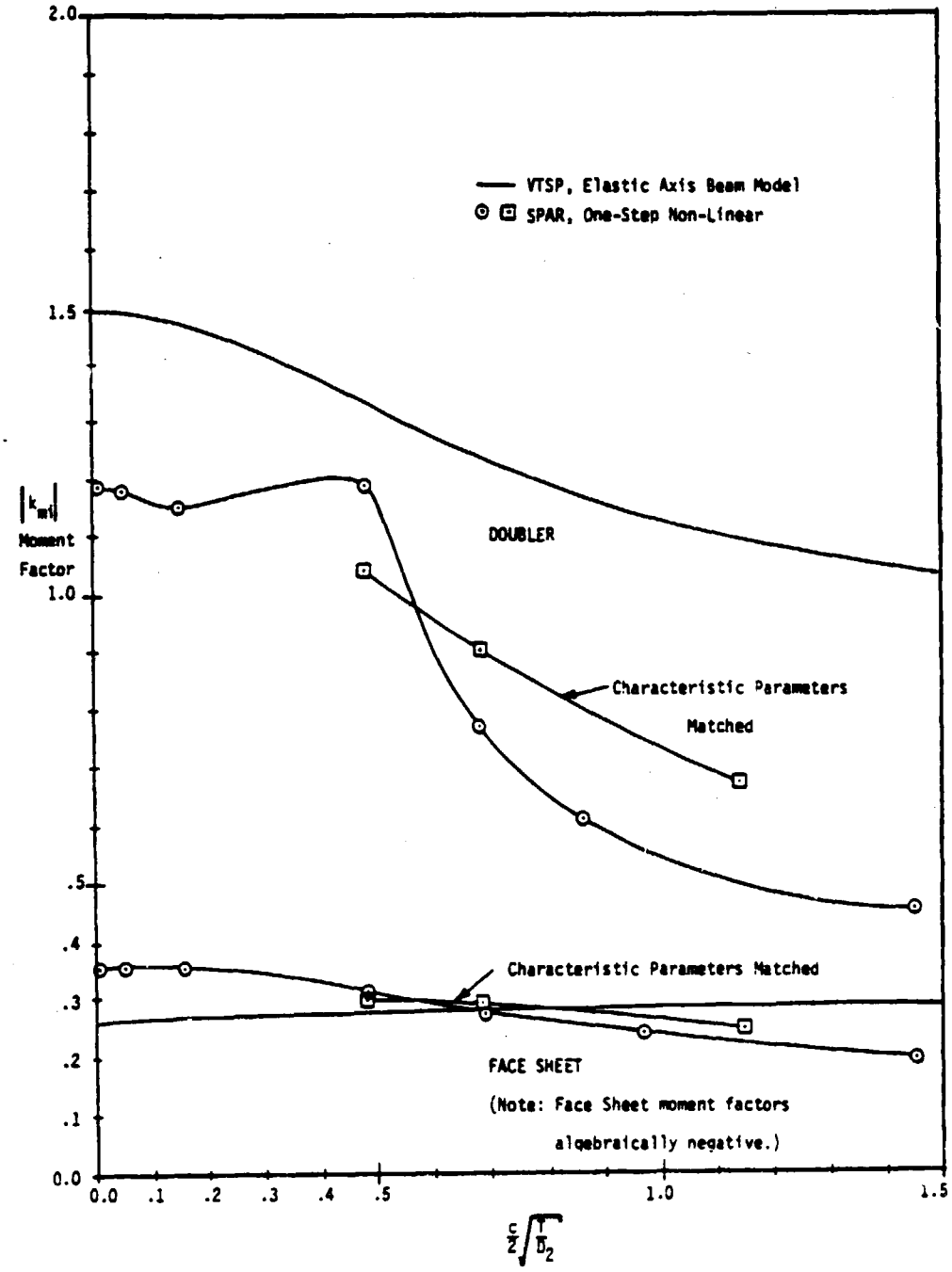

Figure 28: Comparison of VTSP and SPAR Moment Factors

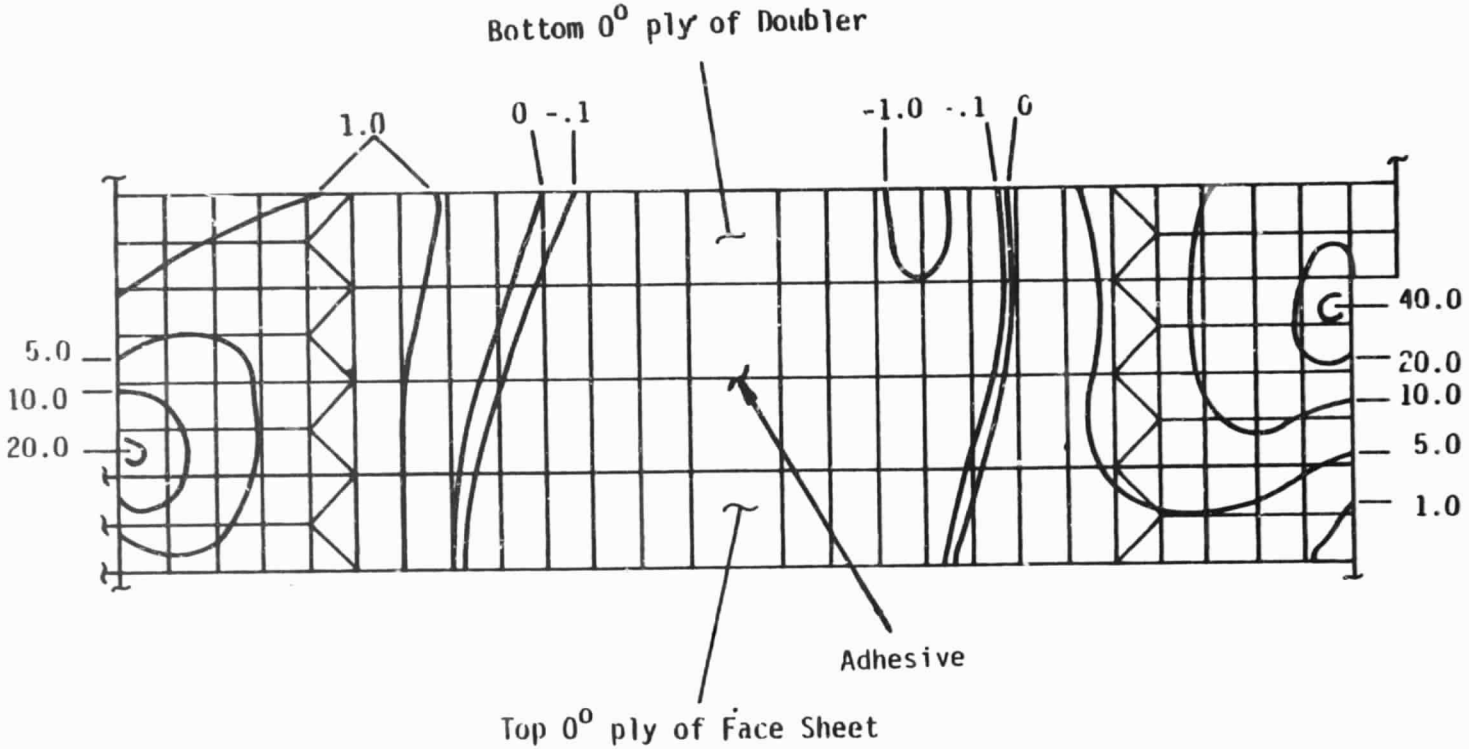

Figure 29: Mechanical Peel Stresses in Overlap Region (ksi)

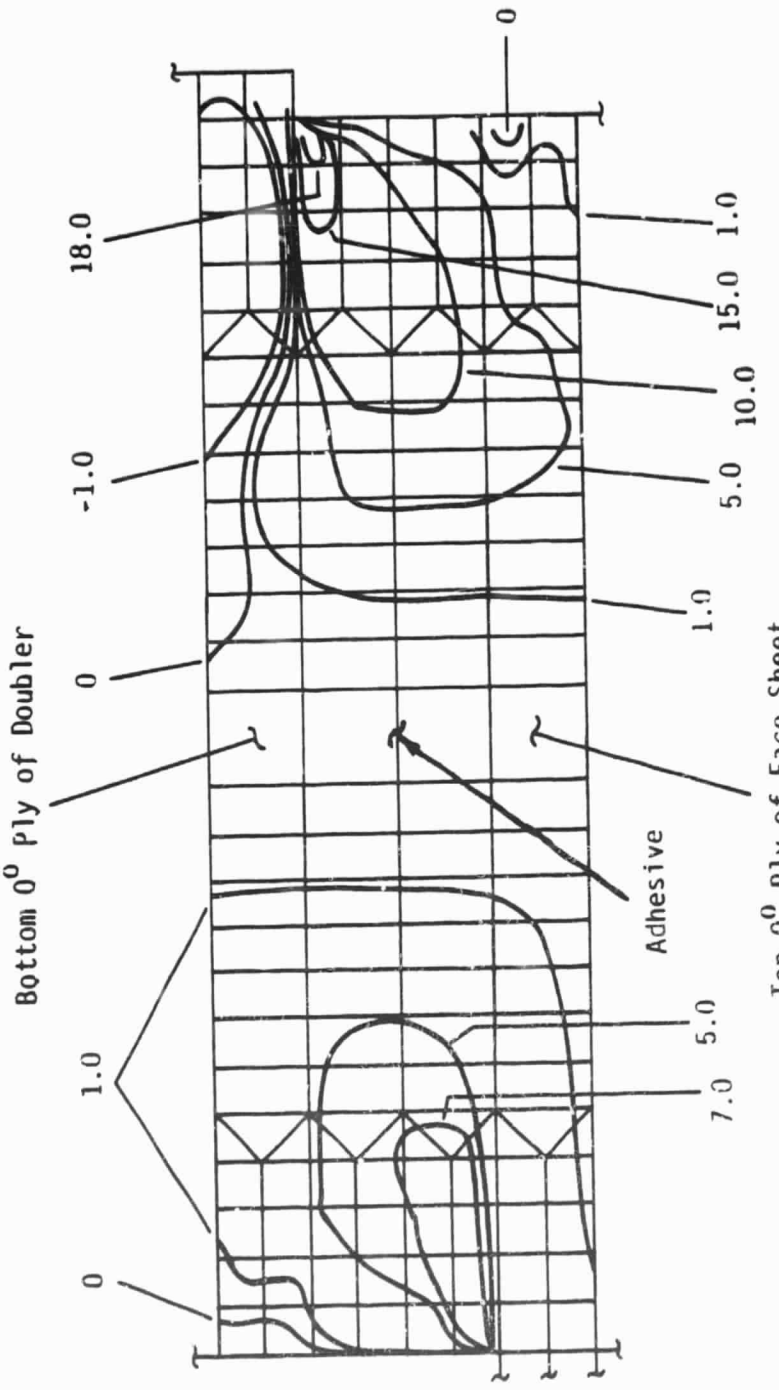

Figure 30: Mechanical Shear Stresses in Overlap Region (ksi)

The region of the finite element model shown in the figures is the adhesive layer and the adjacent plies only. The grid is not drawn to scale. The applied load is 900 lbs/in and the overlap length is .75 inches. The elastic foundation stiffness of the core (not shown in Figures 29 and 30) is 4000 lbs/in^3, since the transverse core modulus (in the thickness direction) is 1000 psi [10], and its semi-thickness is .25 inches.

As it would be reasonable to expect, the peak stresses are to be found in the regions of the re-entrant corners at the two ends of the overlap. It can be seen that the stresses at the right hand or gap side of the overlap are much greater than those at the face sheet side - from 2 to 3 times greater. This result is in agreement with the conclusion drawn in Chapter 6 regarding the region of the splice that is most critical with respect to peak stresses. It should be noted that the gap side of the overlap was consistently subjected to higher stress peaks than the face sheet side in all cases considered with this finite element model. This effect will be discussed later in light of its bearing upon joint efficiency.

Figures 31 and 32 show maximum peel and shear stress concentration factors at the gap side of the overlap as calculated from SPAR results. Stresses are normalized to the applied stress, which is the applied load level divided by the face sheet thickness. Overlap length was changed by adding two columns of .25 inch wide elements to the center of the overlap region. Core stiffness was changed by changing core

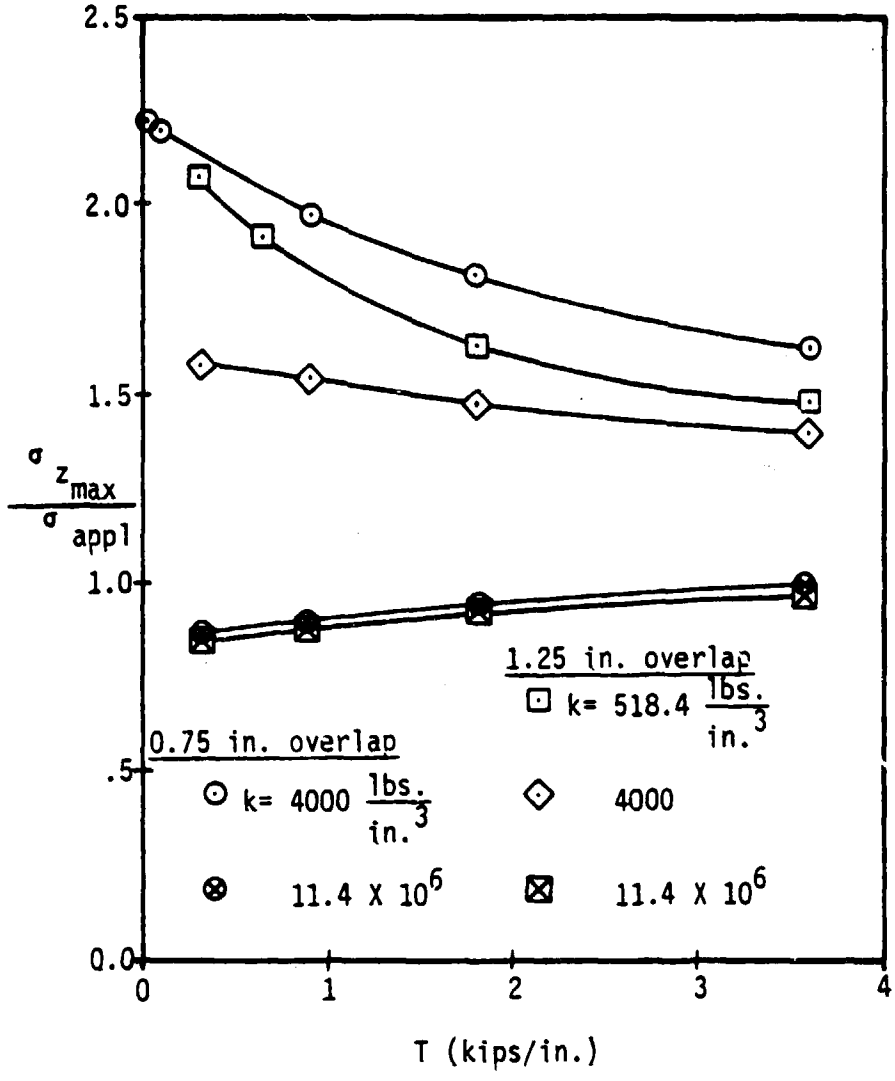

Figure 31: Maximum Peel Stress Concentration Factors

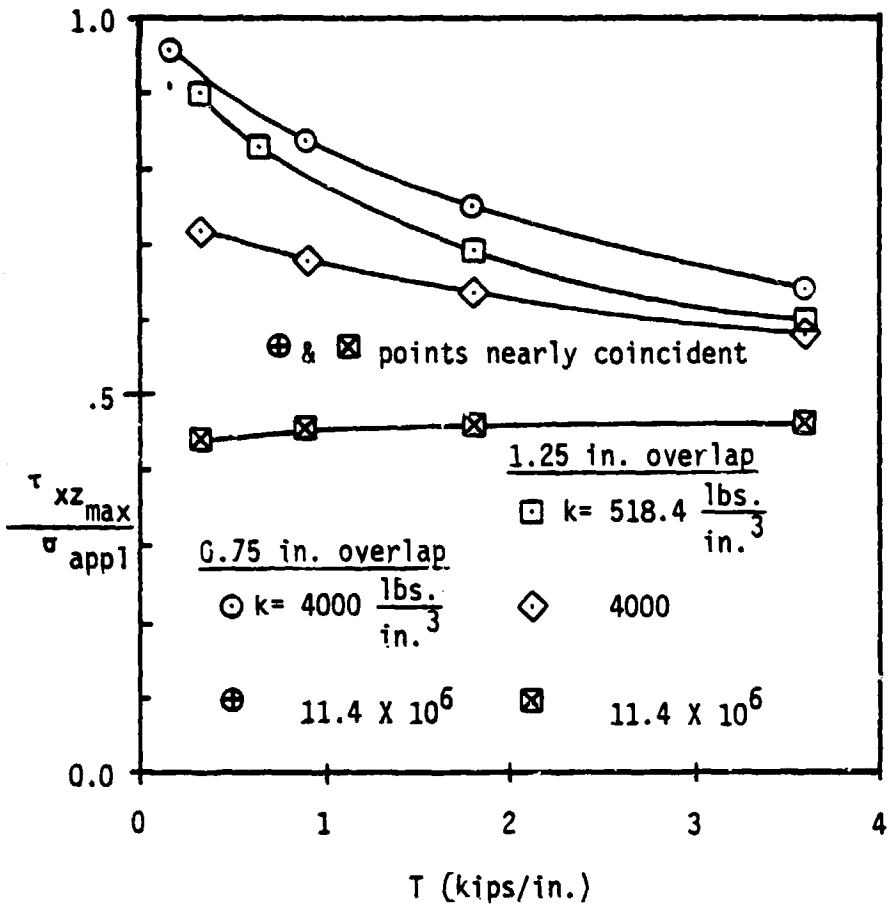

Figure 32: Maximum Shear Stress Concentration Factors

modulus. It can be seen that increasing both overlap and core stiffness effects a reduction in the peak stresses. Again, this result is in accord with conclusions drawn in Chapter 6 from the elastic axis beam model. The figures also show that the influence of overlap is reduced by an increased core stiffness. This effect can also be deduced from the elastic axis beam model, and it is a result which correlates well with the noted behavior of double lap joints. Considering a double lap joint to be analogous to the sandwich splice with an extremely stiff core, one would expect that increasing overlap is not an effective method of strengthening a double lap joint. Hart-Smith [5] reports that, past a certain point at least, increasing overlap does not provide a worthwhile increase in joint strength.

It is also found from the stress concentration curves for the very high core stiffness that the stress concentration factors increase slightly with load - which is a reversal of behavior observed up to this point. It is likely that part of this effect is a result of a lessening of the internal load relief from plate deflection. The deflection is reduced by increasing core stiffness. No additional explanation of this effect can be offered, however.

It was noted previously that the gap side of the overlap consistently experienced higher stresses than did the face sheet side in all cases studied with the finite element model. Figures 33 and 34 show plots of the ratios of the peak peel and shear stresses, and it is clear that the stresses on the gap side are the greater. It would be more desirable if these peak stress ratios could be reduced

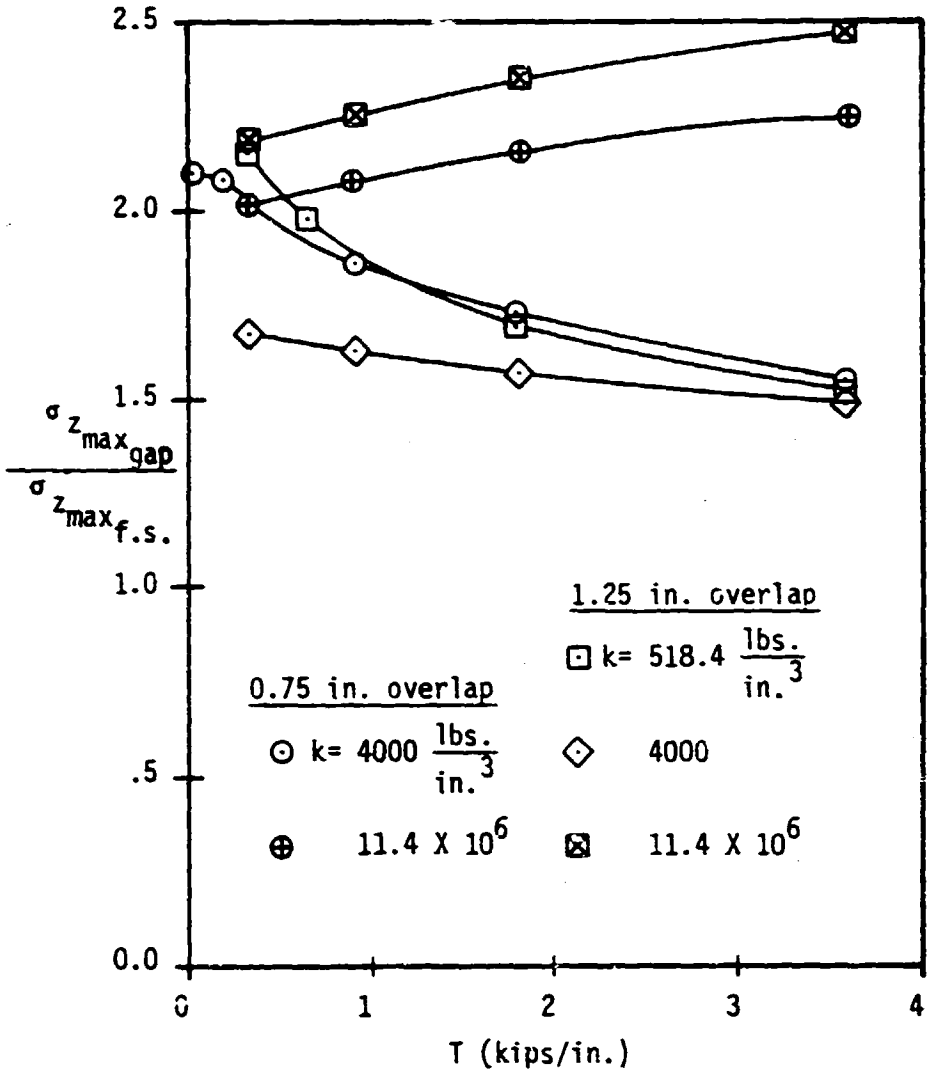

Figure 33: Comparison of Peak Peel Stresses

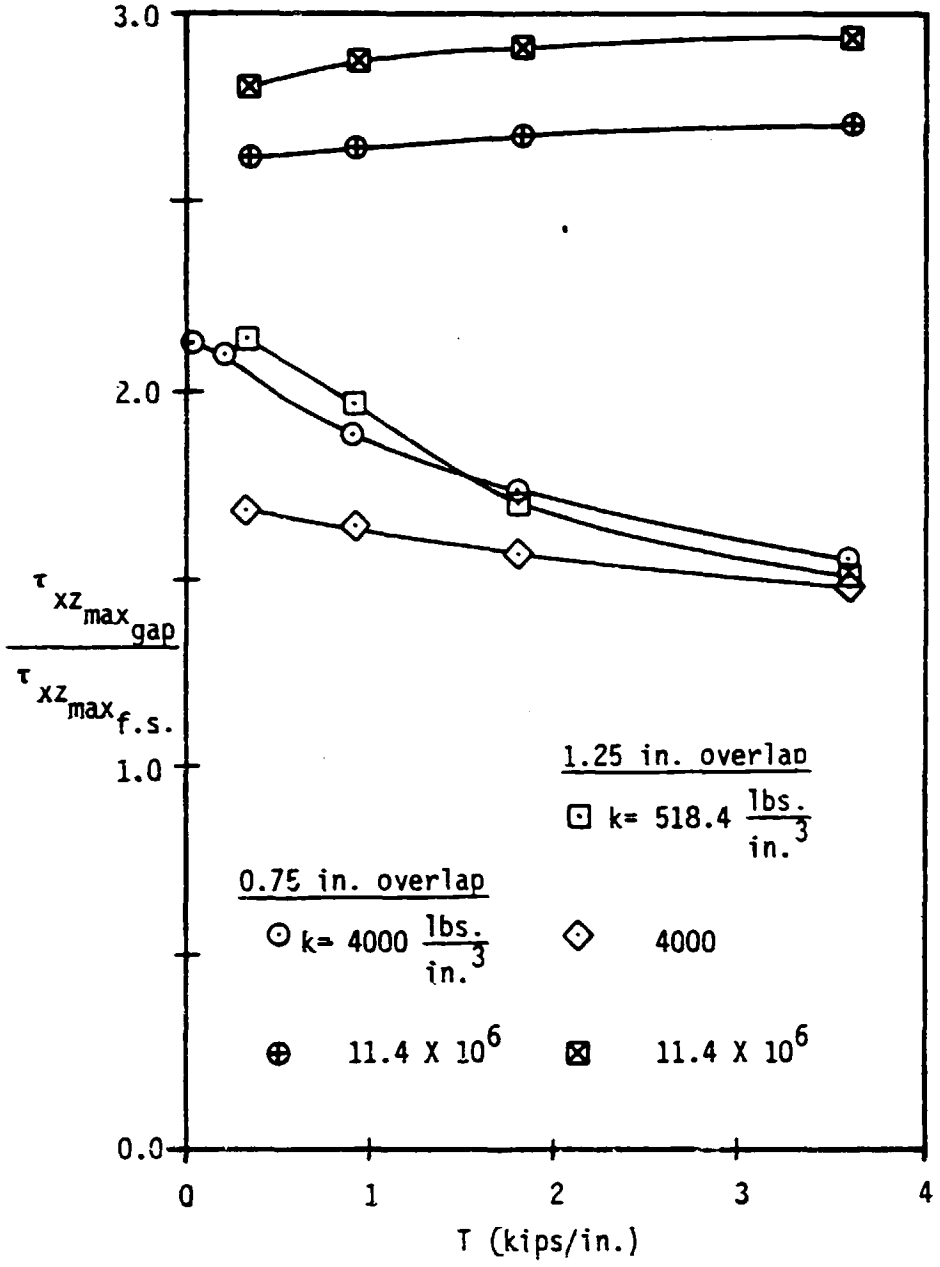

Figure 34: Comparison of Peak Shear Stresses

to unity by reducing the gap side's stresses even further. Peak stress ratios of unity imply that the load transfer through the adhesive is balanced between the two ends of the overlap, and is thus more efficient.

It is also apparent from Figures 33 and 34 that the dependence of the stress ratios upon core stiffness and overlap length is a complex one. Increasing core stiffness initially improves efficiency as does increasing overlap. However, the highest core stiffness curves are seen to be above the others for the most part. Additionally, at the high core stiffness, the curves for the larger overlap are above those for the smaller overlap.

These results suggest that there may be an optimum combination of core stiffness and overlap for which the load transfer through the adhesive for a particular splice is most efficient. This would be but one of many factors that would influence the selection of a core material and an overlap length for use in an actual structure. Some other factors would be the stress levels associated with and the weight penalty imposed by the particular combination chosen.

7.2 Curing Stresses

Because of the non-homogeneity of thermoelastic properties inherent in laminated composite structures, and the usual curing that the laminates require at elevated temperatures, stresses typically develop within the laminates as a result of cooling from curing temperatures. These stresses are commonly referred to as curing stresses.

Figure 35 depicts a contour plot of curing peel stresses predicted by SPAR at the two ends of a 1.25 inch overlap sandwich splice, with a core stiffness of 4000 lb/in^3. The temperature drop of 625°F is in the typical range of a cool down from Graphite/Polyimide and LARC-13 curing temperatures. Other cases were also studied which considered a core stiffness of 518.4 lb/in^3 and an overlap of .75 inches. Any differences between the stress distributions observed in any of the cases were insignificant, and the stress patterns shown in Figure 35 would not be altered for these cases. This result suggests that core stiffness and overlap length have little or no influence on tne magnitude and distribution of curing peel stresses.

It can be seen that one effect of the drop from curing temperatures is to induce compressive peel stresses in the regions where high tensile peel stresses, resulting from tensile mechanical loading, were noted previously. While this might be considered helpful to joint strength, there are high tensile stresses in regions immediately adjacent to the compressive regions. What is more, these tensile stresses are near or exceed the interlaminar tensile strength of Graphite/Polyimide laminates. This would lead one to expect that the joints might fail before mechanical loading is introduced. However, results of investigations [11] into the effects of moisture absorption upon interlaminar stresses near free edges of composite laminates suggest that moisture absorption tends to counter, or relieve, curing stresses in some cases. Whether such effects would also be true of the sandwich panel splice

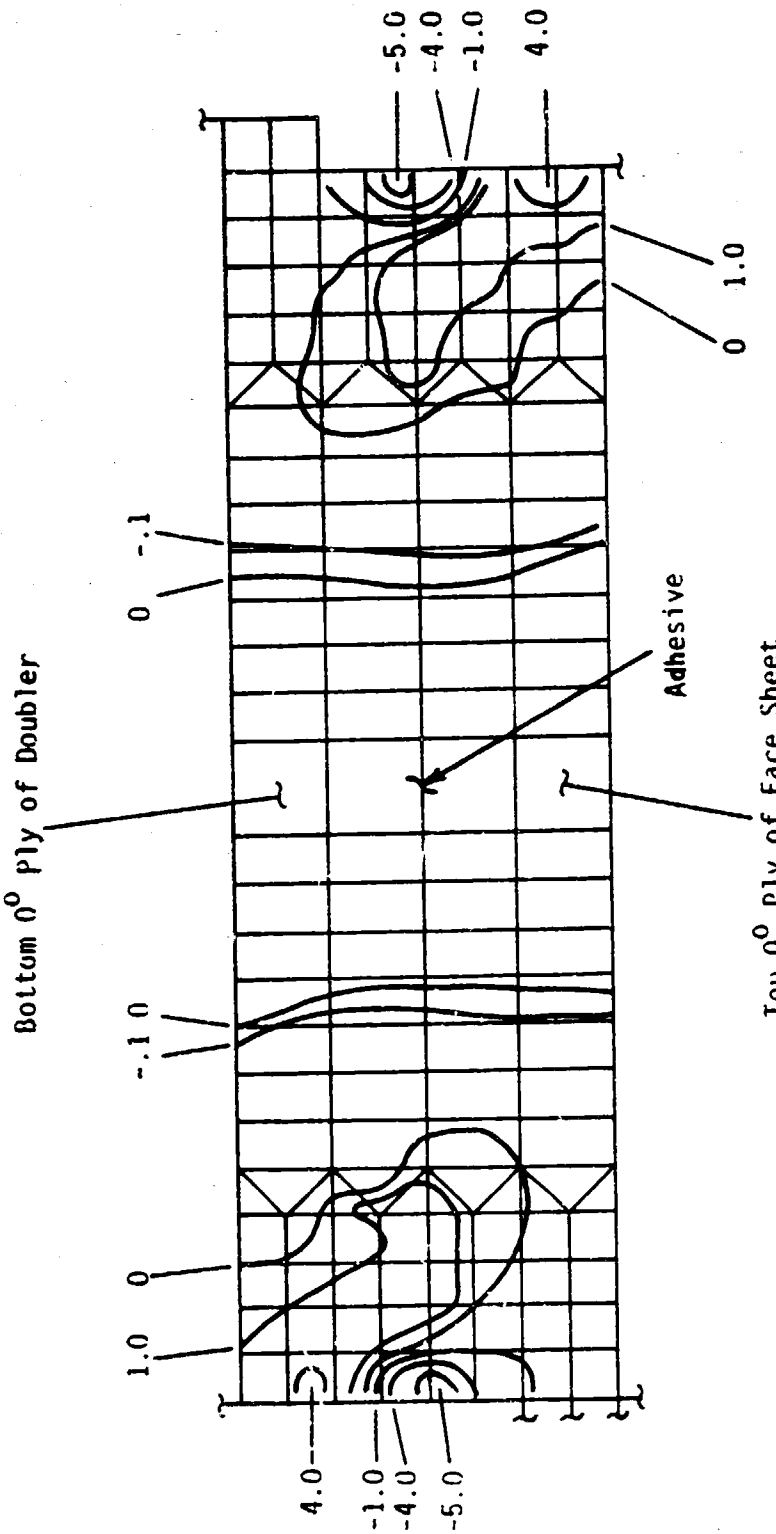

Figure 35: Curing Peel Stresses in Overlap Region (ksi)

is not known. However, the results of failure tests of sandwich panel splices, to be presented, show significant joint strengths.

Chapter 8

EXPERIMENTAL TENSION RESULTS

8.1 Induced Test Variables

In addition to the planned test variables of: laminate configuration; overlap length; temperature; and loading, there are also variables due to uncontrollable influences. These variables fall into two categories: manufacture-induced and test-induced.

The manufacturer of the test specimens used three separate batches of material to fabricate the specimens. The manufacturer receives material as a tape of unidirectional fibers pre-impregnated with semi-cured matrix material, commonly called "prepreg". Five separate rolls of one of the prepreg batches were also used. General experience has shown that the physical properties of the material can vary between supposedly identical prepreg materials. Also to be included in manufacture-induced variables are the so called "process variables". Process variables arise in this instance because no two sets of specimens can be fabricated under exactly the same conditions, even when a great deal of care is taken. General experience has shown that composite material behavior can be sensitive to process variables. One measure of these manufacture-induced test variables is the fiber volume fraction of fabricated composite laminates. Measurements taken by the manufacturer of the test specimens show that the fiber volume fractions of the laminates used in the test specimens varied from a low of 55.7% to a high of 65.9% - a difference of more than 10%.

Test-induced variables arise from the conditions under which the tests are performed. Environmental conditions in these tests could not be controlled; however, the possible influence of test equipment can be controlled. An effort was made to minimize the latter influence by orienting the specimen grips and inserting load pins in an identical fashion from specimen to specimen.

It will be seen that there is some degree of scatter in the test data. An attempt will be made to correlate this scatter with the induced variables. However, because of the small amount of data available, the results of the correlation attempt will still be uncertain.

8.2 Results of Room Temperature Tension Tests

All of the fifteen (15) planned room temperature tension tests were conducted. Of the fifteen tests, five (5) resulted in load tab failures, and the remaining ten in joint failures. In one joint failure case, failure load data was lost.

Figure 36 shows plots of the results of the room temperature tension tests. The data points corresponding to joint failures were used to compute average strengths; the averages are connected by lines in the plots. The data points corresponding to load tab failures were not used in computing average strengths. The abscissa of the plot is recognizeable as one of the characteristic parameters of the overlap region, derived previously in Chapter 6. The ordinate of the plot is the average applied stress in one face sheet at failure, and is computed as one sixth of the failure load (as there are two face sheets subjected to load and the specimens are three inches wide) divided by the face

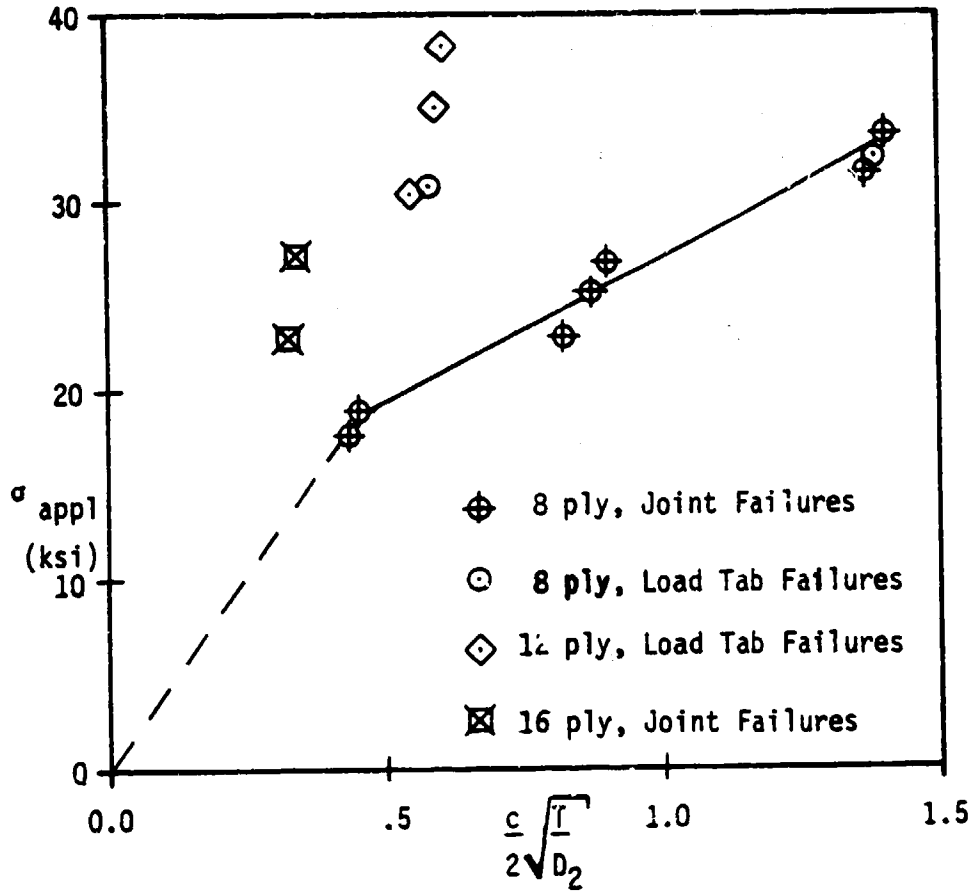

Figure 36: Room Temperature Tension Test Results

sheet thickness. Since laminate thicknesses were not uniform from specimen to specimen, nor consistently so within a given specimen, the individual ply thickness assumed throughout the preceeding analyses was used to compute the applied stresses. Plate bending stiffnesses used for determining abscissa values are those computed with the same assumed ply thickness and the assumed material properties in Table II.

The effect of increasing overlap length, as evidenced by the test results in Figure 36, is consistent with the results of the preceeding analysis in that it causes an increase in joint strength. This result is predictable since the same effect is true of lap joints.

The effect of adding zero degree plies to the outer surfaces of the laminates is not entirely consistent with the results of the elastic axis beam model analysis. It is recalled that the predicted effect of increasing plate bending stiffness was to degrade joint strength. It is apparent that increasing the number of zero degree plies (which also increases plate bending stiffness) at first improves joint strength, but eventually degrades it. It should be noted here that the measured fiber volume fractions for the thickest laminates were at the low end of fiber volume fraction range reported previously. The fiber volume fractions for the thinner laminates were at the high end of the range. This would generally mean that the thick laminates are slightly weaker and more flexible than they would be if their volume fractions were as high as those of the thinner laminates. It is not believed that this variance in fiber volume fraction had a

significant effect upon the observed trend in the test results.

In all of the room temperature tension tests that resulted in joint failures the same damage state, depicted in Figure 37, was observed. Without exception, the zero degree ply at a doubler-adhesive interface was split between the doubler and the adhesive in the vicinity of the gap between the spliced sandwich panels. This behavior is consistent with results of the finite element analysis reported in Chapter 7. No consistent pattern was observed in the widths of the splitting zones.

The results of the elastic axis beam model suggest that joint strength is degraded by increasing the plate bending stiffnesses as it tends to increase the adhesive peel stress peaks for a given load. Increasing the number of zero degree plies at the outer surfaces of a laminate obviously increases the bending stiffness as well as the bending moment capacity of the laminates. Thus, there are two conflicting influences of adding zero degree plies to the laminates in a sandwich splice.

The test results in Figure 36 also show two conflicting influences of adding zero degree plies. It is probable, then, that the 8-ply laminate specimens failed initially through longitudinal tension in the doublers' bottom zero degree plies in the vicinity of the gap where analysis shows large internal bending moments exist. The high peel and shear stresses in this region can then easily cause the observed splitting failure. The 12-ply specimens show improved strength therefore (in excess of the load tab failure loads), since

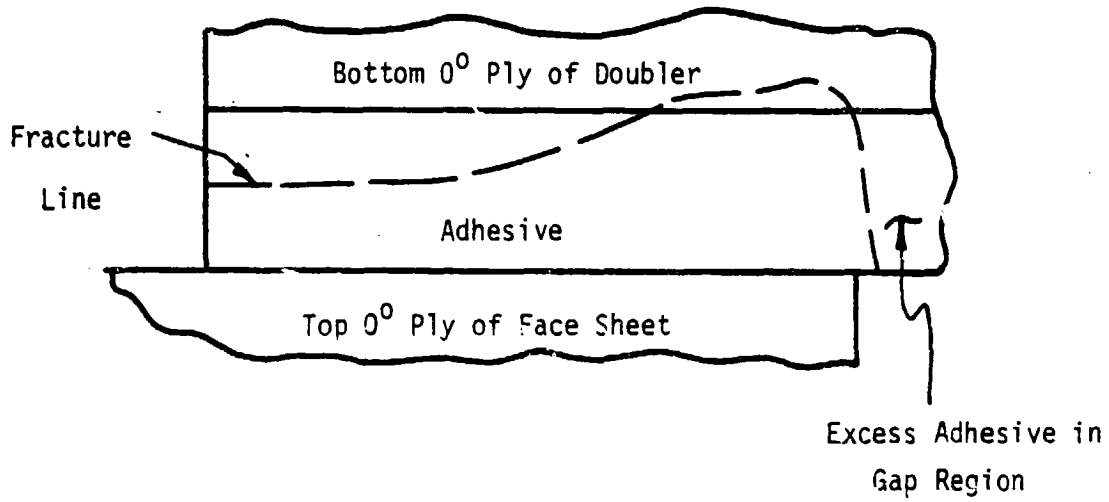

Figure 37: Damage State of Room
Temperature Tension
Test Specimens

the bending capacity of the doublers has been increased. Whether the failure in this case would be controlled by longitudinal tension in the zero degree ply or by high adhesive stress peaks is uncertain, however. It is apparent that the 16-ply specimens failed from the influence of the adhesive stresses rather than the bending tension in the bottom zero degree ply. This conclusion is drawn since the tests showed a reduction in strength from the 12 ply specimens, and this reduction is consistent with conclusions drawn from analysis.

These results suggest, then, that there is an optimum number of zero degree plies that can be placed at the outer surfaces of the laminates to maximize joint strength. This is evident in Figure 38. Figure 38 illustrates the general influence of the number of zero degree plies upon joint strength that has been proposed.

8.3 Elevated Temperature Tension Tests

Of the fifteen planned elevated temperature tension tests, nine (9) were conducted. Of these nine tests, two resulted in load tab failures and another was rendered useless by an operator error. The nine tests show the influence of overlap length upon joint strength for specimens with 8 ply laminates. Figure 39 shows two faces of a test specimen with thermocouple locations indicated. As temperature was increased for these tests, it was found that thermocouples 2 and 3 heated more quickly than the thermocouples that were at the splice center. This was probably due to the potting material at the splice center. This effect made it impossible to obtain stable and equal temperatures at the thermocouple locations in a reasonable amount of time. So, an

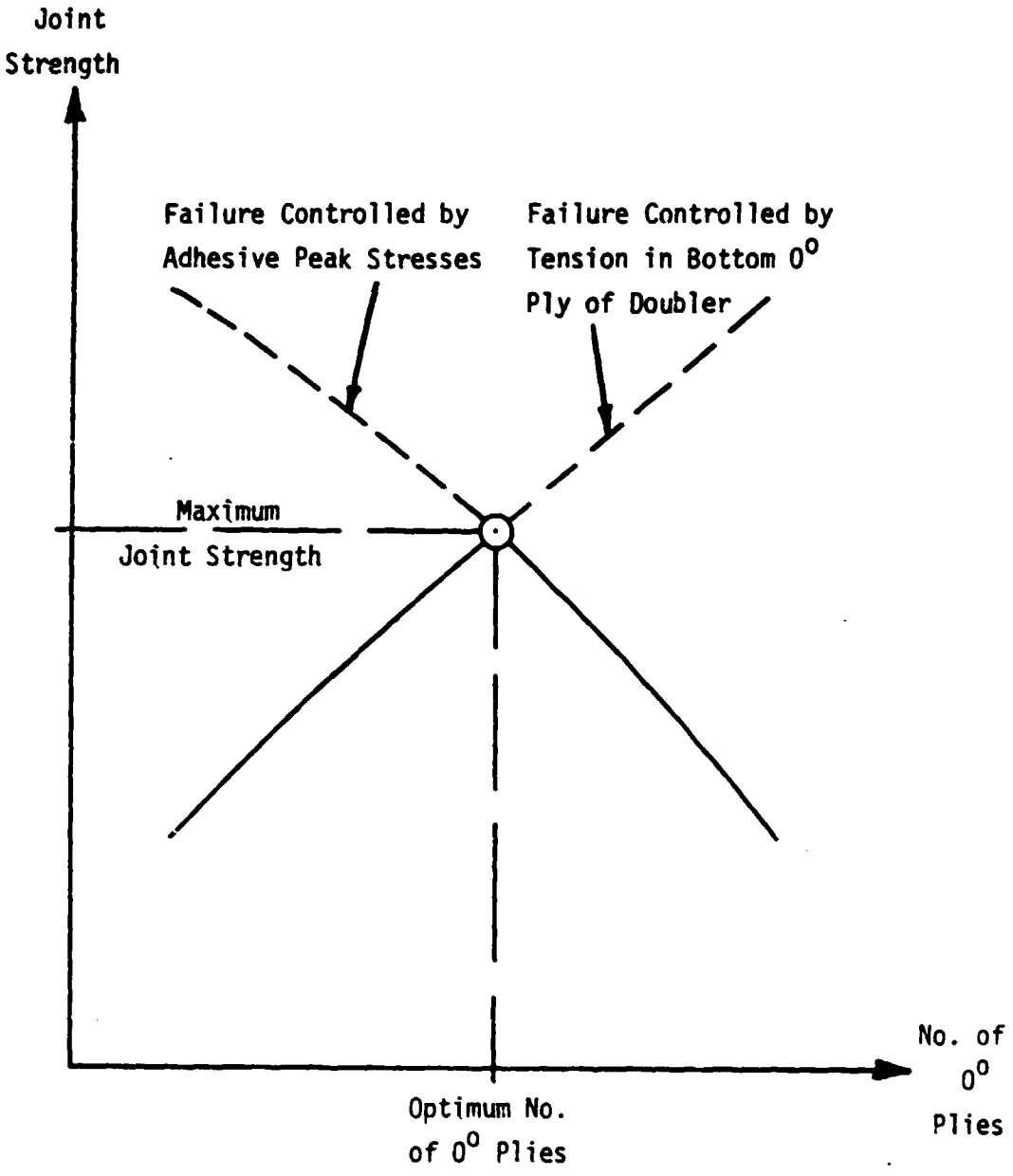

Figure 38: General Influence Upon
Joint Strength of Adding
0^{o} Plies to Laminates

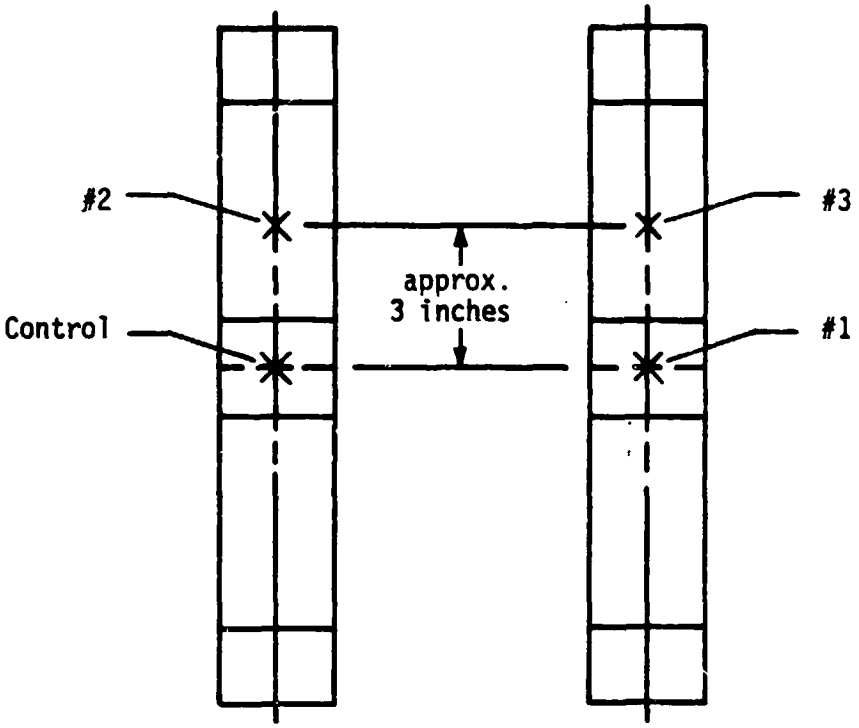

Figure 39: Thermocouple Placement

effort was made to obtain reasonably stable temperatures within or near the range of 550°F to 600°F.

Figure 40 shows the failure data obtained from the elevated temperature tension tests. The abscissa of the plot is thermocouple temperature and the ordinate is applied stress at failure, defined previously. The failure load data points are plotted at the average of the thermocouple temperatures.

Upon comparison of Figures 36 and 40 it would seem that subjecting the test specimens to elevated temperatures does not adversely affect the strength of the joints. However, two conflicting results were noted. The average strength of the .75 inch overlap specimens at elevated temperature is close to that of .75 inch overlap specimens at room temperature. However, the one room temperature specimen that experienced load tab failure was fabricated from the same panel as the corresponding elevated temperature specimens. If these four specimens can be considered nearly identical, then subjecting the specimens to elevated temperature was responsible for an appreciable strength reduction in the .75 inch overlap specimens. This is the first conflicting result. The second conflicting result is to be found in the 1.75 overlap specimen test results. The two elevated temperature data points shown in Figure 40 for these specimens were for specimens fabricated from the same panel as one of the corresponding room temperature specimens. The conflicting result is that the joint strengths of these elevated temperature specimens are greater than the joint strengths of the corresponding room temperature specimens.

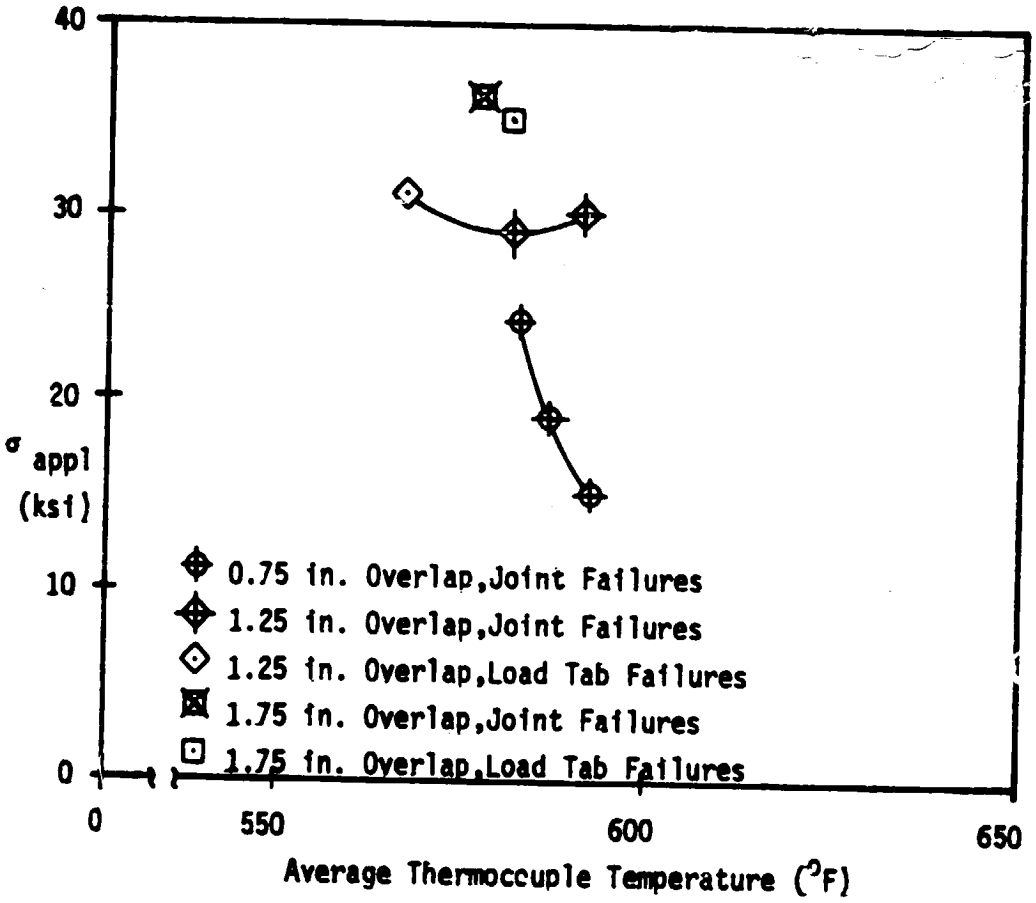

Figure 40: Elevated Temperature Tension
Test Results

Also, the 1.25 inch overlap, room temperature specimens had laminates with fiber volume fractions comparable to those for the elevated temperature specimens. The strengths of elevated temperature specimens are seen to be the greater. Thus, in the balance, evidence thus far supports the statement that elevated temperatures do not adversely affect the tensile strength of the joints.

It is noted lastly that no consistent failure mode was observed in the elevated temperature tension tests as in the room temperature tension tests. The various damage states observed were: splitting of the bottom 0° ply of the doubler in the vicinity of the gap; splitting in the top 0° ply of the face sheet in the vicinity of the outside (or face sheet side) of the overlap; and adhesive failure including neither the face sheet nor the doubler. No conclusions can be drawn from these varying results.

Chapter 9

RESULTS OF STUDY OF COMPRESSION LOADING

9.1 Approach to Problem of Compression Loading

It has been shown in the previous chapters that tensile loading exerted upon a bonded doubler splice of two composite sandwich panels induces high shear and tensile peel stresses at the inner and outer edges of the adhesive layers. It has also been reasoned that these high stresses play a significant role in the failures of these joints in tension.

It is generally known that a reversal of the loading from tension to compression will increase a lap joint's strength. This is primarily a result of the reversal in the direction of the adhesive peel stresses from tension to compression [5]. This effect is certainly true if the physical structure is mathematically linear. For the sandwich splice problem, the mathematical linearity arises from the restriction of small slopes in the deflection shape of the structure's elastic axis. While tensile loading, in all probability, would not cause mathematical non-linearity, compression loading can. This mathematical non-linearity is caused by large slopes in the elastic axis deflection and corresponds to the physical phenomenon of buckling. As a result of the large post-buckling deformations that would be experienced by the sandwich splice, failure could occur in a variety of locations depending upon the support conditions imposed upon the splice structure.

If the splice and the panels being spliced are not very wide and

are laterally supported by surrounding structure, failure could occur as a result of either high adhesive shear stresses at the edges of the adhesive or buckling of the face sheet/doubler bonded structure. If the splice and the panels being spliced are rather wide, panel (or column) buckling may be the cause of joint failure as well as the two possible causes mentioned previously.

In this study, attention was restricted to the manner in which buckling of the sandwich splice might occur. Several approaches were taken to study this problem. One approach was to utilize the features of the VTSP analysis. Results from VTSP are compared to an analysis done by Hetenyi of a clamped-clamped beam on a continuous elastic foundation [12]. Hetenyi's model is equivalent to a sandwich panel with no joint. VTSP and Hetenyi's model were used to study the effects of doubler overlap length, laminate bending stiffness, and gap length upon the critical buckling load of the face sheet/doubler structure.

The results of compression tests of sandwich panel splice specimens are also presented. The specimens were not laterally supported, so buckling of one sort or another was virtually guaranteed. Two unexpected phenomena were observed during the testing and are discussed.

9.2 Results of VTSP (Elastic Axis Beam Model) Analysis

As is evident from the development of the elastic axis beam model in Chapter 3, the plate boundary conditions are not homogeneous. This is due to the moment discontinuities at the regional junctions of the model. The system of boundary condition equations, solved by VTSP,

cannot be treated in the fashion of an eigenvalue problem.

The discontinuous elastic axis representation of the sandwich splice (Figure 3) suggests a similarity between the splice and an eccentrically loaded column. Solutions to the linear model of the eccentrically-loaded column display the behavior shown in Figure 41. As load increases from zero, the deflection at some convenient reference point in the structure (usually the point of maximum deflection) increases as would be expected. At the bifurcation point, the deflection becomes infinite. Past the bifurcation point, the model predicts a complete reversal in the deformation shape of the structure. While this effect is meaningless physically, it is a valid mathematical solution to the linear model.

Figure 42 shows a load-deflection curve obtained from VTSP for compressive loading of a splice with 8 ply laminates, an overlap length of .75 inches, a semi-gap length of .001 inches, and an elastic foundation stiffness of 4000 lbs/in^3. The nature of this curve is the same of that in Figure 41. This similarity is the basis of the criterion used to identify the critical buckling load for the structure. Since VTSP is designed only to solve the system of boundary condition equations for a given set of conditions, the buckling load must be found through iteration. This is accomplished by incrementing load until a reversal of the deflection shape to a mirror image is observed. The load increment is then refined until the reversal in the deflection shape is observed to occur between two sufficiently close (and this is to be decided by the user) values of load. The average of these two

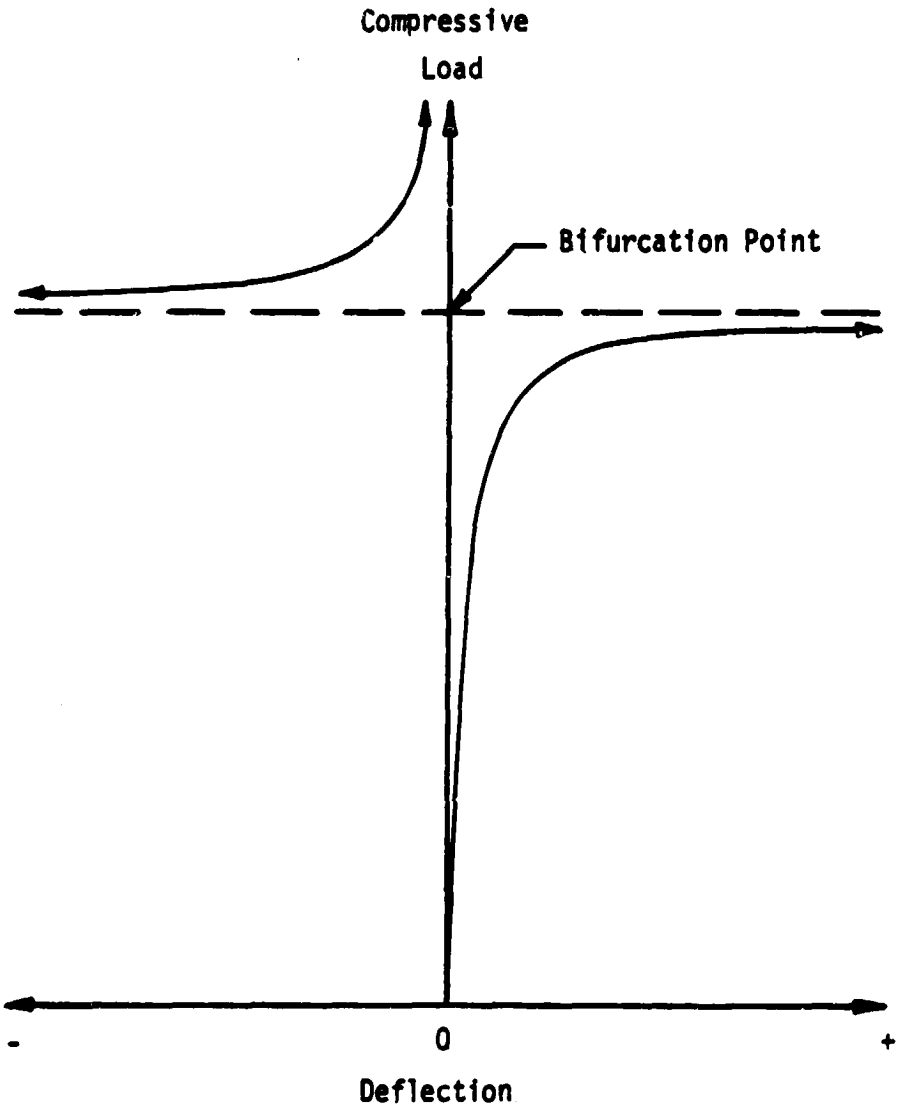

Figure 41: Behavior of Solutions to
Linear Model of an Eccentrically
Loaded Column

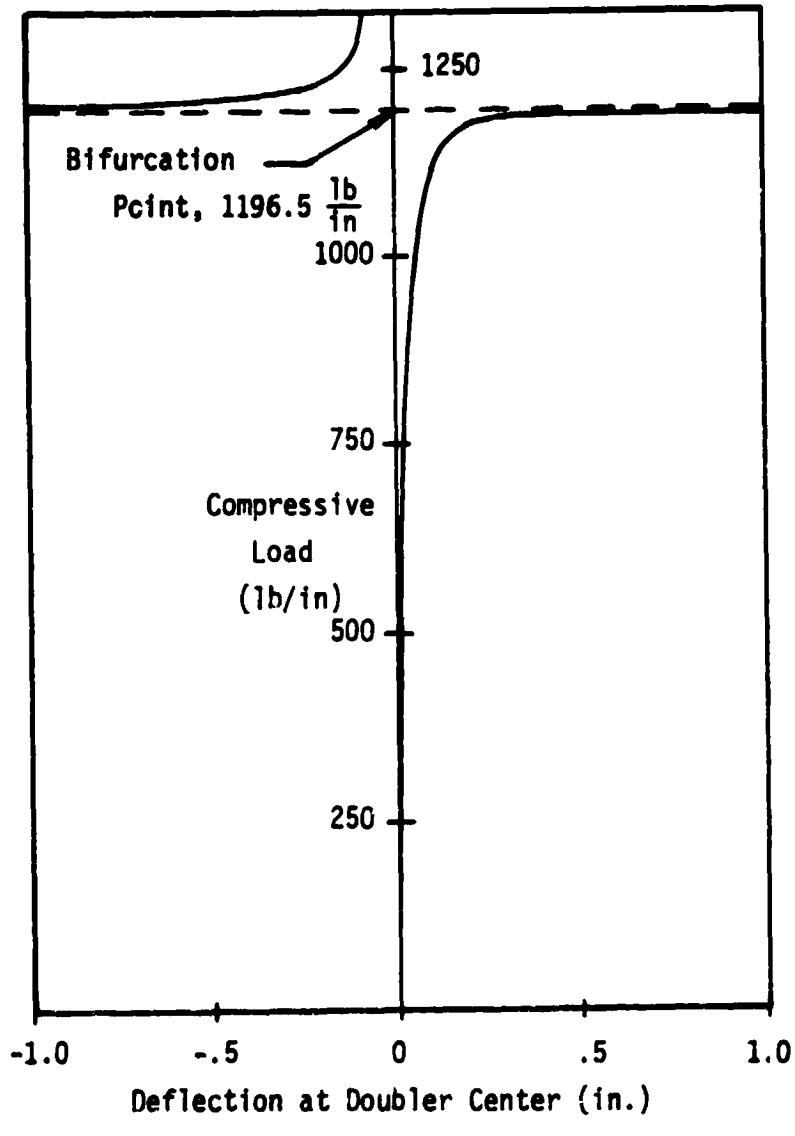

Figure 42: Behavior of VTSP Solutions for Compressive Loading

load values can then be taken as the buckling load. The smallest load increment used for all cases in this study was 1 lb/in.

Recalling the system of boundary condition equations for the elastic axis beam model, it is evident that the system can be written in matrix form. Indeed, the VTSP program solves the system through matrix operations. The square matrix obtained by writing the system in matrix form is of interest. If the boundary conditions were homogeneous, the determinant of the square matrix would be zero for load values equal to buckling loads. In all the cases studied with VTSP, the reversal of the deflection shape that was considered indicative of buckling was accompanied by a change in sign of the determinant of the square boundary condition matrix.

Hetenyi [12] presents the solution for the buckling loads of a clamped-clamped beam on an elastic foundation. An approximate equation for the critical buckling load, as a function of beam length and bending stiffness, and elastic foundation stiffness, is given by Hetenyi as

$$P_{cr} = 4(\frac{\pi}{L})^2 D + 2\sqrt{kD} \qquad (25)$$

The exact solution is a transcendental equation which must be solved iteratively.

Figure 43 illustrates the effect of overlap length on critical buckling strength as predicted by VTSP, and includes a comparison with the solution from Equation 25. The calculations were done for laminates with 8 plies, and an elastic foundation stiffness of 4000 lb/in^3.

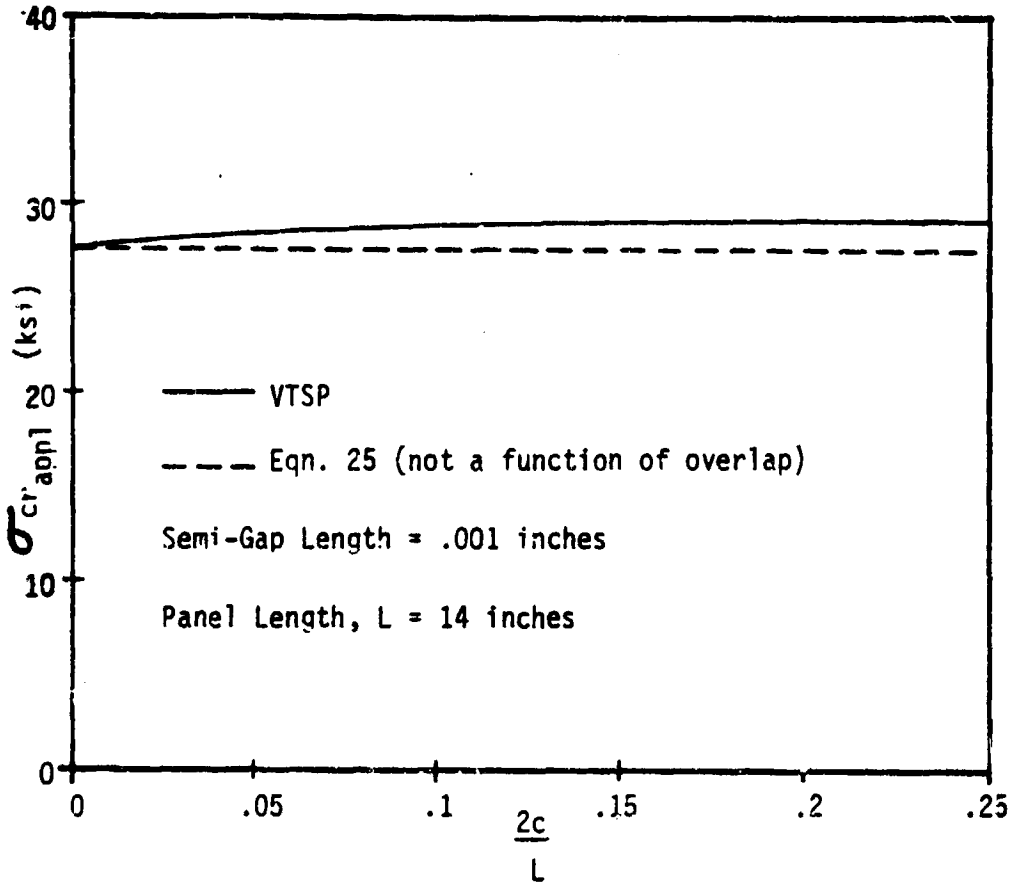

Figure 43: Effect of Overlap on
Critical Buckling Strength

Panel length was kept constant at a total of 14 inches (plus the gap size). The applied stress to one face sheet is calculated in the same fashion as in Chapter 7. It can be seen that increasing overlap affords slight increases in critical buckling strength over the buckling strength of just a plain panel with no joint. This is a sensible result since local stiffening is provided by the doubler.

Figure 44 shows the effect of increasing bending stiffness, by adding 0° plies to the outer surfaces of the laminates, upon critical buckling strength. As would be expected, increasing bending stiffness increases the joint structure's buckling strength. Comparison with solutions of Equation 25, however, suggests that adding 0° plies to the laminates effects an improvement in buckling strength over the strength of a joint-less panel only up to a point. Past this point, the joint's buckling strength is less than that of a jointless panel. It is not certain why this effect is observed. Possibly, the strength improvement that accompanies the presence of the doubler for the 8 ply laminates is being countered by the increased eccentricity in the elastic axis that accompanies the addition of 0° plies.

It was shown in Chapter 6 how increasing the size of the gap between the spliced panels can improve the tensile strength of the splice. It is obvious that increasing this gap size should decrease the buckling strength of the joint. Figure 45 illustrates this effect. It can be seen that increasing the gap length causes an eventual reduction in buckling strength to below the buckling strength of a jointless panel. However, it is also evident that increasing

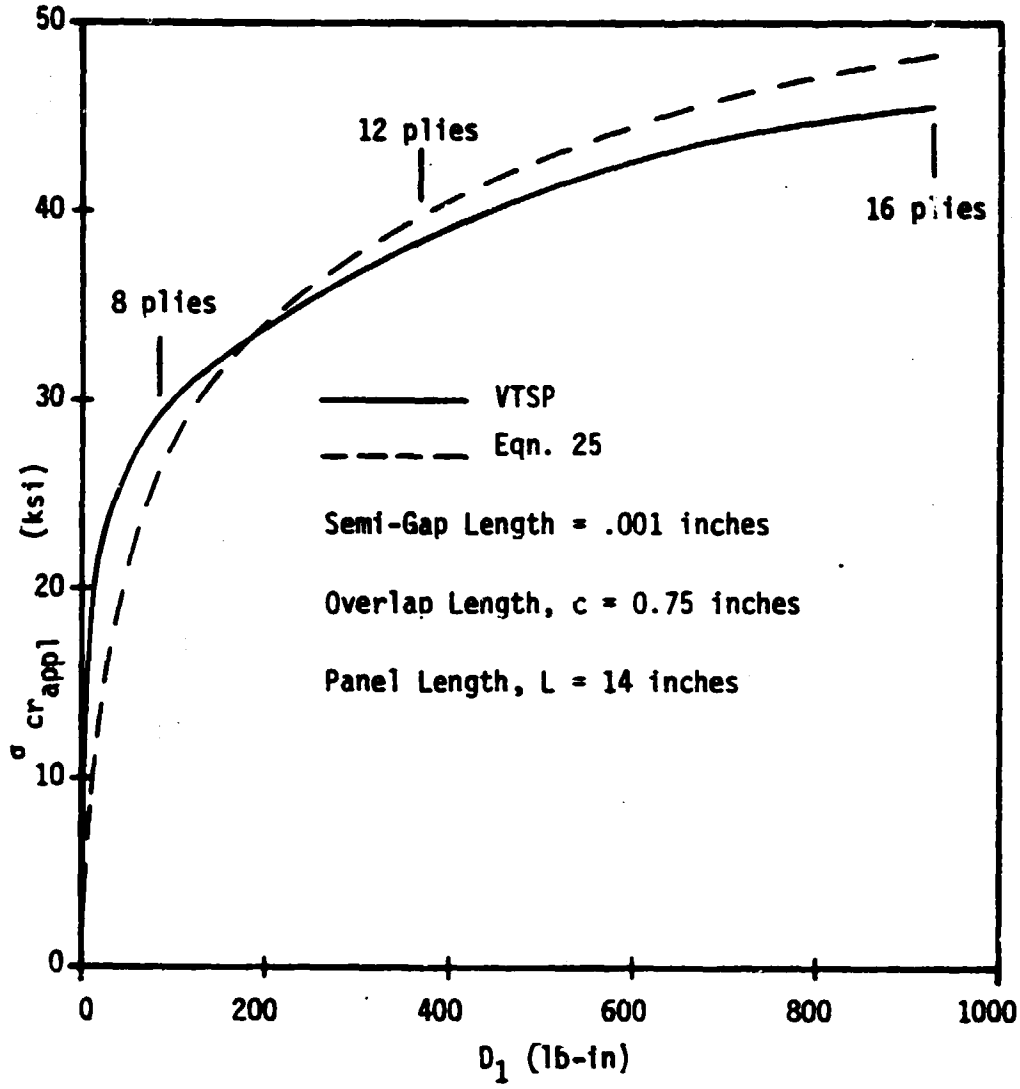

Figure 44: Effects of Bending Stiffness upon Critical Buckling Strength

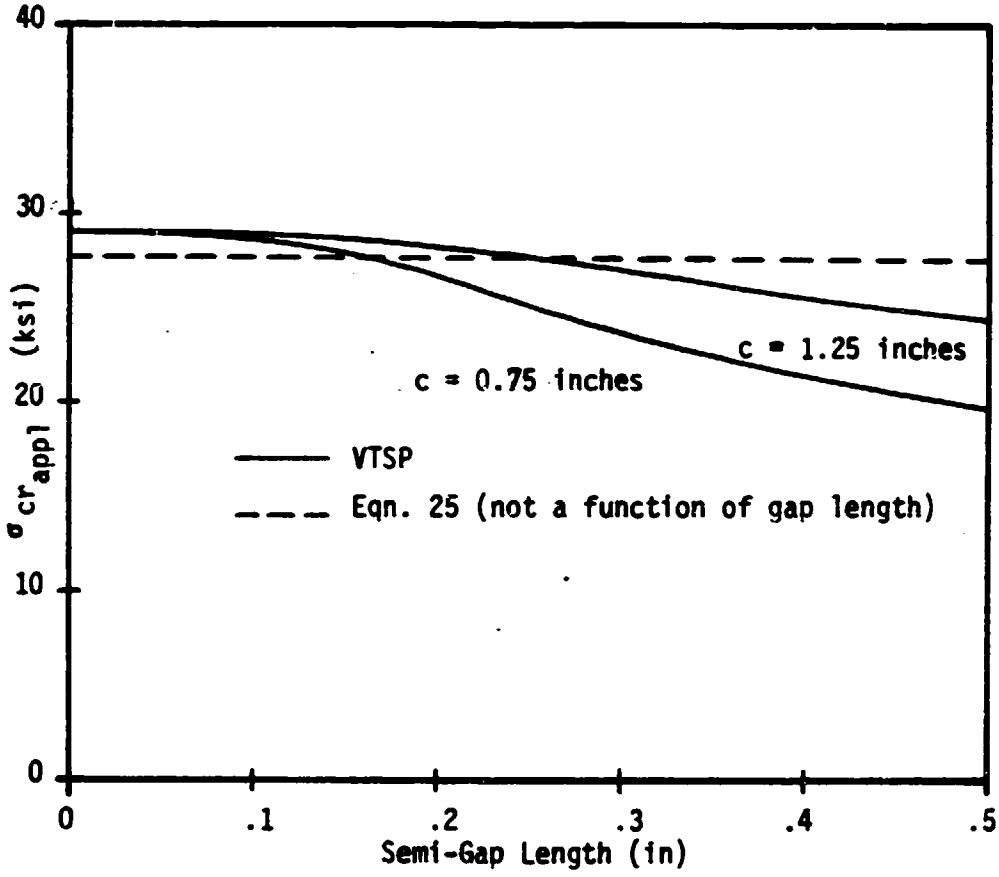

Figure 45: Effect of Gap Length on Critical Buckling Strength

overlap can permit a considerable increase in gap length without a major reduction in the buckling strength.

9.3 Results of Compression Tests

Of the fifteen (15) planned room temperature compression tests, fourteen (14) were conducted. Of the fifteen planned elevated temperature compression tests, three (3) were conducted. Additionally, two (2) spare specimens were tested in compression at room temperature.

All of the compression tests resulted in column buckling. Some of these were accompanied by joint failures. In particular, the specimens which experienced joint failure were ones with 8 ply laminates and overlaps of .75 and 1.25 inches, and ones with 16 ply laminates and an overlap of 1.25 inches. Figure 46 illustrates the typical deformed shape of the failed specimens. In all cases, the buckling damage zone had the appearance of a shear crimping failure, a common failure mode for sandwich panels in compression. Also, the damage zone consistently appeared at about two thirds of the distance from the inner edge of the load tab to the center of the joint. If one considers half of the test specimen to be a column, clamped at the load tab and pinned at the joint, the location of the damage zone of the buckled specimen is seen to correspond to the point of maximum deflection in the first buckling mode shape of a clamped-pinned column (Fig. 47). This is one of the unexpected phenomena mentioned previously. What was expected was overall column buckling. The reason for this behavior is not certain. It is possible that the

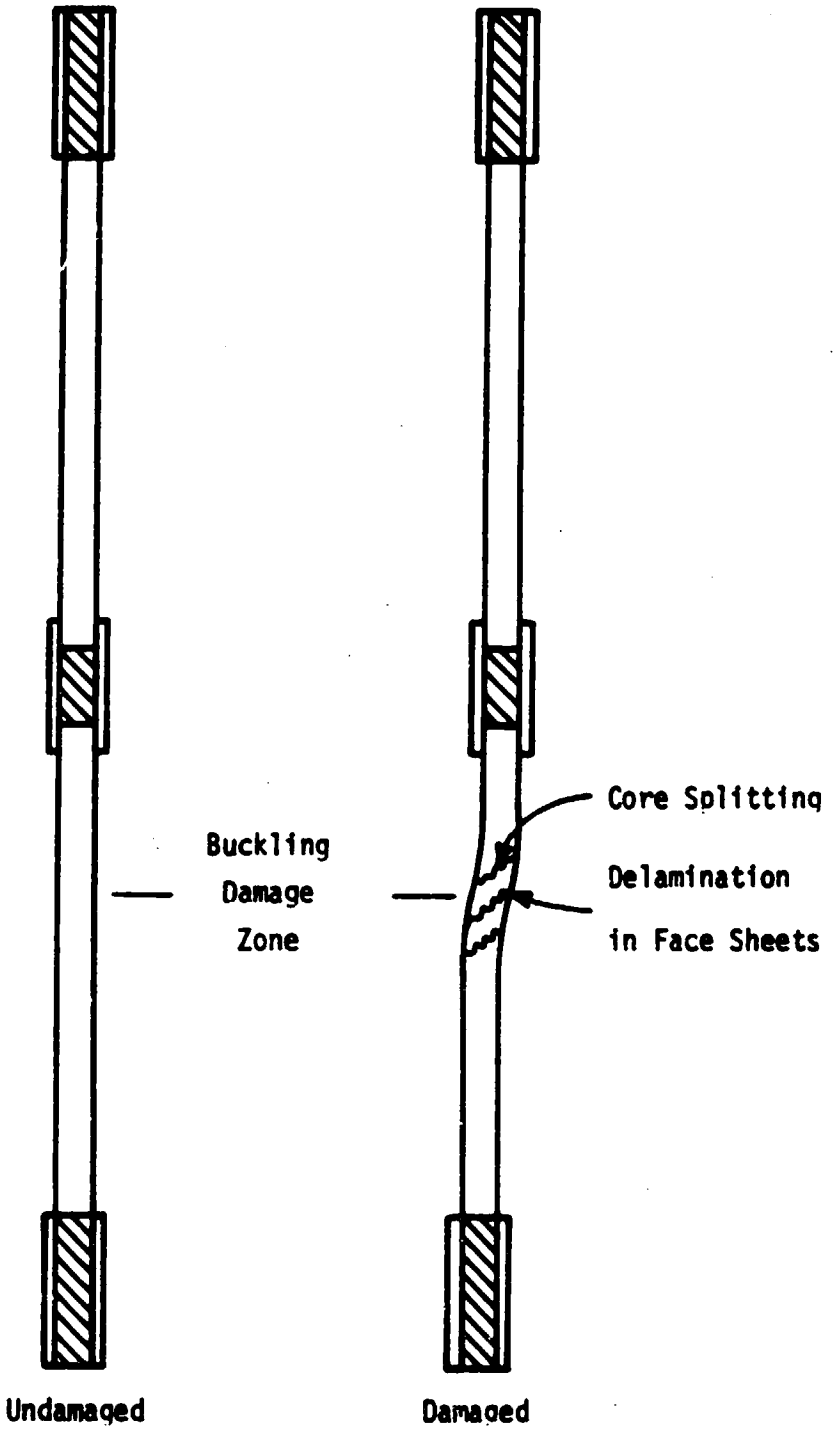

Figure 46: Typical Damage State of
Failed Compression Specimens

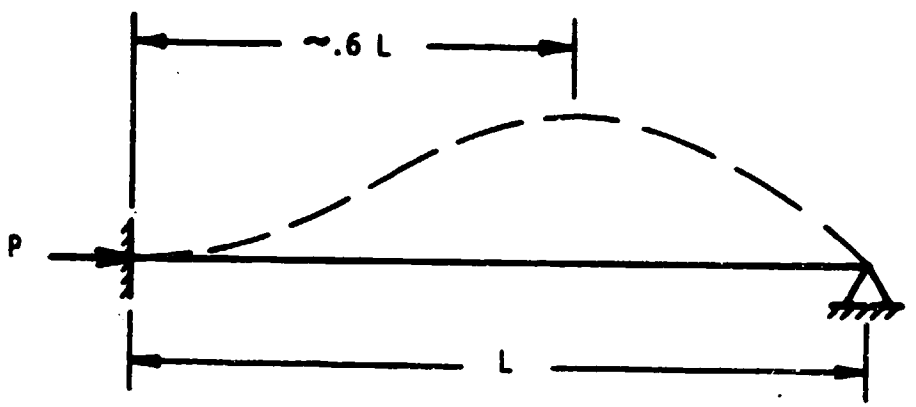

Figure 47: First Buckling Mode Shape of a Clamped-Pinned Column

joint region provided sufficient local stiffening to prevent overall column buckling. In one test, the specimen was seen to take on a slight S shape shortly before failure. So, it is also possible that there were misalignments in the specimen grips or in the prepared specimens. These misalignments could have induced moments on the specimens, bending them into S shapes, and thus forcing the observed buckling mode.

A second unexpected phenomenon was observed in only four cases; two of the .75 inch overlap specimens, and two of the 1.25 inch overlap specimens. While these specimens were being loaded, a "kink" was seen to occur in the Load/Ram Deflection curve. These kinks were accompanied by a sharp noise (not as loud as the ultimate failure) and, in several cases, a cloud of dust about the joint region that had the color of the adhesive and potting material. Figure 48 shows the two types of Load/Ram Deflection curves observed during compression testing. The two spare specimens were tested in an attempt to determine how much tension strength the joint had after experiencing a kink in the Load/Ram Deflection curve. Neither of these spares exhibited the kink.

Figure 49 and 50 show the results of the compression tests and illustrate the effects of overlap length and laminate bending stiffness on the critical buckling strength. The ordinates of these plots are the average stress applied to one face sheet, and are calculated in the fashion defined in Chapter 7. Also shown on these plots are the results of analyses of two analytical models intended to approximate

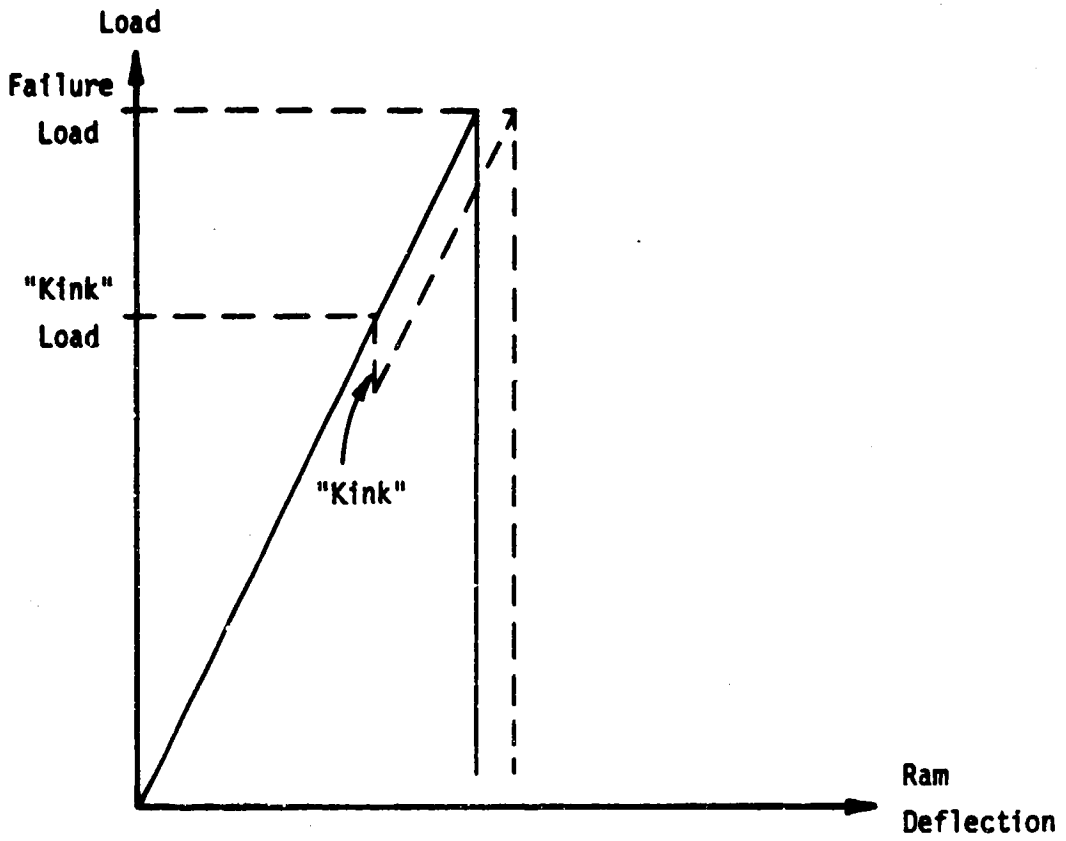

Figure 48: Typical Load/Ram Deflection Curves
Observed During Compression Tests

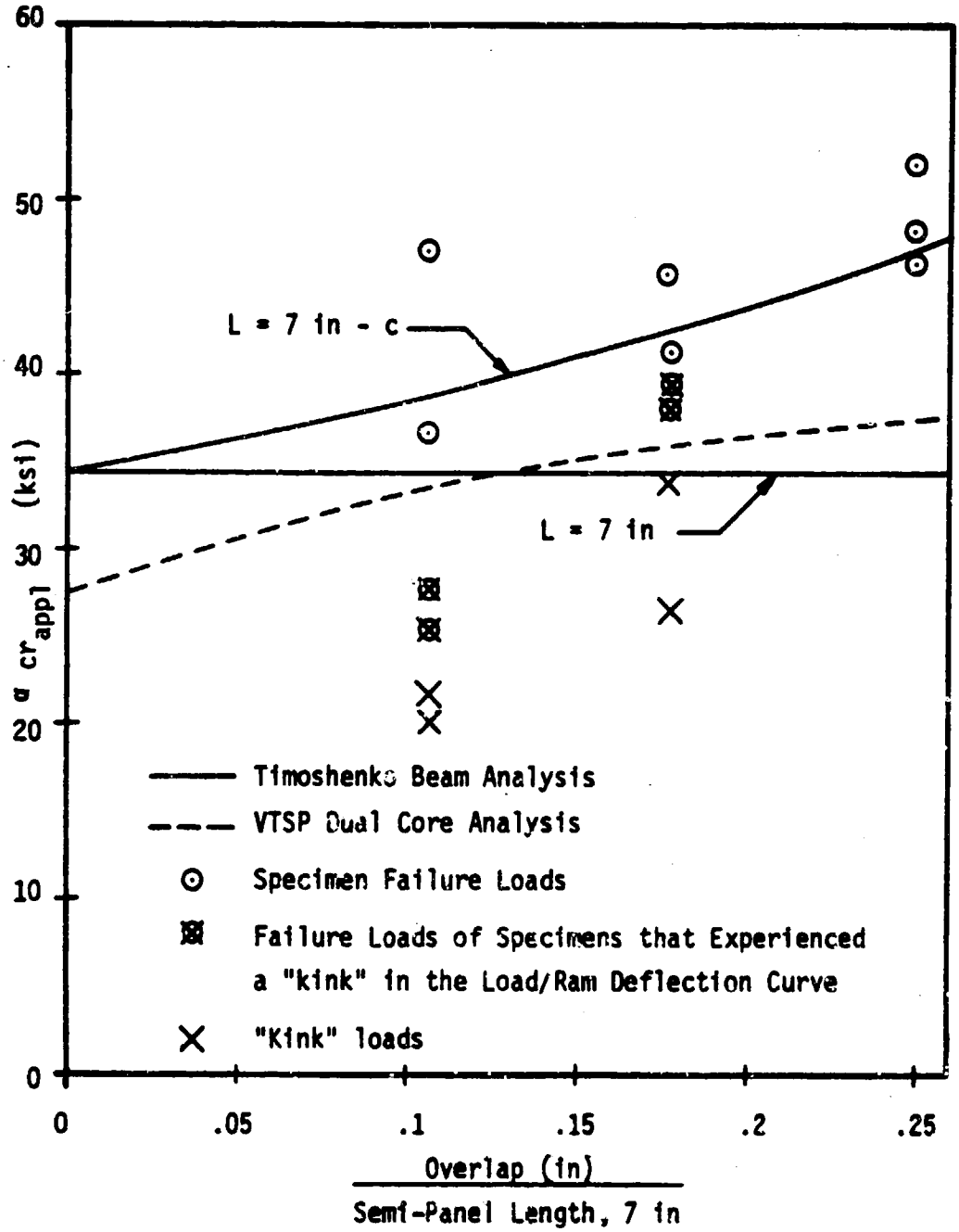

Figure 49: Effect of Overlap on Critical Buckling Strength

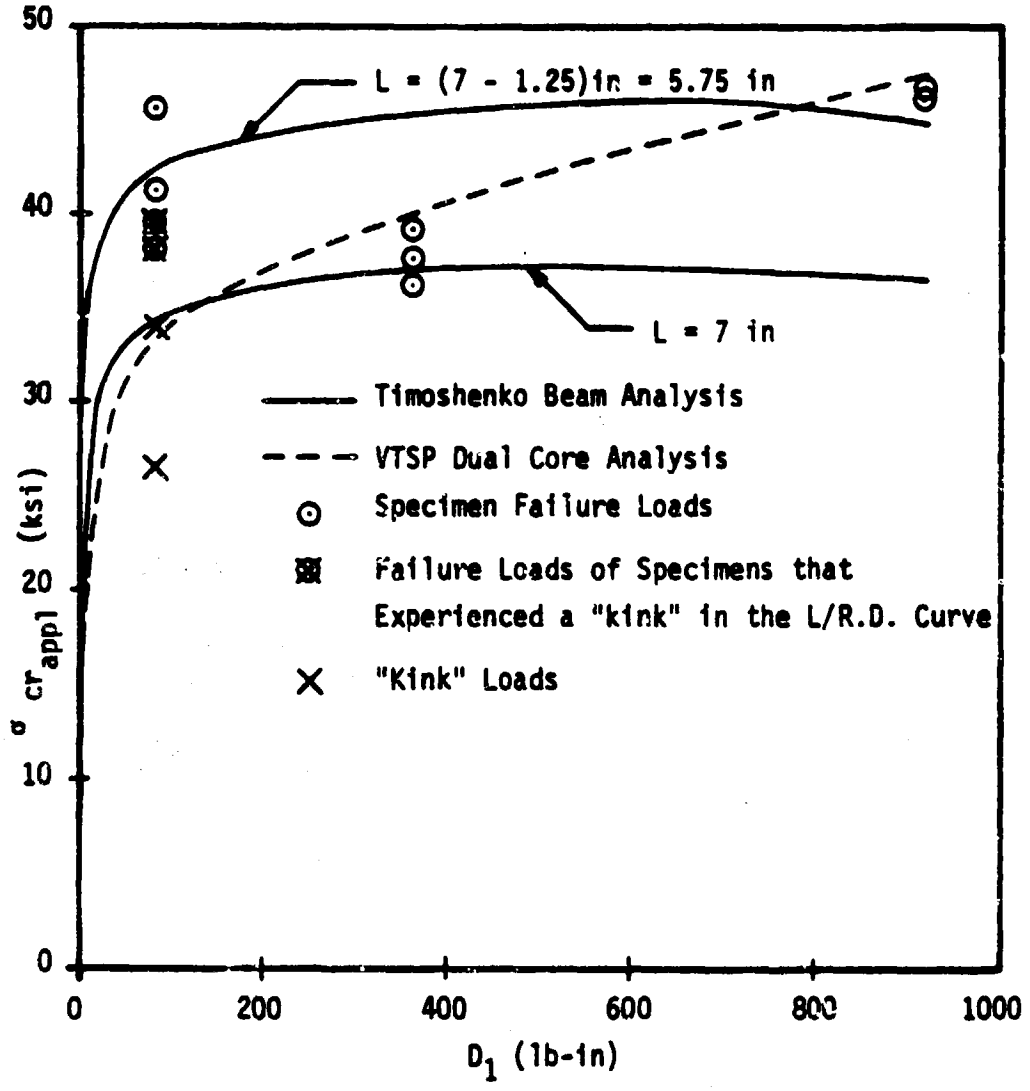

Figure 50: Effect of Face Sheet Bending Stiffness on Critical Buckling Strength

the test specimens. One of these models was the VTSP program with the elastic foundation stiffness beneath the overlap equal to 10^6 lb/in^3. The rest of the elastic foundation was assigned a stiffness of 4000 lb/in^3, corresponding to the actual stiffness of the core. The "dual core" model is intended to approximate the effects of the stiff core potting at the splice center.

The other model used to analyse the compression specimen behavior was a Timoshenko Beam model of a clamped-pinned column. The Timoshenko Beam theory includes the effect of shear flexibility in computing buckling loads [13]. The resulting equation for the critical buckling load, as modified for a sandwich panel, is given in [13] as

$$P_{cr} = \frac{\sqrt{1 - \frac{4n}{hG} P_e} - 1}{\frac{2n}{hG}} \qquad (26)$$

where

P_e = Euler Load, $(\frac{4.49}{L})^2 D_s$

L = Column Length

D_s = Sandwich Panel Bending Stiffness (as defined in [10])

n = Cross Section Correction Factor

= 1.2 for Solid Rectangle [13]

h = Distance Between Face Sheet Middle Surfaces

G = Longitudinal/Transverse Shear Modulus of Core

= 1000 psi [10]

In each of figures 49 and 50 there are two curves for the Timoshenko Beam model. One curve was developed for a column length equal to the

semi-specimen length of 7.0 inches. The second curve was developed for a column length equal to the semi-specimen length less the overlap length. These two pairs of Timoshenko Beam model curves are intended to account for the probable local stiffening effects of the core potting and the doubler.

It can be seen that the critical buckling loads predicted by the analytical models and the tested buckling loads are, for the most part, in the same neighborhood. Thus, it is possible that laminate buckling (modeled with the VTSP program) and column buckling (modeled with the Timoshenko Beam) are related phenomena, the former precipitating the latter. It is also possible that the kinks observed in some of the Load/Ram Deflection curves are related to laminate (face sheet/doubler structure) buckling since the dust clouds that were observed came from the joint vicinity - indicating an event there. In any case, the correlations between theory and experiment, visible in Figures 49 and 50, suggest that the two types of buckling, laminate and column, are each potential failure modes, and should be considered in any design that incorporates the type of splice investigated in this study.

Because of the restricted time available for testing, only three elevated temperature compression tests could be conducted. The specimens tested were those with 8 ply laminates and overlap of .75 inches. Figure 51 shows these test results. One of the two spare specimens tested was cut from the same panel that the three elevated temperature compression specimens were. Thus, it should provide a

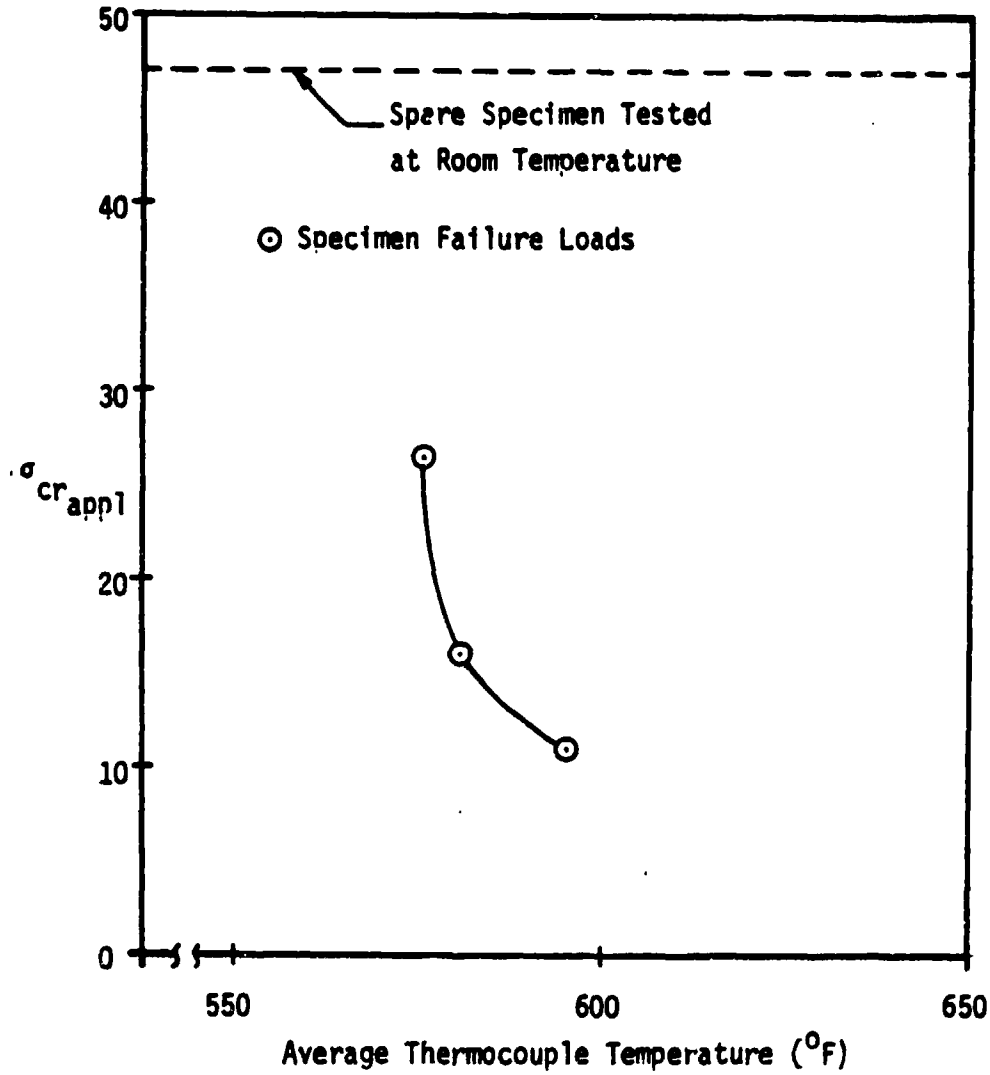

Figure 51: Elevated Temperature
Compression Test Results

meaningful comparison, and its failure load is included in Figure 51. It can be seen that elevated temperature degrades buckling strength drastically. Joint failure accompanied the buckling only in the case of the strongest specimen. No kinks in the load/ram deflection curves occurred.

Upon comparison of Figures 49 and 51, it can be seen that the strength of the strongest elevated temperature specimen compares favorably with the strengths of room temperature specimens with the same configuration. However, the other elevated temperature specimens were definitely weaker than the corresponding room temperature specimens. It should be noted here that the laminates on the elevated temperature specimens had fiber volume fractions near the high end of the range reported in Chapter 8. The room temperature specimens had laminates with fiber volume fractions near the low end of the range. This nonuniformity in fiber volume fractions could have had an influence on the behavior being observed here.

Chapter 10

CONCLUSIONS AND RECOMMENDATIONS

10.1 Conclusions

The results of an investigation into the behavior of adhesively bonded doubler splices of two composite material sandwich panels have been presented. Three approaches were taken in this investigation: an analytical beam model; a finite element model; and experimental testing.

The beam model shows that conditions may exist such that the face sheet and doubler moment factors, at the face sheet and gap sides of the overlap, respectively, are a strong function of only two parameters. These parameters involve four quantities that, to a large extent, characterize the splices. These four quantities are: the applied load level (tensile); the doubler overlap length; the stiffness of the sandwich core; and the bending stiffness of the bonded face sheet/doubler structure, constituting the overlap. By taking advantage of this functional dependence, a study of the general behavior of a wide variety of such splices can be accomplished. In an actual splice the functional dependence is not entirely accurate since factors such as adhesive flexibility are also involved.

An important effect of the applied load level is the deformation of the doubler and face sheets in the splice. As in the case of the single lap joint, this deformation and the internal loads of the doubler and face sheets are interdependent, leading to a geometric

structural non-linearity between stress and deflection.

The critical location for the failure of sandwich panel splices in tension is at the gap side of the doubler overlap region. It is here that the adhesive stress peaks are found to be the greatest. Experimental tests show that tensile failures of splices constructed of graphite/polyimide laminates are characterized by a splitting of the bottom ply of the doubler (at the doubler/adhesive interface) in the vicinity of the gap side of the overlap.

Increasing overlap length improves joint strength for both tensile and compressive edge loads. The effect of overlap length is strong for tensile loading and for the compressive stability of the splice specimens tested in the course of this study. However, it seems that overlap does not have a strong influence on the compressive stability of the face sheet/doubler structure, except in that larger overlaps allow slight increases in the gap length - without a significant degradation of the critical buckling strength. Increasing the gap length improves the splice's tensile strength of the splice by reducing the bending moment in the doubler.

Increasing the stiffness of the sandwich core improves joint strength in both tension and compression. This occurs because the core provides a restraint against face sheet rotation, and thus the curvature, of the plates at the edges of the overlap. Comparison of finite element and experimental results show that stiffening the core locally at the center of the splice (at the gap side of the overlap) can provide a significant increase in tensile strength. Also, it is possible that

there is an optimum combination of core stiffness and overlap length for which the load transfer through the adhesive layer is closest to being balanced between the two ends of the overlap.

The results of the present investigation suggest that there are two possible modes of failure in tension for the splice. The first mode is initiated by a longitudinal tension failure of the bottom 0° ply of the doubler at the splice center. The high adhesive peel stresses in this vicinity then cause the failed ply to split longitudinally, precipitating total failure of the splice. The second mode of failure is initiated by the high adhesive peel stresses at the splice center which, again, cause the bottom 0° ply of the doubler to split longitudinally.

The first failure mode is dominant for thin laminates, and adding 0° plies to the outer surfaces of the laminates increases the tensile strength of the splice by increasing the capacity of the doubler to withstand the longitudinal bending stresses. However, increasing the bending stiffness of the laminates also aggravates the adhesive stress peaks to the point where the second failure mode becomes dominant. The tensile strength of the splice is then degraded by the addition of further 0° plies to the outer surfaces of the laminates. As a result, there is an optimum number of 0° plies that can be added to the laminates to maximize the tensile strength of the splice.

The effect upon buckling strength of adding 0° plies to the splice's laminates is uncertain, since the results of analysis and experiment conflict. Either the analytical modeling does not adequately simulate

reality, or induced test variables have produced scatter in the experimental data. If the latter case is true, adding 0° plies to the laminates effects a gradually diminishing increase in the critical buckling strength of the spliced panel structure.

Subjecting the spliced panels to elevated temperature (in the 550° to 600°F range) does not appear to markedly degrade the joint's tensile strength. Elevated temperature does appear to degrade the buckling strength of the splice specimens tested in the course of this investigation.

10.2 Recommendations

The effect of local stiffening of the core at the splice center should be considered in more detail. This method of restraining the overlap ends against rotation could, as evidenced by test results, provide a significant strength increase without an excessive weight penalty. Further study of this possibility could be accomplished, to some extent, with a slight modification of the elastic axis beam model, presented previously. The local core reinforcement could be modeled as a spring attached to the splice at the junction of two elastic axes. The mathematical modification would involve a discontinuity in the shear force at the junction, and would appear in the appropriate shear boundary condition. The use of the elastic axis beam model is restricted because adhesive flexibility is ignored. One possibility for improvement of the model is to expand the elastic axis beam model in the fashion in which Hart-Smith [4] expands the single lap joint

model of Goland and Reissner [2]. However, experience with the elastic axis beam model strongly suggests that developing, checking, and interpreting results from the associated computer program would be a formidable task. It is likely that analytical, finite element, and experimental studies of specific details may be the most feasible approach to studying this splice.

It has been suggested that there exists an optimum number of 0° plies that could be added to the outer surfaces of the laminates in the splice to maximize joint strength. It is recommended that this possibility be studied further and verified.

The effect of increasing the gap length between the sandwich panel face sheets should also be investigated more thoroughly. Analysis has suggested that a very small increase in gap length could effect an improvement in tensile strength without significantly degrading the buckling strength of the combined face sheet/doubler structure.

The expressions developed in Appendix A for adhesive peel stress show that, if the shear force is ignored, the peel stress varies with the square root of the equivalent elastic foundation stiffness of the adhesive layer (its transverse Young's modulus divided by its thickness). This suggests that making the adhesive layer less stiff in the regions of the peel stress peaks will reduce the peaks, and strengthen the joint. One method would be to chamfer the face sheet and doubler as shown in Figure 52. Hart-Smith [5] reaches the same conclusion for double lap joints. Accomplishing this with composite laminates may prove troublesome, however, because of residual curing stresses at the edges of

the laminates. These stresses might cause a laminate to deform, or curl, out of plane if a portion of its edge is machined away.

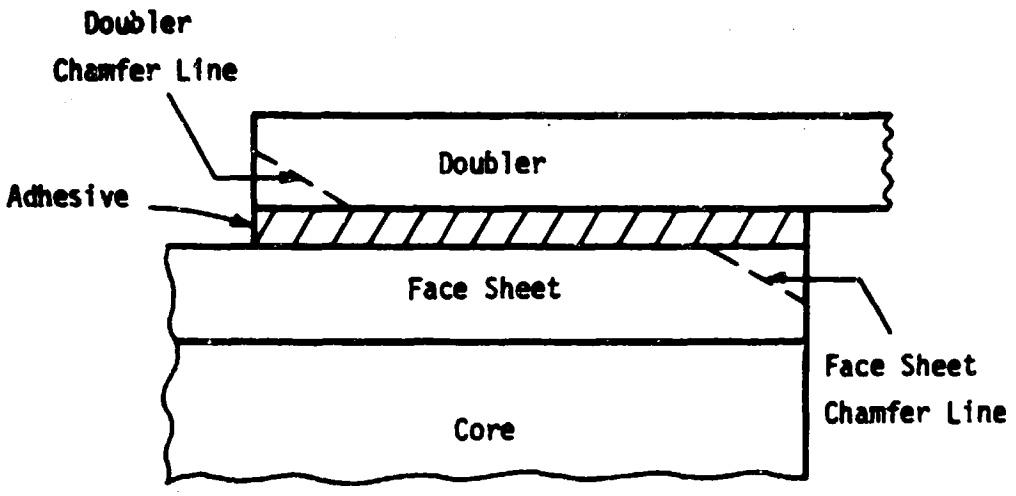

Figure 52: Chamfering the Face Sheet
and Doubler Edges

REFERENCES

1. Mallon, J. A. and Beck, E. J., "Structural Analysis of Bonded Honeycomb Welded Joints," American Astronautical Society, Southeastern Symposium on Missiles and Aerospace Vehicle Sciences, Vol. II, 1966, pp. 100-1 - 100-11.

2. Goland, M. and Reissner, E., "The Stresses in Cemented Joints," Journal of Applied Mechanics, Vol. 11, No. 6, 1944, pp. A-17 - A-27.

3. Lutters, Samuel F. and Bonassar, Maron J., "Development of Adhesive-Bonded Joints for Glass Resin Composite Sandwich Structures," Proj. DA-1-T-02440, United Aircraft Corp., Stratford, Conn. (Sikorsky Aircraft Div.). 1968.

4. Hart-Smith, L. J., "Adhesive-Bonded Single-Lap Joints," NASA CR 112236, 1973.

5. Hart-Smith, L. J., "Adhesive-Bonded Double-Lap Joints," NASA CR 112235, 1973.

6. Amijima, Sadao, Fujiz, Toru, and Yoshida, Akira, " Two Dimensional Stress Analysis on Adhesive Bonded Joints," Proceedings of the Twentieth Japan Congress on Materials Research. The Society of Materials Science, Japan, Kyoto, Japan, 1977, pp. 275-281.

7. Humphreys, E. A. and Herakovich, C. T., "Nonlinear Analysis of Bonded Joints with Thermal Effects," VPI-E-77-19 (NASA Grant NGR 47-004-090), Virginia Polytechnic Institute and State University, June 1977 (available as NASA CR-153263).

8. Cooper, P. A. and Sawyer, J. W., "A Critical Examination of Stresses in an Elastic Single Lap Joint," NASA TP 1507, September, 1979.

9. Whetstone, W. D., "SPAR System Reference Manual - System Level 13A. Volume I: Program Execution, NASA CR-158970, 1978.

10. Structural Sandwich Composites, Military Handbook, MIL-HDBK-23A, Department of Defense, 30 December 1968.

11. Farley, G. L. and Herakovich, C. T., "Influence of Two-Dimensional Hygrothermal Gradients on Interlaminar Stresses Near Free Edges," Advanced Composite Materials - Environmental Effects, ASTM STP 658, J. R. Vinson, Ed., American Society for Testing and Materials, 1978, pp. 143-159.

12. Hetenyi, M., "Beams on Elastic Foundations," The University of Michigan Press, Ann Arbor, Michigan, 1946.

13. Timoshenko, Stephen P., and Gere, James, M., "Theory of Elastic Stability," McGraw-Hill Book Company, New York, 1961.

14. Pike, R. A., Novak, R. C., and DeCrescente, M. A., "An Evaluation of FM-34 Polyimide Adhesive," 30th Anniversary Technical Conference, 1975, Reinforced Plastics/Composites Institute, The Society of the Plastics Industry, Inc.

APPENDIX A

SUPPLEMENTARY ANALYSIS OF ADHESIVE PEEL STRESSES

APPENDIX A

Figure A.1 shows the shear factor curves for a splice with the characteristics:

$$D_2 = 540.4 \text{ lb/in}$$

$$C = .75 \text{ in}$$

T and k variable,

where shear factor is defined, after Goland and Reissner, as

$$k_v = - \frac{Vc}{T(t+n)}.$$

Here,

V = shear force

c = overlap length

T = applied edge load

t = laminate thickness

n = adhesive thickness.

It can be seen that the shear factor in the doubler is very small, being .001 inches from a zero shear boundary condition at the gap center.

Now, Figures A.2a and A.2b show the face sheet and gap sides of the overlap, respectively. The loads shown conform to the positive sign conventions of the beam analysis. For the purpose of this analysis it is convenient to reverse the position shown in Figure A.2a to that shown in Figure A.2c. Thus, what was a positive shear force in Figure A.2a is a negative shear force in A.2c. Figures A.2b and A.2c will be refered to as the "doubler model" and the "face sheet model" respectively.

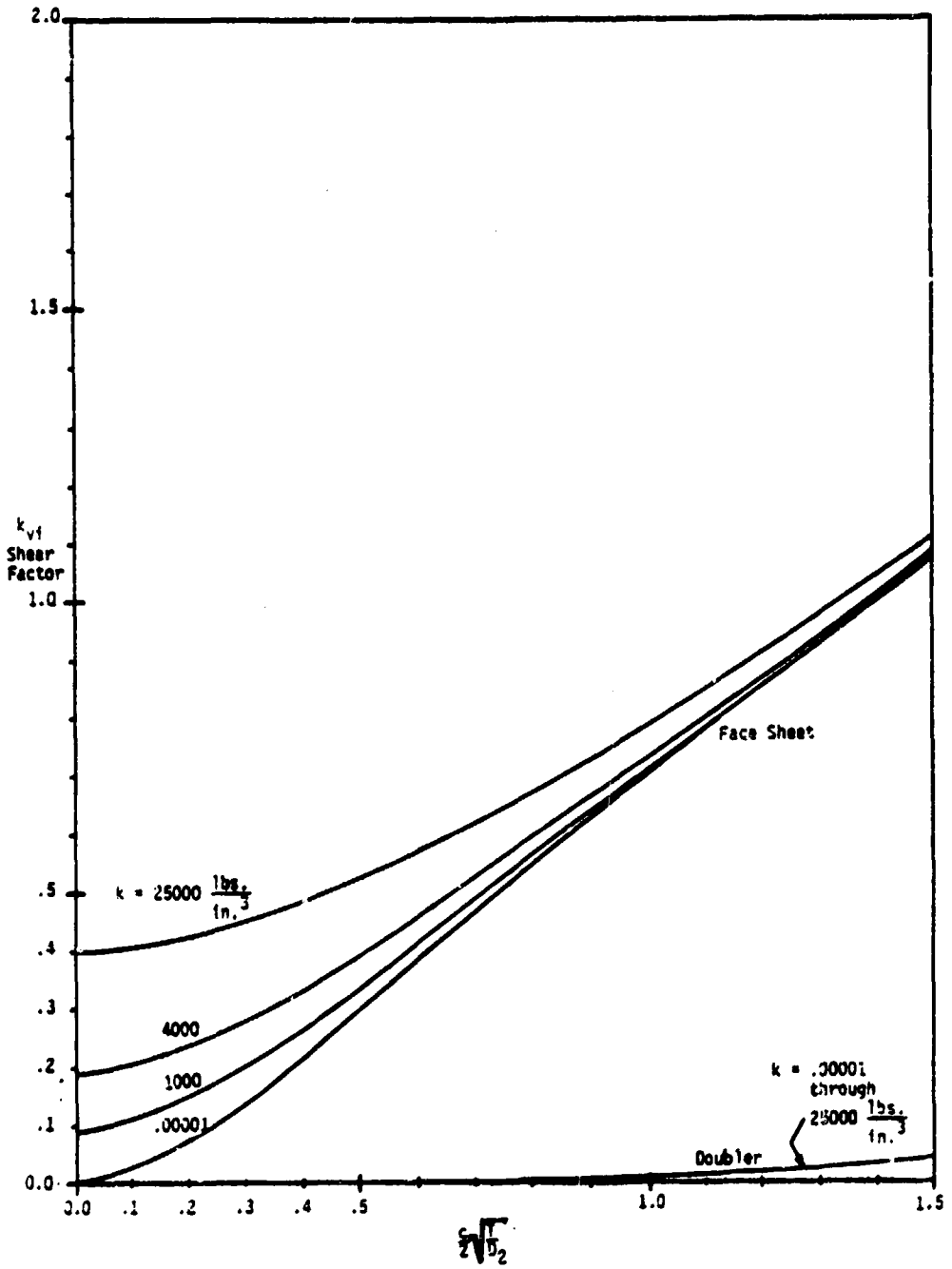

Figure A.1: Shear Factors

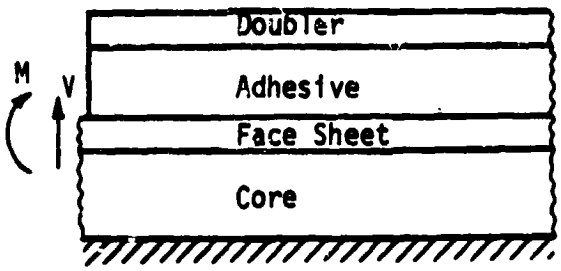

a: Face Sheet Moment and Shear

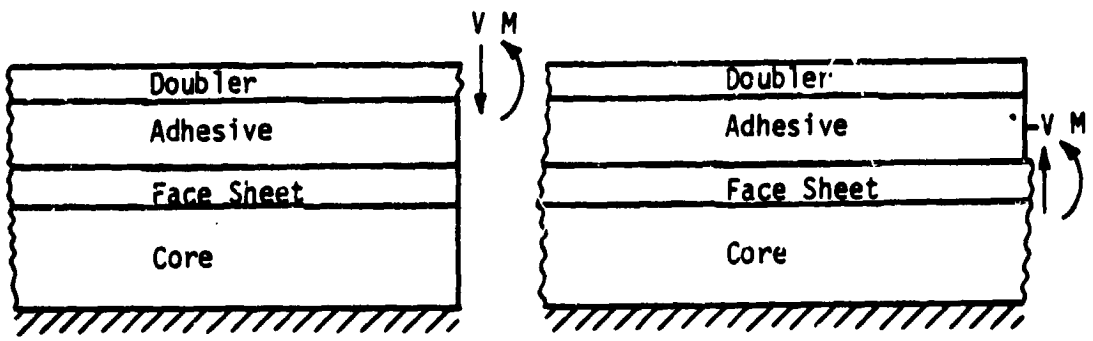

b: Doubler Model

c: Face Sheet Model

Figure A.2: Overlap Region Models for Adhesive Peel Stress Analysis

The governing equation for a semi-infinite beam (plate) on an elastic foundation subjected to shear and moment at one end is

$$w'''' + \frac{k}{D} = 0.$$

Figure A.3 shows the boundary conditions to be of the form:

$$w(-\infty) = 0 \qquad w''(0) = -\frac{M}{D}$$

$$w'(-\infty) = 0 \qquad w'''(0) = -\frac{V}{D}.$$

The solution to the governing equation, after two constants are elminated by the boundary conditions at minus infinity, is

$$w = C_1 e^{\lambda x} \cos \lambda x + C_2 e^{\lambda x} \sin \lambda x,$$

where

$$\lambda = \sqrt[4]{\frac{k}{4D}}.$$

The solution at $x = 0$ is found to be

$$w(0) = \frac{V - M\lambda}{2D\lambda^3}.$$

If the face sheet in the doubler model is considered rigid, k in the above analysis becomes

$$k = k_{adh} = \frac{E_{adh}}{\eta}.$$

The bending stiffness is that of a single $[0,45,90,-45]_s$ graphite/polyimide laminate. The adhesive peel stress at the adhesive edge is then

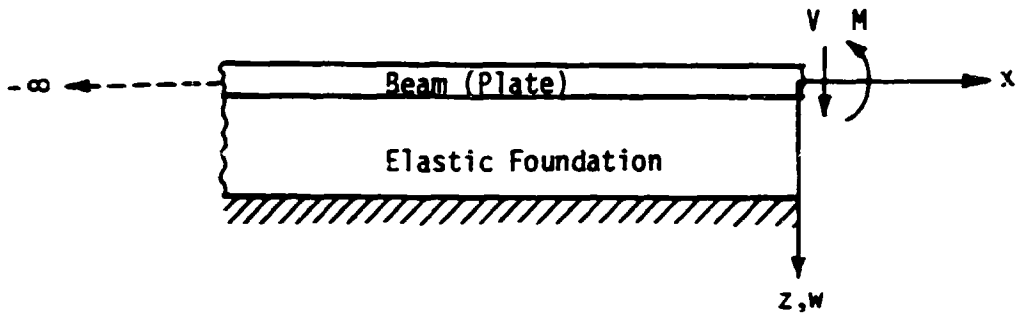

Figure A.3: Semi-Infinite Beam (Plate) on an Elastic Foundation

$$\sigma = - k_{adh}\, w(0) = - \frac{k_{adh}}{2D\lambda^3} (V-M\lambda).$$

If the doubler in the face sheet model is considered rigid, k becomes

$$k = k_{adh} + k_{core} = \frac{E_{adh}}{\eta} + k_{core}.$$

The bending stiffness is the same as for the doubler model (the doubler and the face sheet being identical laminates). The adhesive peel stress at the adhesive edge is then

$$\sigma = + k_{adh}\, w(0) = \frac{k_{adh}}{2D\lambda^3} (V-M\lambda).$$

Obtaining the shears and moments from the shear and moment factor curves, a comparison between the peel stresses in the two models can be made. For the doubler model:

$$k = k_{adh} = \frac{E_{adh}}{\eta} = \frac{2.6\times10^6 \text{psi}}{.005 \text{ in}} = 5.2 + 10^8 \frac{\text{lb}}{\text{in}^3}$$

$$D = 81.1 \text{ lb/in}$$

$$c = .75 \text{ in}$$

$$e_3 = \frac{t+\eta}{2} = \frac{.0416+.005}{2} \text{ in} = .0233 \text{ in.}$$

For a core stiffness of 4000 lb/in^3 and a load of 1000 lb/in, the doubler's shear and moment are:

$$V_3 = -k_{V_3} \frac{T(t+\eta)}{c} = -(.003) \frac{1000(.0466)}{.75} \frac{\text{lb}}{\text{in}}$$

$$= -.1864 \frac{\text{lb}}{\text{in}}$$

$$M_3 = k_{M_3}(Tc_3) = 1.313(1000)(.0233)\ \frac{lb/in}{in}$$

$$= 30.59\ \frac{lb/in}{in}\ .$$

Thus the adhesive peel stress is,

$$\sigma = 7.745x10^4 psi.$$

If the shear force is ignored,

$$\sigma = 7.746x10^4 psi.$$

For the face sheet model:

$$k = k_{ahd} + k_{core} = (5.2x10^8+4000)\ \frac{lb}{in^3}$$

$$= 5.20004x10^8\ \frac{lb}{in^3} \approx k_{adh}$$

$$D = 81.1\ lb/in$$

$$c = .75\ in$$

$$c_1 = \frac{t+n}{2} = .0233\ in.$$

The face sheet shear and moment (taking into account the sign reversed for the shear) are:

$$V_1 = -(-k_{v_1}\ \frac{T(t+n)}{c}) = -(-(.395)\ \frac{1000(.0466)}{.75})\ \frac{lb}{in}$$

$$= 24.54\ lb/in$$

$$M_1 = k_{m_1}(Te_1) = (-.265)(1000)(.0233)\ \frac{lb/in}{in}$$

$$= -6.17 \frac{lb/in}{in}$$

Thus the adhesive peel stress is,

$$\sigma = 1.737 \times 10^4 psi.$$

If the shear force is ignored,

$$\sigma = 1.562 \times 10^4 psi.$$

The peel stress in the doubler model is substantially greater than that in the face sheet model.

If the plates that were assumed rigid for this analysis were allowed flexibility, the face sheet and doubler models would be closer to reality. Refering to Figure A.4a, a flexible face sheet should add to the deflection of the doubler but should not alter appreciably the stretching, and thus the peel stress, experienced by the adhesive. However, refering to Figure A.4b, a flexible doubler should deform so as to relieve some of the adhesive stretching, and thus the peel stress.

This analysis suggests, then, that:

1) The shear loads in the sandwich splice do not have a strong influence upon the adhesive peel stresses at the adhesive edges.
2) The doubler side of the overlap is the more critical for peel stresses.

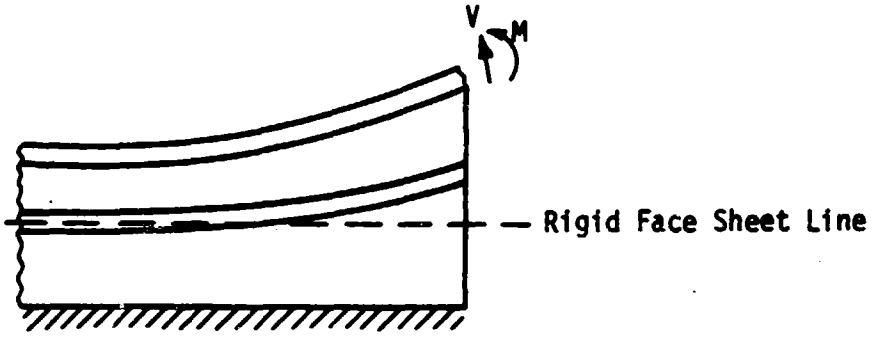

a: Fully Flexible Doubler Model

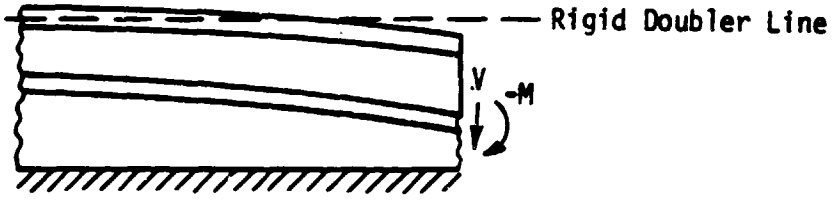

b: Fully Flexible Face Sheet Model

Figure A.4: Fully Flexible Overlap Region Models